ROBUST AND INTELLIGENT CONTROL OF UNMANNED AERIAL VEHICLES

İNSANSIZ HAVA ARAÇLARININ AKILLI VE GÜRBÜZ KONTROLÜ

ABDURRAHMAN BAYRAK

PROF. DR. MEHMET ÖNDER EFE

Supervisor

Submitted to

Graduate School of Science and Engineering of Hacettepe University

as a Partial Fulfillment to the Requirements

for the Award of the Degree of Doctor of Philosophy

in Computer Engineering

January 2023

ABSTRACT

ROBUST AND INTELLIGENT CONTROL OF UNMANNED AERIAL VEHICLES

Abdurrahman BAYRAK

Doctor of Philosophy, Computer Engineering

Supervisor: Prof. Dr. Mehmet Önder EFE

January 2023, 128 pages

Quadrotors from the family of unmanned aerial vehicles have an important place for human life, because over the last decade, they have been used in many areas both civilian and military applications, such as search, surveillance, rescue, tracing, aerial photography and postal service due to their size and maneuverability. Therefore, there are a great amount of the studies about the modelling and control of the quadrotors in the literature. Despite all these efforts, the modelling and control of the quadrotors is still among the subjects which are frequently studied to make them more autonomous. What makes them so important is that they have hover, vertical take-off and landing VTOL ability and agile mobility. With these features, even complex tasks can be successfully accomplished.

Quadrotor that is an under-actuated and nonlinear coupled system, has four rotors and six degrees of freedom (6 DOF) involving the both translational and rotational dynamical equations. Its unstable nature has required many different control methods. The most remarkable control methods among them are optimal control, robust control, adaptive control and intelligent control. The main goal of these control strategies is to achieve the best performance in the quadrotor control. However, there are many factors that affect the

performance of the quadrotors such as unmodelled dynamics, parameter uncertainties, all external force and moment disturbances, payload changes and sensor measurement noises during the quadrotor flights. In order to deal with these factors, many linear and non-linear controllers including above control strategies have been developed. Disturbance/Uncertainty Estimator (D/UE) based control, or in other words, disturbance observer based control (DOBC) that compensates the external disturbances and system uncertainties is one of the efficient robust control approaches and they are frequently used in modern control systems. In this thesis, widely used DOBC approaches in the literature are discussed in detail, usage structures for quadrotor control architectures are studied and a new machine learning assisted DOBC approach is proposed.

This thesis study can be summarized in three main subjects. Firstly, an analysis and synthesis of widely used linear disturbance observer based robust control approaches are presented. The main objective is to provide an exhaustive comparison of disturbance observer based robust control approaches and to handle the structural details of each approach for gaining insight about the complexity of each approach. Toward this goal, nine performance and robustness equations portraying useful insights for understanding and analyzing control systems are derived by examining their common and equivalent block diagrams. Four of them have been selected as a Gang of Four (GoF) equations, namely, Complementary Sensitivity Function (CSF), Sensitivity Function (SF), Disturbance Sensitivity Function (DSF) and Noise Sensitivity Function (NSF). Robustness and disturbance rejection performance analysis of all linear disturbance observer based control schemes and Classical Feedback Control (CFC) scheme are done using GoF equations. With these representations, two tables discussing all prime issues and facilitating the selection of the best approach have been obtained. Our research stipulates critical facts and figures of each scheme by considering the derived GoF equations, which can be used for choosing the most appropriate disturbance observer based control approach for a given robust control problem. It is concluded that the Uncertainty Disturbance Estimator (UDE) approach is superior when time delay type uncertainty is involved in the model. Unfolding this is critical as time delay is an inevitable fact in most industrial control systems. The findings also emphasize that Time

Domain Disturbance Observer Based Control (TDDOBC) approach is proficient if there is no process time delay.

Secondly, we present a short tutorial introduction to disturbance observer based control approaches for the quadrotors. With this tutorial, researchers, engineers and students would be able to implement disturbance observer based model-in-loop simulations and experiments more easily to design robust autopilot system for the quadrotors. To achieve this, the modeling and controlling of a quadrotor are explained and all linear disturbance observer based control approaches in the literature are adapted its overall nonlinear architecture. Disturbance observer based control design steps are given in detail by design challenges. To show their disturbance rejection capabilities and practical applicability, two flight simulation scenarios are carried out. For all simulation cases, we only take into account the external disturbances in rotational motions. While we give the attitude trajectory commands to quadrotor attitude control architecture in the first scenario, we issue both way-point and trajectory commands to an outer loop controlling the translational motions in the second one. Presented disturbance observer based control approaches have successfully completed the given reference commands in the presence of the external disturbances even under the measurement noise. Moreover, simulation experiments have shown that UDE approach transmit the external disturbance and measurement noise effects to the actuators directly. As a result, for UDE approach, it should be kept in mind that flight accidents may occur due to excessive electronic speed controller heating. Baseline attitude controller without disturbance observer based control approach have failed to follow the given reference commands. The simulation studies have also proved the practical applicability of these methods, which are successful even under measurement noise.

As the final and main purpose, we introduce a machine learning assisted disturbance/uncertainty estimator based control scheme. The aim of the proposed method is to update the nominal model directly used by the conventional disturbance observer based control architecture and approximate it to the perturbed/uncertain system using machine learning approaches. This enhances the disturbance rejection performance of the system remarkably. The performance deterioration capacity of lumped disturbances, which

are the mixed effect of disturbances entering through the control channels and modeling uncertainties, are decomposed in our approach and handled separately. For this study, harmonic disturbance model and constant unstructured uncertainty model are considered, and ϵ-Support Vector Regression approach is used together with an online adaptation algorithm. A numerical example is given to demonstrate the merits and effectiveness of the proposed approach. Simulation results show that the proposed method outperforms the conventional disturbance/uncertainty estimator based control architecture by increasing disturbance estimation performance of the system.

Keywords: robust control, disturbance observer based control, robustness and performance analysis, time domain disturbance observer based control, uncertainty disturbance estimator, disturbance rejection, quadrotor control, robust autopilot design, disturbance/uncertainty estimator machine learning, ϵ-Support Vector Regression

ÖZET

İNSANSIZ HAVA ARAÇLARININ AKILLI VE GÜRBÜZ KONTROLÜ

Abdurrahman BAYRAK

Doktora, Bilgisayar Mühendisliği

Danışman: Prof. Dr. Mehmet Önder EFE

Ocak 2023, 128 sayfa

İnsansız hava araçları ailesinden olan quadrotorlar, son on yılda arama, gözetleme, kurtarma, iz sürme, havadan fotoğraflama ve posta hizmetleri gibi hem sivil hem de askeri birçok alanda kullanılması nedeniyle insan yaşamı için boyutları ve manevra kabiliyetleri nedeniyle önemli bir yere sahiptir. Bu nedenle literatürde quadrotorların modellenmesi ve kontrolü ile ilgili çok sayıda çalışma bulunmaktadır. Tüm bu çalışmalara rağmen, quadrotorların modellenmesi ve kontrolü, onları daha otonom hale getirme hala sıklıkla çalışılan konular arasında yer almaktadır. Onları bu kadar önemli kılan, havada asılı kalma, dikey kalkış ve iniş (VTOL) kabiliyetine ve çevik hareket kabiliyetine sahip olmalarıdır. Bu özellikler sayesinde, karmaşık görevler bile başarıyla gerçekleştirilebilir.

Düşük tahrikli ve doğrusal olmayan kuplajlı bir sistem olan Quadrotor, hem öteleme hem de dönme dinamik denklemlerini içeren dört rotora ve altı serbestlik derecesine (6-DOF) sahiptir. Kararsız doğası, birçok farklı kontrol yöntemi geliştirmeyi gerekli kılmıştır. Bunlar arasında en dikkat çekici kontrol yöntemleri optimal kontrol, gürbüz kontrol, uyarlamalı kontrol ve akıllı kontroldür. Bu kontrol stratejilerinin temel amacı, quadrotor kontrolünde en iyi performansı elde etmektir. Ancak quadrotor uçuşları sırasında modellenmemiş dinamikler, parametre belirsizlikleri, tüm dış kuvvet ve moment bozulmaları, faydalı yük

değişimleri ve sensör ölçüm gürültüleri gibi quadrotorların performansını etkileyen birçok faktör bulunmaktadır. Bu faktörlerle başa çıkmak için, yukarıdaki kontrol stratejilerini içeren birçok doğrusal ve doğrusal olmayan denetleyiciler geliştirilmiştir. Disturbance/Uncertainty Estimator (D/UE) tabanlı kontrol veya başka bir deyişle, dış bozucuları ve sistem belirsizliklerini telafi eden bozucu gözlemci tabanlı kontrol (DOBC), verimli gürbüz kontrol yaklaşımlarından biridir ve modern kontrol sistemlerinde sıklıkla kullanılmaktadır. Bu tezde, litertürde yaygın bir şekilde kullanılan DOBC yaklaşımları ayrıntılı olarak ele alınmış, quadrotor kontrol mimarileri için kullanım yapıları çalışılmış ve yeni bir makine öğrenimi destekli DOBC yaklaşımı önerilmiştir.

Bu tez çalışması üç ana başlıkta özetlenebilir. İlk olarak, yaygın olarak kullanılan lineer bozunum gözlemcisine dayalı gürbüz kontrol yaklaşımlarının bir analizi ve sentezi sunulmaktadır. Temel amaç, bozulma gözlemcisine dayalı gürbüz kontrol yaklaşımlarının kapsamlı bir karşılaştırmasını sağlamak ve her bir yaklaşımın karmaşıklığı hakkında fikir edinmek için her bir yaklaşımın yapısal ayrıntılarını ele almaktır. Bu amaca yönelik olarak, ortak ve eşdeğer blok diyagramları incelenerek, kontrol sistemlerini anlamak ve analiz etmek için yararlı içgörüler sunan dokuz performans ve gürbüzlük denklemi türetilmiştir. Bunlardan dördü, GoF denklemleri olarak seçilmiştir: Tamamlayıcı Duyarlılık Fonksiyonu (CSF), Duyarlılık Fonksiyonu (SF), Bozulma Duyarlılık Fonksiyonu (DSF) ve Gürültü Duyarlılık Fonksiyonu (NSF). Tüm lineer bozulma gözlemcisi tabanlı kontrol şemalarının ve Klasik Geri Besleme Kontrolü (CFC) şemasının gürbüzlük ve bozulmayı reddetme performans analizi, GoF denklemleri kullanılarak yapılır. Bu temsillerle, tüm ana konuları tartışan ve en iyi yaklaşımın seçimini kolaylaştıran iki tablo elde edilmiştir. Araştırmamız, belirli bir gürbüz kontrol problemi için en uygun bozucu gözlemci tabanlı kontrol yaklaşımını seçmek için kullanılabilecek türetilmiş GoF denklemlerini göz önünde bulundurarak her şemanın kritik gerçeklerini ve rakamlarını şart koşar. Modelde zaman gecikmesi tipi belirsizlik yer aldığında UDE yaklaşımının üstün olduğu sonucuna varılmıştır. Çoğu endüstriyel kontrol sisteminde zaman gecikmesi kaçınılmaz bir gerçek olduğundan, bunun ortaya çıkarılması kritiktir. Bulgular ayrıca, herhangi bir işlem süresi gecikmesi yoksa, TDDOBC yaklaşımının yeterli olduğunu vurgulamaktadır.

İkinci olarak, quadrotorlar için bozucu gözlemci tabanlı kontrol yaklaşımlarına kısa bir öğretici giriş sunulmuştur. Bu öğretici giriş ile, araştırmacılar, mühendisler ve öğrenciler, quadrotorlar için gürbüz bir otopilot sistemi tasarlamak üzere bozucu gözlemci tabanlı döngü içi model simülasyonlarını ve deneyleri daha kolay bir şekilde uygulayabileceklerdir. Bunu başarmak için, bir quadrotorun modellenmesi ve kontrolü açıklanmış ve literatürdeki tüm doğrusal bozucu gözlemci tabanlı kontrol yaklaşımları quadrotorun doğrusal olmayan kontrol mimarisine uyarlanmıştır. Bozulma gözlemcisi tabanlı kontrol tasarım adımları, tasarım zorlukları ile ayrıntılı olarak verilmektedir. Bozulmayı reddetme yeteneklerini ve pratik uygulanabilirliğini göstermek için iki uçuş simülasyon senaryosu gerçekleştirilmiştir. Tüm simülasyon durumları için, sadece dönme hareketlerindeki dış bozulmalar hesaba katılmıştır. İlk senaryoda quadrotor konum kontrol mimarisine konum yörünge komutları verilirken, ikinci senaryoda öteleme hareketlerini kontrol eden bir dış döngüye hem yol noktası hem de yörünge komutları verilmiştir. Sunulan bozucu gözlemci tabanlı kontrol yaklaşımları, verilen referans komutlarını, ölçüm gürültüsü altında bile harici bozucuların varlığında başarıyla yerine getirmiştir. Ayrıca simülasyon deneyleri, UDE yaklaşımının harici bozulma ve ölçüm gürültüsü etkilerini doğrudan aktüatörlere ilettiğini göstermiştir. Sonuç olarak UDE yaklaşımı için aşırı elektronik hız kontolcüsü donanımı ısınması nedeniyle uçuş kazalarının oluşabileceği akılda tutulmalıdır. Bozulma gözlemcisi tabanlı kontrol yaklaşımı olmayan temel durum kontrolörü, verilen referans komutlarını takip edememiştir. Simülasyon çalışmaları, ölçüm gürültüsü altında bile başarılı olan bozucu gözlemci tabanlı kontrol yöntemlerinin pratik uygulanabilirliğini de kanıtlamıştır.

Nihai ve ana amaç olarak, makine öğrenimi destekli bozunum/belirsizlik tahmincisi tabanlı bir kontrol şeması sunulmuştur. Önerilen yöntemin amacı, geleneksel bozucu gözlemci tabanlı kontrol mimarisi tarafından doğrudan kullanılan nominal modelin güncellenmesi ve makine öğrenmesi yaklaşımlarının kullanılması ile bozulmuş/belirsiz sisteme yaklaştırılmasıdır. Bu, sistemin bozulma reddetme performansını önemli ölçüde artırır. Kontrol kanallarından giren bozulmaların ve modelleme belirsizliklerinin karışık etkisi olan toplu bozulmaların performans bozulma kapasitesi, yaklaşımımızda ayrıştırılmış ve ayrı ayrı ele alınmıştır. Bu çalışma için harmonik bozulma modeli ve sabit

yapılandırılmamış belirsizlik modeli ele alınmış ve bir çevrimiçi uyarlama algoritması ile birlikte ϵ-Support Vector Regresyon yaklaşımı kullanılmıştır. Önerilen yaklaşımın yararlarını ve etkinliğini göstermek için sayısal bir örnek verilmiştir. Benzetim sonuçları, önerilen yöntemin, sistemin bozucu tahmin performansını artırarak geleneksel bozucu/belirsizlik tahmincisi tabanlı kontrol mimarisinden daha iyi bir performans sergilediğini göstermektedir.

Keywords: gürbüz kontrol, bozunum gözlemcisine dayalı kontrol, gürbüzlük ve performans analizi, bozunum reddetme, quadrotor kontrol, gürbüz otopilot tasarımı, makine öğrenimi, ϵ-Support Vector Regression

CONTENTS

Page

TABLES

FIGURES

ABBREVIATIONS

UAV	:	**U**nmanned **A**erial **V**ehicle
VTOL	:	**V**ertical **T**akeoff and **L**anding
D/UE	:	**D**isturbance/ **U**ncertainty **E**stimator
DOE	:	**D**isturbance/**O**bserver **E**stimator
DOBC	:	**D**isturbance **O**bserver **B**ased **C**ontrol
LPF	:	**L**ow **P**ass **F**ilter
2-DoF	:	**2**-**D**egree **o**f **F**reedom
D/U	:	**D**isturbance/**U**ncertainty
MIMO	:	**M**ultiple **I**nput **M**ultiple **O**utput
ADRC	:	**A**ctive **D**isturbance **R**ejection **C**ontrol
CDOBC	:	**C**onventional **D**isturbance **O**bserver **B**ased **C**ontrol
TF	:	**T**ransfer **F**unction
GoF	:	**G**ang **o**f **F**our
CSF	:	**C**omplementary **S**ensitivity **F**unction
SF	:	**S**ensitivity **F**unction
DSF	:	**D**isturbance **S**ensitivity **F**unction
NSF	:	**N**oise **S**ensitivity **F**unction
ESO	:	**E**xtended **S**tate **O**bserver
TDDOBC	:	**T**ime **D**omain **D**isturbance **O**bserver **B**ased **C**ontrol
ISMC	:	**I**ntegral **S**liding **M**ode **C**ontrol
OEBDOBC	:	**O**utput **E**rror **B**ased **D**isturbance **O**bserver **B**ased **C**ontrol
EID	:	**E**quivalent **I**nput **D**isturbance
UDE	:	**U**ncertainty **D**isturbance **E**stimator
TDC	:	**T**ime **D**elay **C**ontrol
PID	:	**P**roportional **D**erivative **I**ntegral
PD	:	**P**roportional **I**ntegral

LQR	:	**L**inear **Q**uadratic **R**egulator
MPC	:	**M**odel **P**redictive **C**ontrol
BSC	:	**B**ack **S**tepping **C**ontrol
SMC	:	**S**liding **M**ode **C**ontrol
GC	:	**G**eometric **C**ontrol
CFC	:	**C**lassical **F**eedback **C**ontrol
CCF	:	**C**ontrollable **C**anonical **F**orm
OCF	:	**O**bservable **C**anonical **F**orm
FFT	:	**F**ast **F**ourier **T**ransform
SSMoFFT	:	**S**ingle **S**ided **M**agnitude of **F**ast **F**ourier **T**ransform
MAV	:	**M**ean **A**bsolute **V**alue
ZC	:	**Z**ero **C**rossing
ML	:	**M**achine **L**earning
LTI	:	**L**inear **T**ime **I**nvariant
SVM	:	**S**upport **V**ector **M**achine
SVR	:	**S**upport **V**ector **R**egression
ϵ-**SVR**	:	ϵ-**S**upport **V**ector **R**egression
MSE	:	**M**ean **S**quare **E**rror
PCA	:	**P**rincipal **C**omponent **A**naylsis

1. INTRODUCTION

Quadrotors from the family of unmanned aerial vehicles (UAVs), have been widely used for many different civilian and military purposes thanks to their low cost, agile maneuverability, Vertical Takeoff and Landing (VTOL) property, small size and hover capability. In recent years, the fact that many people prefer rotary wing unmanned aerial vehicles in many areas such as photography, search and rescue, emergency response and swarm applications shows that control of the quadrotors is still among the hot topics. Nonlinear, multi-variable, coupled and under-actuated dynamics of the quadrotors make modelling and control of them a challenging design problem. Furthermore, uncertainty and unavoidable external disturbances such as wind, unmodeled dynamics, neglected aerodynamic effects, variable weight suspended payloads, measurement and input noise make controller design even more difficult. While wind and variable weight suspended payloads are the environmental factors, unmodeled dynamics and measurement noise are caused by the modelling errors and available sensors, respectively.

The aim of the robust control is to deal with these plant uncertainties and disturbances that widely exist in all realistic feedback systems. Since 1970s, significant number of linear and nonlinear robust control methods eliminating the adverse effects of disturbances and uncertainties have been presented in the literature. Disturbance/Uncertainty Estimator (D/UE) based control, or in other words, disturbance observer based control (DOBC) that compensates the external disturbances and system uncertainties is one of the efficient robust control approaches and they are frequently used in modern control systems. DOBC actually is a patch over existing classical feedback controller, which has good stability and tracking performance yet it is vulnerable to external disturbances and uncertainties. The main idea of DOBC approaches is to estimate the lumped disturbances including both unknown dynamics and external disturbances, and to achieve robustness of the overall system via cancellation/rejection/attenuation of estimated disturbances by considering a number of design issues (e.g. nominal plant, reference model, Low Pass Filter (LPF) design etc.) with their two Degrees of Freedom (2-DoF) control structures. 2-DoF control structure adds an

inner loop that is activated in presence of the uncertainties and disturbances to classical feedback control that includes a baseline controller. While the baseline controller specifies the performance and stability of the control system, the inner loop determines the disturbance rejection and uncertainty handling capabilities [2].

Numerous research outcomes have been reported on DOBC so far, which increases the robustness of the system by estimating the total difference between the nominal model and the perturbed/uncertain system without affecting the system performance, and a certain level of closed loop performance has been reached [3]. However, the most DOBC structures reported in the literature generally assume the existence of an equivalent input disturbance on the control input and estimate mixed effect of disturbance and uncertainty as a lumped signal, [4]. Utilizing the disturbance observer's dynamical description, it becomes nearly impossible to figure out how much of the lumped D/U estimations are associated to the disturbance and how much is associated to uncertainty. This sets up our motivation. In this thesis study, we propose a new adaptive method based on machine learning approaches that increases disturbance estimation performance by approximating to the amount of system uncertainty. To our best knowledge, unmixing the lumped disturbances via an adaptive scheme is first attempted in the current study. Adaptive DOBC structures in the literature include generally composite controller design, data driven and nonlinear controller based augmented structures [5–8]. In [5], a novel control scheme combining nonlinear DOBC with H_∞ control structure was presented for complex multiple-input-multiple-output (MIMO) flight control system. The authors in [6] designed an adaptive multi-variable finite-time disturbance observer to estimate model uncertainties, external disturbances, and actuator faults for reusable launch vehicles. For piezoelectric ultrasonic actuator-based surgical device, an enhanced adaptive robust DOBC scheme including sliding mode was proposed in [7]. In [8], a data driven disturbance observer based control scheme including the active disturbance rejection control (ADRC) approach is discussed. However, the cited body of literature estimates the lumped D/U and remedies are based on the lumped effect of the disturbances and plant uncertainties.

In this thesis study, we also present a short tutorial introduction to DOBC approaches for attitude control of the quadrotors by applying five different linear DOBC methods existing

in the literature. We also analyze disturbance suppression capabilities of them in detail by discussing design challenges and practical applicability.

1.1. Scope Of The Thesis

Although there are a number of DOBC schemes, robust stability and robustness performance analysis are still the problems that worth studying in this field [9–11]. In the studies of Sariyildiz et al, analysis and design of conventional disturbance observer based control approach is presented [10, 11]. However, there is not a common way to synthesize and analyze the other DOBC approaches. The only common issue known is that the designed LPF dynamics directly effects the disturbance rejection capability of the control system. Reference signal tracking capability, rejection of external disturbances, measurement noise and process variations are the basic requirements for a robust control system design. In this thesis study, performance and robustness analysis equations of the DOBC approaches described in the literature are derived under the presence of a number of requirements.

After presenting a comprehensive comparison of these disturbance observer based robust control approaches by considering the advantages and disadvantage of each method such as time delay and measurement noise sensitivity, and derived the robustness and performance equations providing useful insights for choosing the best DOBC approach, we have applied DOBC approaches to attitude control of the quadrotors by discussing design challenges and practical applicability.

This thesis mainly focuses on the subject area towards decomposition algorithms that handle the adverse effects of input disturbances and plant uncertainties separately. The lumped estimation uses the difference between the nominal model and the perturbed/uncertain plant. Our purpose is to update the nominal model iteratively to match its response to that of the perturbed/uncertain system by using machine learning approaches thereby leading to an improvement in the disturbance rejection performance of the system. The proposed method is applicable to all DOBC schemes that exploit the nominal plant information. In order to exemplify the efficacy of the proposed technique, we use the algorithm proposed in [1].

1.2. Contributions

The main contributions of this thesis can be summarized as follows:

- This thesis study gives an exhaustive comparison of disturbance observer based robust control approaches. Toward this goal, nine relations between the input and the output signals including both the baseline controller and the inner loop are derived from the classical feedback control for all DOBC schemes described above. Spectra of these nine Transfer Functions (TFs) can provide useful insights for understanding and analyzing control systems under DOBC approaches. However, in this study, the only gang of four (GoF) equations are considered, these are Complementary Sensitivity Function (CSF), Sensitivity Function (SF), Disturbance Sensitivity Function (DSF), and Noise Sensitivity Function (NSF).

- Present study stipulates the critical facts and figures of each scheme by considering the derived GoF equations, which can be used for choosing the most appropriate DOBC approach for a given robust control problem including both minimum-phase uncertain and time-delay systems from disturbance rejection capability to design challenges.

- In this thesis, the one finds the structural details of each approach and gains insight about the complexity of each approach, which is undoubtedly essential in practice. Therefore, a discussion, which is not specific to a particular plant model, is presented and a second order plant model with some uncertainty in the form of time delay is considered. Although the studied plant model is an abstract one, this makes it possible to compare the most critical aspects peculiar only to DOBC algorithms.

- After reading this work, one would have a clear understanding of which approach to choose and what to expect. From this point of view, one can extend the results seen here to a large class of dynamic systems especially the second order ones appearing typically in mechanics.

- This study presents a short tutorial introduction to disturbance observer based control approaches for the quadrotors. With this tutorial, researchers, engineers and students

would be able to implement disturbance observer based model-in-loop simulations and experiments more easily to design robust autopilot system for the quadrotors.

- Machine learning offers a framework based on numerical data & optimization algorithms and we exploit the observed quantities towards unmixing a mixed signal in a feedback control framework. The most important contribution of the current study is to postulate an algorithm for handling the input disturbances by adaptively modifying the nominal plant dynamics.

1.3. Organization

The organization of the thesis is as follows:

- Chapter 1 presents our motivation, contributions and the scope of the thesis.
- Chapter 2 gives a background overview for disturbance observer based control approaches.
- Chapter 3 provides an exhaustive comparison of disturbance observer based robust control approaches and to handle the structural details of each approach for gaining insight about the complexity of each approach.
- Chapter 4 introduces a short tutorial introduction to disturbance observer based control approaches for the quadrotors.
- Chapter 5 proposes a machine learning assisted disturbance/uncertainty estimator based control scheme.
- Chapter 6 demonstrates the experimental results indicate that the proposed method outperforms the conventional disturbance/uncertainty estimator based control architecture by increasing disturbance estimation performance of the system.
- Chapter 7 states the summary of the thesis and possible future directions.

2. BACKGROUND OVERVIEW

2.1. Disturbance Observer Based Control

The disturbance observer was firstly proposed by Ohnishi in order to estimate external disturbances and structural uncertainties [12–14]. Extended State Observer (ESO), so called Active Disturbance Rejection Control (ADRC) that was proposed by Han, appears as another popular robust control scheme [15, 16]. Thanks to Ohnishi's and Han's inspirations to other researchers, in the last few decades, several DOBC structures are reported in the literature [1, 2, 9, 13, 17–27].

The first general DOBC scheme, abbreviated as Conventional Disturbance Observer Based Control (CDOBC), was proposed by Ohishi et al [13]. Chang et al have recommended a disturbance observer design and analysis toolbox for MATLAB to find acceptable Q-Filter for CDOBC approach [22]. They have also studied the robust stability and nominal performance recovery analyses, which help engineers to construct CDOBC approach. A discussion on discrete implementation of CDOBC approach has presented for motion control systems [23]. Efe and Kasnakoğlu have inserted a signum function into CDOBC loop and obtained an enhanced bandwidth CDOBC scheme [24]. A disturbance attenuation problem for a missile system using a recently proposed disturbance observer based robust control method is presented in the work of Yang et al [17], which is called Time Domain Disturbance Observer Based Control (TDDOBC). In study of Kürkçü et al, authors have proposed the novel DOBC method combining Integral Sliding Mode Control (ISMC) with an $\mathcal{H}_\infty$ controller named as Output Error Based Disturbance Observer Based Control (OEBDOBC) [1]. The works of She et al are the motivating studies for the Equivalent Input Disturbance (EID) approach in order to improve disturbance rejection performance of control systems [18, 19]. An improved EID approach is presented and validated on position control of a ball-and-beam system experimentally [26]. Zhong et al have proposed Uncertainty Disturbance Estimator (UDE) method that is an alternative control strategy to Time Delay Control (TDC) scheme [20, 21]. Aharon et al have presented a guideline including analysis of

UDE approach considering actuator dynamics and applied it to power control of a multimode bi-directional non-inverting buck-boost converter [27]. The recent and advanced DOBC approaches addressing both linear and nonlinear cases can be found in the works of Chen et al [2, 9]. Moreover, the reader may refer to paper of Sariyildiz et al for a detailed overview of DOBC from origin to present [3].

2.2. Disturbance Observer Based Control for Quadrotors

In the literature, numerous studies focus on the control of the quadrotors ([28]). The most common controller structure is the Proportional Integral Derivative (PID) control which is widely used in commercial quadrotors ([29–32]). The other common control structures in the literature include both linear and nonlinear controllers: Linear Quadratic Regulator (LQR), Model Predictive Control (MPC), Back-Stepping Control (BSC), Sliding Mode Control (SMC), H-infinity Control and Geometric Control (GC). ([33–44]).

[28] have presented an exhaustive review of recent advances for position, altitude and attitude control of multi-rotor aerial vehicles from linear to nonlinear control approaches. Readers can refer to their work for a range of multi-rotor aerial vehicles control approaches such as intelligent control, robust control, adaptive control, fractional order control, data-driven control, disturbance observer based control (DOBC), active disturbance rejection control (ADRC), and more. Among these control approaches, the ADRC and DOBC have recently gained popularity not only in the control of quadrotors, but also in the control of most industrial mechanical systems including external disturbances and unknown dynamics which are widely encountered in most control problems. Especially for practical applications, the ADRC and DOBC approaches emerge as robust control methods given the complexity of quadrotor control as well as unknown external disturbances and uncertainties. The ADRC approach is also known as extended state observer (ESO). Tracking differentiator, ESO and state error feedback control law are the main parts to design an ADRC approach. [45], have proposed a new double closed-loop ADRC approach for the quadrotors.

[46] have used the CDOBC approach to reject external disturbances caused by wind in the rotational motion of a quadrotor. To further improve the trajectory tracking precision of a quadrotor, a Linear Dual DOBC scheme is proposed by [47] with modification of the CDOBC approach. A new disturbance suppression scheme that is sliding mode observer based EID approach for the under-actuated subsystem of a quadrotor is presented in the work of [48]. The authors in [49] have proposed a UDE based robust control method that is validated in real-time applications for the attitude and the altitude control of quadrotors. In another work, the authors in [50] have proposed a modified UDE control approach, and have validated it with real time quadrotor experiments. They have obtained much better performance even under the presence of large time delays. TDDOBC is applied to quadrotors by proposing a robust disturbance observer-based feedback linearization approach to eliminate adverse effects to the formation flight of multiple quadrotors ([51]).

Mathematical modelling of the quadrotors are another challenging area due to we must consider aerodynamic effects, actuator and sensor dynamics. So far, different data driven methods using experimental input output data and allowing tuning of the controller parameters have often used ([52]). These methods allow us fast deployment of the control system besides an accurate modeling of the system. As some DOBC approaches require priory knowledge of nominal plant or inverse of nominal plant, the merging data driven methods and DOBC structures emerges as an open field that needs to be studied. [53] have obtained data driven model by means of fuzzy rules emulating a neural network and proposed a discrete time disturbance observer improving closed loop performance with an output feedback controller considering input output information.

3. RELATED WORK

3.1. Classical Feedback Control (CFC)

Fig. 3.1 shows CFC block diagram including two blocks, namely, the feedback block K and the feedforward block F. In the figure, $\widehat{P}$ is the disturbed uncertain plant. Let e denote the reference tracking error. Consider the diagram shown in Fig. 3.1 assume that the capital letters denote the Laplace transform of the relevant variables.

From Fig. 3.1, the following equations can be written:

$$E = FR - Y_r \tag{1}$$

$$U = KE \tag{2}$$

$$X_r = \widehat{P}(U + D) \tag{3}$$

$$Y_r = X_r + N \tag{4}$$

The nine TFs for a CFC system can be obtained by using Eq. (1), (2), (3), and (4) as follows:

$$U = \frac{KF}{1 + K\widehat{P}}R - \frac{K\widehat{P}}{1 + K\widehat{P}}D - \frac{K}{1 + K\widehat{P}}N \tag{5}$$

$$X_r = \frac{K\widehat{P}F}{1 + K\widehat{P}}R + \frac{\widehat{P}}{1 + K\widehat{P}}D - \frac{K\widehat{P}}{1 + K\widehat{P}}N \tag{6}$$

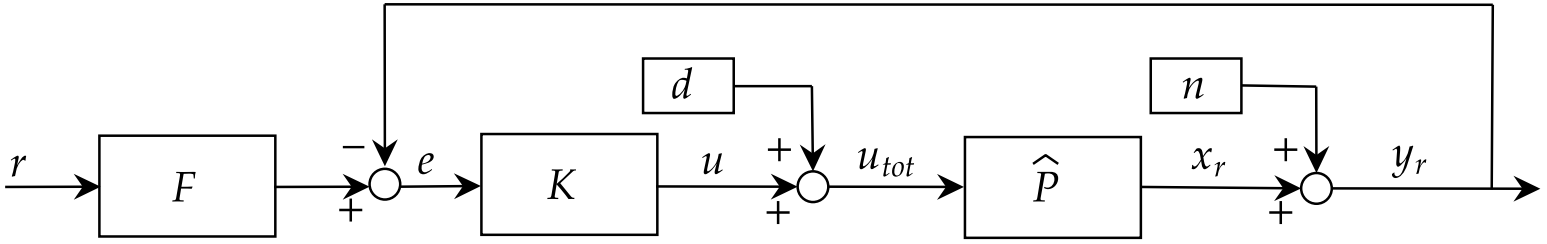

Figure 3.1 General block diagram of CFC

$$Y_r = \frac{K\widehat{P}F}{1+K\widehat{P}}R + \frac{\widehat{P}}{1+K\widehat{P}}D + \frac{1}{1+K\widehat{P}}N \tag{7}$$

3.2. Conventional Disturbance Observer Based Control (CDOBC) Approach

Let d_l denote the lumped disturbances and $\hat{d}$ denote the estimation of lumped disturbances. Let u_{tot} denote the corrected control signal. Let P, P^{-1} and Q are the nominal model of plant, the inverse of nominal plant and disturbance observer filter, respectively. Fig. 3.2 illustrates the original form of CDOBC [13]. Its equivalent block diagram can be obtained by replacing $\widehat{P}$ with P and d with d_l. The difference between the original form and the equivalent form is that the equivalent form employs P as the plant whereas the original form employs $\widehat{P}$, the uncertain model. As a consequence of this, $\hat{d}$ variable directly equals to lumped disturbance. On the other hand, $\hat{d}$ variable in the original form is the estimation of the lumped disturbances, obtaining which is the ultimate goal in any DOBC mechanism. Lumped disturbances include both the external disturbances and the internal disturbances caused by model uncertainties.

The following equation can be written by using the noiseless plant output in Fig. 3.2 and CDOBC equivalent block diagram.

$$(U+D)\widehat{P} = (U+D_l)P \tag{8}$$

As a consequence, the lumped disturbances are obtained as given by

$$D_l = P^{-1}\widehat{P}D + (P^{-1}\widehat{P} - 1)U \tag{9}$$

From CDOBC equivalent block diagram, we have

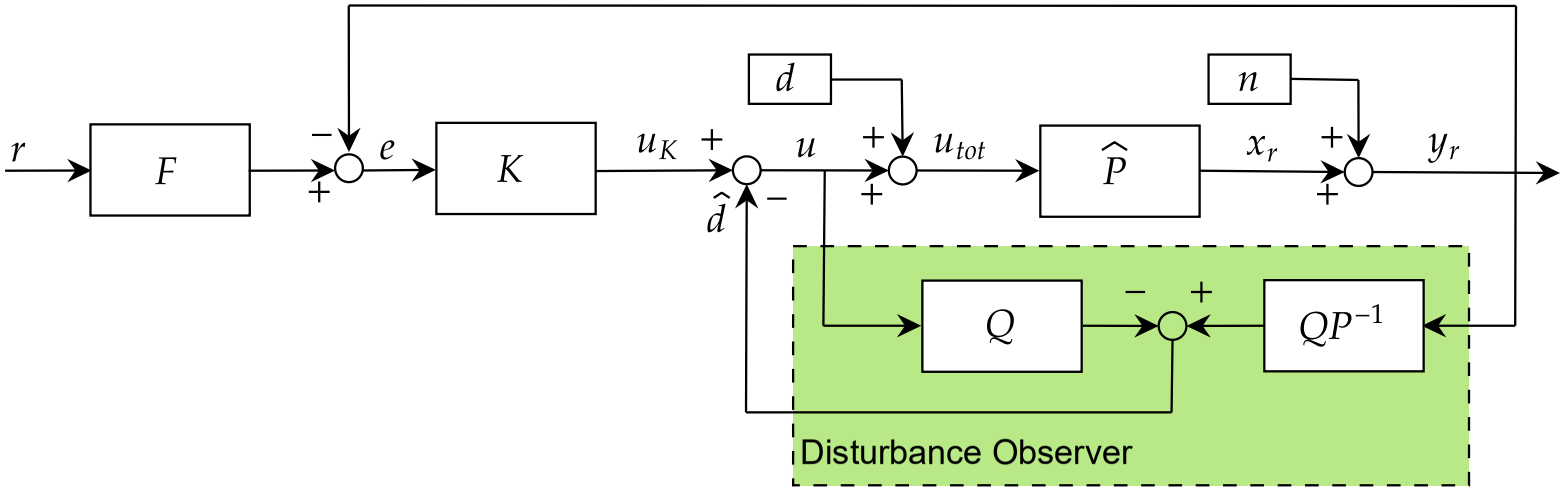

Figure 3.2 General block diagram of CDOBC

$$\hat{D} = Q(D_l + P^{-1}N) \tag{10}$$

When we write the plant output, $X_r(s)$ as $X_r(s) = P(s)U - Q(s)N - P(s)(1 - Q(s))D$ following can be said: To suppress the effects of noise, Q should go to zero. On the other hand, in order to avoid the adverse effects of the disturbance, Q should go to unity. These two requirements are conflicting and this fact leads to the design of the LPF denoted by Q. We know that disturbance ($D(s)$) has low frequency components and noise ($N(s)$) has high frequency components, this fact entails choosing an appropriate pass band for the LPF.

From Fig. 3.2, it can be seen that the CDOBC structure contains the CFC structure. Therefore, the first five equations in CFC section can be used with following correction for derivation of the nine relations.

$$U_K = KE \tag{11}$$

$$U_{tot} = U + D \tag{12}$$

Corrected control signal U is as follows.

$$U = U_K - \hat{D} \tag{13}$$

Having these in mind, the nine relations for a CDOBC system can be obtained as below. From (9), (10), (11) and (13), we have

$$
\begin{aligned}
U = & \frac{KF}{1+K\widehat{P}+Q(P^{-1}\widehat{P}-1)}R \\
& -\frac{\widehat{P}(K+QP^{-1})}{1+K\widehat{P}+Q(P^{-1}\widehat{P}-1)}D \\
& -\frac{K-QP^{-1}}{1+K\widehat{P}+Q(P^{-1}\widehat{P}-1)}N
\end{aligned} \tag{14}
$$

From (3), (12) and (14), we have

$$
\begin{aligned}
X_r = & \frac{\widehat{P}CF}{1+\widehat{P}C+Q(P^{-1}\widehat{P}-1)}R \\
& +\frac{\widehat{P}(1-Q)}{1+\widehat{P}C+Q(P^{-1}\widehat{P}-1)}D \\
& -\frac{\widehat{P}(C+QP^{-1})}{1+\widehat{P}C+Q(P^{-1}\widehat{P}-1)}N
\end{aligned} \tag{15}
$$

From (4) and (15), we have

$$
\begin{aligned}
Y_r = & \frac{\widehat{P}CF}{1+\widehat{P}C+Q(P^{-1}\widehat{P}-1)}R \\
& +\frac{\widehat{P}(1-Q)}{1+\widehat{P}C+Q(P^{-1}\widehat{P}-1)}D \\
& +\frac{1-Q}{1+\widehat{P}C+Q(P^{-1}\widehat{P}-1)}N
\end{aligned} \tag{16}
$$

3.3. Output Error Based Disturbance Observer Based Control (OEBDOBC) Approach

Fig. 3.3 illustrates the original form of OEBDOBC [1]. Its equivalent block diagram can be obtained by replacing $\hat{P}, d$ pair with P, d_l pair, respectively. K_{obs} block requires an observer design. Let y_n denote the nominal plant output and y_{obs} denote the observer output.

The following equation can be written by using the noiseless plant output in Fig. 3.3 and OEBDOBC equivalent block diagram.

$$(U + D)\hat{P} = (U + D_l)P \tag{17}$$

As a consequence, the lumped disturbances are obtained as below.

$$D_l = P^{-1}\hat{P}D + (P^{-1}\hat{P} - 1)U \tag{18}$$

From OEBDOBC equivalent block diagram, we have

$$\hat{D} = Q_k P D_l + Q_k N \tag{19}$$

where, Q_k is as follows:

$$Q_k = \frac{K_{obs}}{1 + K_{obs}P} \tag{20}$$

From Fig. 3.3, it can be seen that the OEBDOBC structure contains the CFC structure. The nine relations for the OEBDOBC system can be obtained as follows. From (2), (13), (18), (19) and (20), we have

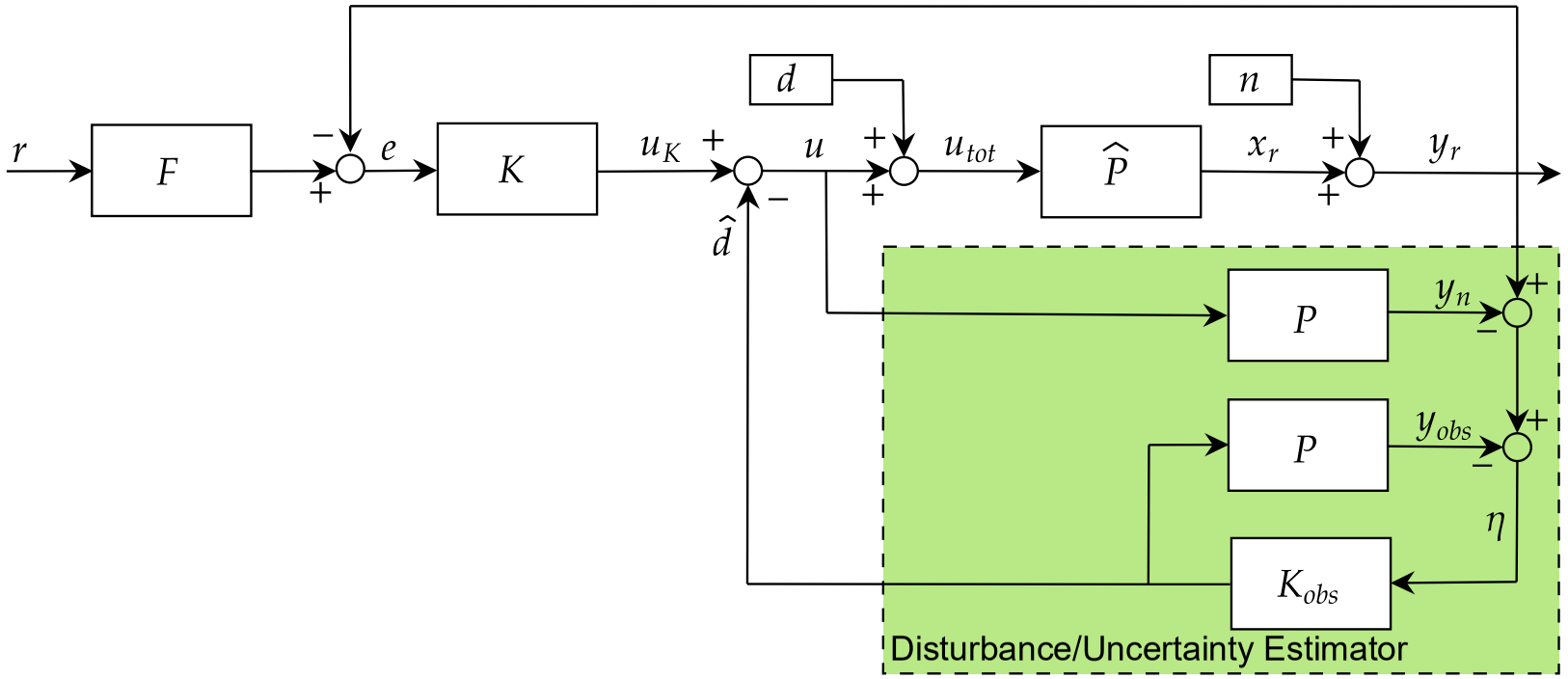

Figure 3.3 General block diagram of OEBDOBC.

$$
\begin{aligned}
U = & \frac{CF}{1+\hat{P}C+Q_kP(P^{-1}\hat{P}-1)}R \\
& -\frac{\hat{P}(C+Q_k)}{1+\hat{P}C+Q_kP(P^{-1}\hat{P}-1)}D \\
& -\frac{C+Q_k}{1+\hat{P}C+Q_kP(P^{-1}\hat{P}-1)}N
\end{aligned} \tag{21}
$$

From (3), (12) and (21), we have

$$
\begin{aligned}
X_r = & \frac{\hat{P}CF}{1+\hat{P}C+Q_kP(P^{-1}\hat{P}-1)}R \\
& +\frac{\hat{P}(1-Q_kP)}{1+\hat{P}C+Q_kP(P^{-1}\hat{P}-1)}D \\
& -\frac{\hat{P}(C+Q_k)}{1+\hat{P}C+Q_kP(P^{-1}\hat{P}-1)}N
\end{aligned} \tag{22}
$$

From (4) and (22), we have

$$
\begin{aligned}
Y_r = & \frac{\hat{P}CF}{1+\hat{P}C+Q_kP(P^{-1}\hat{P}-1)}R \\
& +\frac{\hat{P}(1-Q_kP)}{1+\hat{P}C+Q_kP(P^{-1}\hat{P}-1)}D \\
& +\frac{1-Q_kP}{1+\hat{P}C+Q_kP(P^{-1}\hat{P}-1)}N
\end{aligned} \tag{23}
$$

It can be seen that $Q = Q_kP$ from (21), (22) and (23). If K_{obs} is chosen as given below, OEBDOBC and CDOBC approaches display identical performances.

$$
K_{obs} = \frac{Q}{P(1-Q)} \tag{24}
$$

3.4. Equivalent Input Disturbance (EID) Approach

Fig. 3.4 illustrates the original form of EID structure [18, 19]. Its equivalent block diagram can be obtained by replacing $\hat{P}, d$ pair with P, d_l pair, respectively. In the figure, Q_e is the disturbance filter. In the diagram depicted in Fig. 3.4, $\mathbf{A_n}, \mathbf{B_n}, \mathbf{C_n}$ are system matrix, control matrix and output matrix of nominal plant in Controllable Canonical Form (CCF), respectively. $\mathbf{L_e}$ block is the observer gain. Further, $\hat{\mathbf{x}}, \hat{y}$ denote the observer plant state and its output, respectively.

The following equation can be written by using the noiseless plant output in Fig. 3.4 and EID approach equivalent block diagram.

$$(U + D)\hat{P} = (U + D_l)P \tag{25}$$

As a consequence, the lumped disturbances are modeled by:

$$D_l = P^{-1}\hat{P}D + (p^{-1}\hat{P} - 1)U \tag{26}$$

Performing the aforementioned substitutions, from the equivalent structure of the EID approach, we have

$$\hat{D} = k_1 D_l + k_2 U + k_3 N \tag{27}$$

where, $k_1 = \frac{(\mathbf{B_e^+ L_e} - b_e)PQ_e}{1+(a_e-1)Q_e}$, $k_2 = \frac{((\mathbf{B_e^+ L_e} - b_e)P - a_e)Q_e}{1+(a_e-1)Q_e}$, $k_3 = \frac{(\mathbf{B_e^+ L_e} - b_e)Q_e}{1+(a_e-1)Q_e}$, $k_1 = Pk_3$, $k_2 = k_1 - \frac{a_e Q_e}{1+(a_e-1)Q_e}$, $a_e = (\mathbf{B_e^+ L_e})(\mathbf{C_n}(\mathbf{HB_n}))$, $b_e = (\mathbf{B_e^+ L_e})(\mathbf{C_n}(\mathbf{HL_e}))$, $\mathbf{H} = (s\mathbf{I} - \mathbf{A_n} + \mathbf{L_e C_n})^{-1}$ and $\mathbf{B_e^+} = (\mathbf{B_n}^T \mathbf{B_n})^{-1}(\mathbf{B_n}^T)$. ($\mathbf{A_n} \in \mathbb{R}^{q\times q}$, $\mathbf{B_n} \in \mathbb{R}^{q\times 1}$, $\mathbf{C_n} \in \mathbb{R}^{1\times q}$, $\mathbf{L_e} \in \mathbb{R}^{q\times 1}$, $\mathbf{B_e^+} \in \mathbb{R}^{1\times q}$, $\hat{\mathbf{X}} \in \mathbb{R}^{q\times 1}$, $\mathbf{H} \in \mathbb{R}^{q\times q}$).

EID approach requires an observer design and a LPF (Q_e) design independently. From Fig. 3.4, it can be seen that the EID structure contains the CFC structure too.

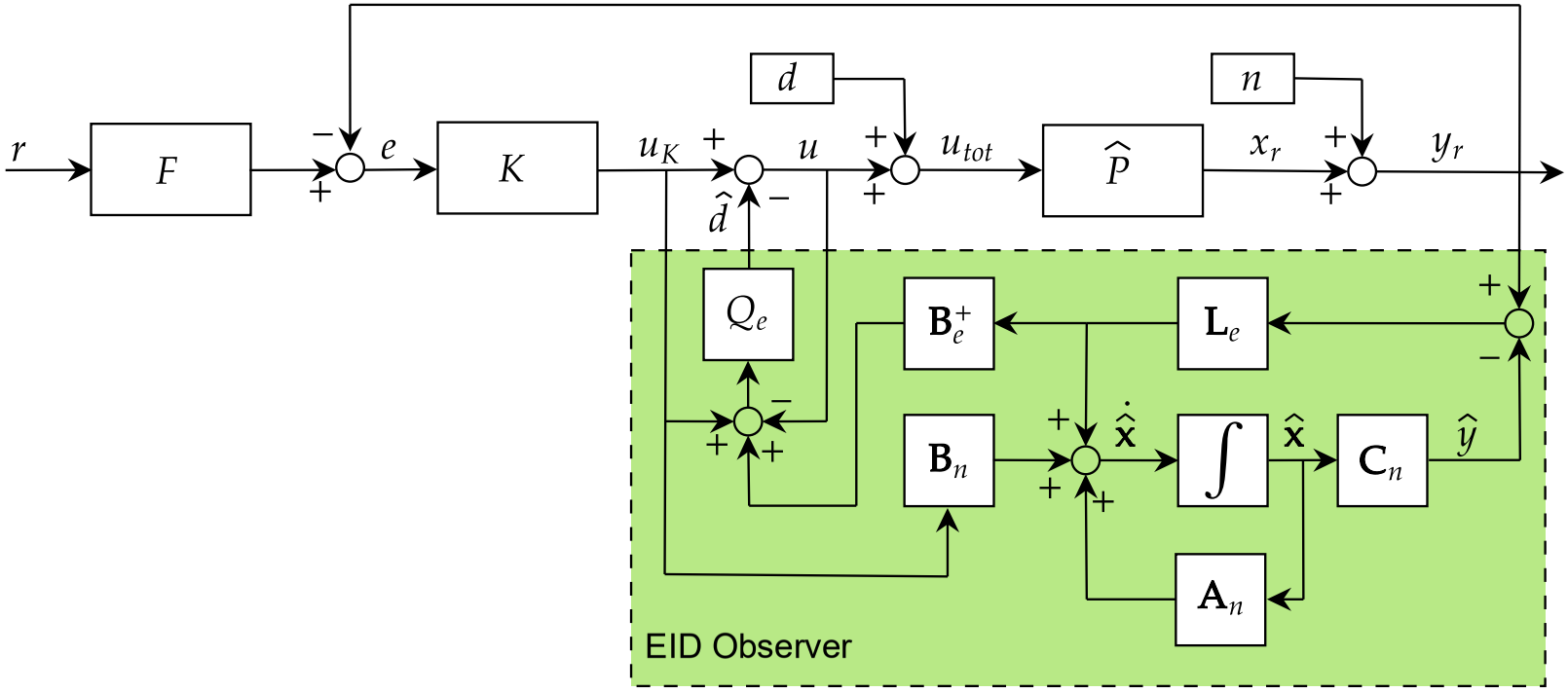

Figure 3.4 General block diagram of EID approach.

The nine relations for an EID system can be obtained as follows. From (2), (13), (26) and (27), we have

$$\begin{aligned} U = & \frac{CF}{1+\hat{P}C+k_1(P^{-1}\hat{P}-1)+k_2}R \\ & -\frac{\hat{P}(C+k_1P^{-1})}{1+\hat{P}C+k_1(P^{-1}\hat{P}-1)+k_2}D \\ & -\frac{C+k_3}{1+\hat{P}C+k_1(P^{-1}\hat{P}-1)+k_2}N \end{aligned} \tag{28}$$

From (3), (12) and (28), we have

$$\begin{aligned} X_r = & \frac{\hat{P}CF}{1+\hat{P}C+k_1(P^{-1}\hat{P}-1)+k_2}R \\ & +\frac{\hat{P}(1-k_1+k_2)}{1+\hat{P}C+k_1(P^{-1}\hat{P}-1)+k_2}D \\ & -\frac{\hat{P}(C+k_3)}{1+\hat{P}C+k_1(P^{-1}\hat{P}-1)+k_2}N \end{aligned} \tag{29}$$

From (4) and (29), we have

$$\begin{aligned} Y = & \frac{\hat{P}CF}{1+\hat{P}C+k_1(P^{-1}\hat{P}-1)+k_2}R \\ & +\frac{\hat{P}(1-k_1+k_2)}{1+\hat{P}C+k_1(P^{-1}\hat{P}-1)+k_2}D \\ & +\frac{1-k_1+k_2}{1+\hat{P}C+k_1(P^{-1}\hat{P}-1)+k_2}N \end{aligned} \tag{30}$$

3.5. Time Domain Disturbance Observer Based Control (TDDOBC) Approach

Fig. 3.5 illustrates the original form of TDDOBC structure [17]. Its equivalent block diagram can be obtained by replacing $\mathbf{A_p}, \mathbf{B_p}, \mathbf{C_p}, d$ variables with $\mathbf{A_n}, \mathbf{B_n}, \mathbf{C_n}, d_l$, respectively. While $\mathbf{A_n}, \mathbf{B_n}, \mathbf{C_n}$ are system matrix, control matrix and output matrix of nominal plant in CCF, respectively, $\mathbf{A_p}, \mathbf{B_p}, \mathbf{C_p}$ are system matrix, control matrix and output matrix of disturbed uncertain plant in CCF, respectively. In the figure, $\mathbf{L_a}$ stands for the observer gain, $\mathbf{x}, \mathbf{x_n}, x_s$ denote the plant state, its noiseless output and its noisy output, respectively. The variable z in the figure denotes an auxiliary variable.

The following equality can be written by using the noiseless plant output in Fig. 3.5 and TDDOBC equivalent block diagram, which is obtained after the above stated substitutions.

$$(U + D)\hat{P} = (U + D_l)P \tag{31}$$

As a consequence, the lumped disturbances are obtained as follows.

$$D_l = P^{-1}\hat{P}D + (P^{-1}\hat{P} - 1)U \tag{32}$$

From TDDOBC equivalent block diagram, we have

$$\hat{D} = z + \mathbf{L_a}\mathbf{x_n} \tag{33}$$

The block labeled W in Fig. 3.5 introduces the following dynamics.

$$\dot{z} = -\mathbf{L_a}\mathbf{B_n}(z + \mathbf{L_a}\mathbf{x_n}) - \mathbf{L_a}(\mathbf{A_n}\mathbf{x_n} + \mathbf{B_n}u) \tag{34}$$

From (76) and (77), we obtain

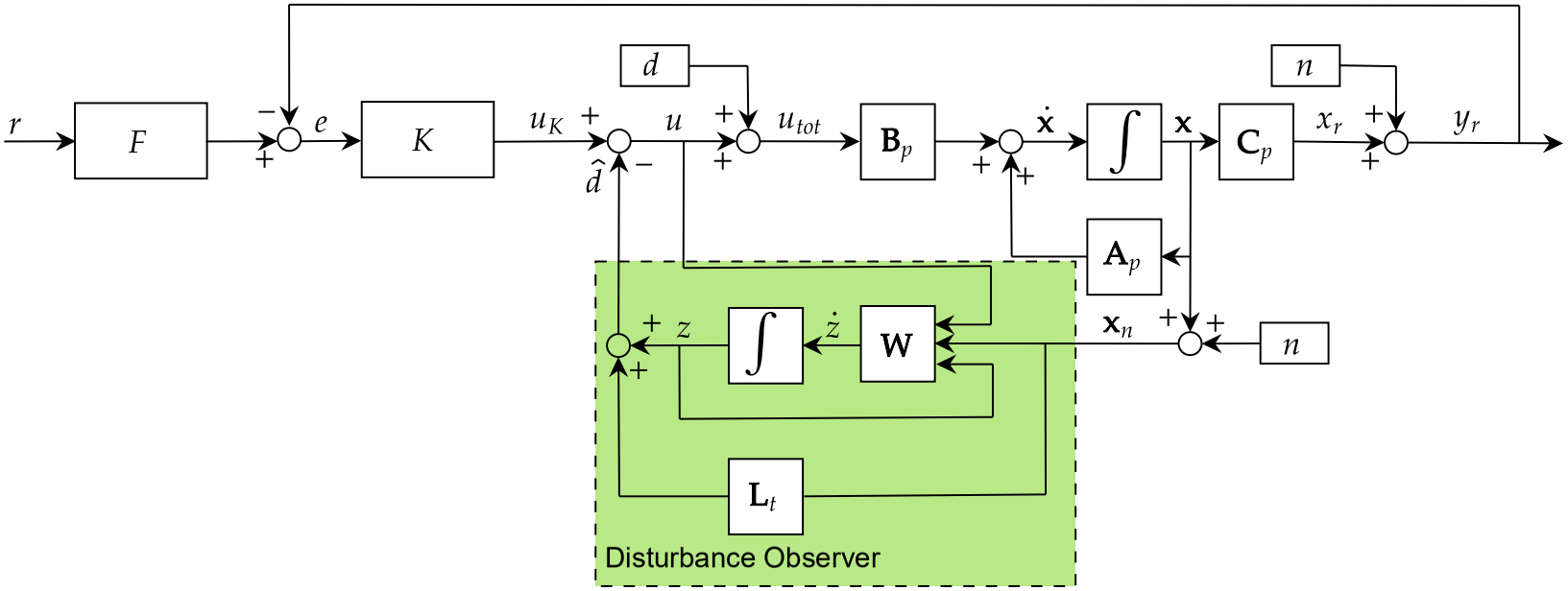

Figure 3.5 General block diagram of TDDOBC.

$$\hat{D} = (G_1 - G2)U + G_1 D_l + G_3 N \tag{35}$$

where, $\mathbf{a_t} = -(\mathbf{L_a B_n})\mathbf{L_a} - \mathbf{L_a A_n} + (s + \mathbf{L_a B_n})\mathbf{L_a}$, $\mathbf{b_t} = (s\mathbf{I} - \mathbf{A_n})^{-1}\mathbf{B_n}$, $G_1 = \frac{\mathbf{a_t b_t}}{s + \mathbf{L_a B_n}}$, $G_2 = \frac{\mathbf{L_a B_n}}{s + \mathbf{L_a B_n}}$, $G_3 = \frac{\mathbf{a_t m}}{s + \mathbf{L_a B_n}}$, $\mathbf{m} = [1, \ldots, 1]^T$, ($\mathbf{a_t} \in \mathbb{R}^{1\times q}$, $\mathbf{b_t} \in \mathbb{R}^{q\times 1}$, $\mathbf{L_a} \in \mathbb{R}^{1\times q}$, $\mathbf{x_n} \in \mathbb{R}^{q\times 1}$, $\mathbf{A_n} \in \mathbb{R}^{q\times q}$, $\mathbf{B_n} \in \mathbb{R}^{q\times 1}$, $\mathbf{m} \in \mathbb{R}^{q\times 1}$).

TDDOBC approach requires an observer design. From Fig. 3.5, it can be seen that the TDDOBC structure contains the CFC structure. Therefore, the first five equations in CFC section can be used with following corrections for the derivation of the nine TFs.

$$X_r = \hat{P} U_{tot} \tag{36}$$

$$Y_r = X_r + N \tag{37}$$

From (2), (13), (32) and (35), we have

$$\begin{aligned} U = & \frac{CF}{1 + \hat{P}C + G_1 P^{-1}\hat{P} - G_2} R \\ & - \frac{\hat{P}(C + G_1 P^{-1})}{1 + \hat{P}C + G_1 P^{-1}\hat{P} - G_2} D \\ & - \frac{C + G_3}{1 + \hat{P}C + G_1 P^{-1}\hat{P} - G_2} N \end{aligned} \tag{38}$$

From (12), (36) and (38), we have

$$
\begin{aligned}
X_r = & \frac{\hat{P}CF}{1+\hat{P}C+G_1P^{-1}\hat{P}-G_2}R \\
& +\frac{\hat{P}(1-G_2)}{1+\hat{P}C+G_1P^{-1}\hat{P}-G_2}D \\
& -\frac{\hat{P}(C+G_3)}{1+\hat{P}C+G_1P^{-1}\hat{P}-G_2}N
\end{aligned} \tag{39}
$$

From (37) and (39), we have

$$
\begin{aligned}
Y_r = & \frac{\hat{P}CF}{1+\hat{P}C+G_1P^{-1}\hat{P}-G_2}R \\
& +\frac{\hat{P}(1-G_2)}{1+\hat{P}C+G_1P^{-1}\hat{P}-G_2}D \\
& +\frac{1+\hat{P}(G_1P^{-1}-G_3)-G_2}{1+\hat{P}C+G_1P^{-1}\hat{P}-G_2}N
\end{aligned} \tag{40}
$$

3.6. Uncertainty Disturbance Estimator (UDE) Approach

Fig. 3.6 illustrates the original form of the UDE approach [20, 21]. UDE approach is based on a reference model, an error feedback gain and a LPF (G_f). Unlike other DOBC schemes, UDE structure does not contain the CFC structure. In Fig. 3.6, $\mathbf{A_m}, \mathbf{B_m}$ are system matrix and control matrix of the reference plant model, respectively, $\mathbf{A_p}, \mathbf{B_p}, \mathbf{C_p}$ are system matrix, control matrix and output matrix of disturbed uncertain plant in Observable Canonical Form (OCF), respectively. $\mathbf{A_n}$ is the system matrix of nominal plant in OCF. Besides, $\mathbf{K_m}$ is the feedback gain, $\mathbf{x_m}$ denote the reference model plant state, $\mathbf{x}, \mathbf{x_r}, \mathbf{x_n}$ denote the disturbed uncertain plant state, its noiseless output and its noisy output, respectively.

The following equations can be obtained from Fig. 3.6.

$$
\mathbf{X_m} = (s\mathbf{I} - \mathbf{A_m})^{-1}\mathbf{B_m}FR \tag{41}
$$

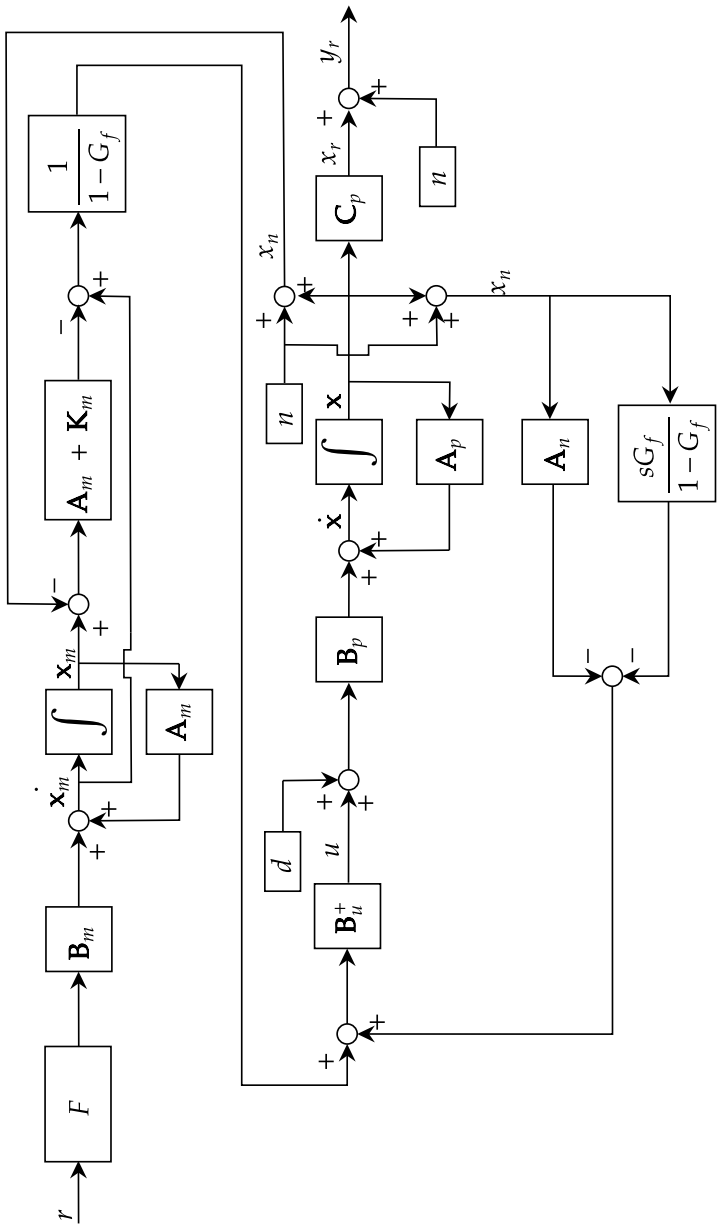

Figure 3.6 General block diagram of UDE approach.

Control signal U is as follows:

$$\begin{aligned} U = G_1(\mathbf{B_u^+}((s\mathbf{I})\mathbf{X_m})) \\ -G_1(\mathbf{B_u^+}(\mathbf{V_m}(\mathbf{X_m} - \mathbf{X_n}))) \\ -\mathbf{B_u^+}\mathbf{A_n}\mathbf{X_n} - G_2\mathbf{B_u^+}\mathbf{X_n} \end{aligned} \tag{42}$$

$$\mathbf{X_n} = \mathbf{X} + \mathbf{m}N \tag{43}$$

$$\mathbf{X} = (s\mathbf{I} - \mathbf{A_p})^{-1}\mathbf{B_p}(U + D) \tag{44}$$

$$X_r = \mathbf{C_p}\mathbf{X} \tag{45}$$

$$Y_r = X_r + N \tag{46}$$

where, $G_1 = \frac{1}{1-G_f}$, $G_2 = \frac{sG_f}{1-G_f}$, $\mathbf{V_m} = (\mathbf{A_m} + \mathbf{K_m})$, $\mathbf{B_u^+} = (\mathbf{B_n}^T\mathbf{B_n})^{-1}\mathbf{B_n}^T$, $\mathbf{m} = [1, \ldots, 1]^T$, ($\mathbf{X_m} \in \mathbb{R}^{q\times 1}$, $\mathbf{X_n} \in \mathbb{R}^{q\times 1}$, $\mathbf{X} \in \mathbb{R}^{q\times 1}$, $\mathbf{A}_* \in \mathbb{R}^{q\times q}$, $\mathbf{B}_* \in \mathbb{R}^{q\times 1}$, $\mathbf{C}_* \in \mathbb{R}^{1\times q}$, $\mathbf{V_m} \in \mathbb{R}^{q\times q}$, $\mathbf{K_m} \in \mathbb{R}^{q\times q}$, $\mathbf{B_u^+} \in \mathbb{R}^{1\times q}$, $\mathbf{m} \in \mathbb{R}^{q\times 1}$).

The nine relations for an UDE system can be obtained as follows. From (41), (42), (43) and (44), we have

$$\begin{aligned} U = \frac{a_u F}{1 - \mathbf{b_u}((s\mathbf{I} - \mathbf{A_p})^{-1}\mathbf{B_p})}R \\ -\frac{-\mathbf{b_u}((s\mathbf{I} - \mathbf{A_p})^{-1}\mathbf{B_p})}{1 - \mathbf{b_u}((s\mathbf{I} - \mathbf{A_p})^{-1}\mathbf{B_p})}D \\ -\frac{-\mathbf{b_u}\mathbf{m}}{1 - \mathbf{b_u}((s\mathbf{I} - \mathbf{A_p})^{-1}\mathbf{B_p})}N \end{aligned} \tag{47}$$

where, $a_u = G_1(\mathbf{B_u^+}((s\mathbf{I}-\mathbf{V_m})((s\mathbf{I}-\mathbf{A_m})^{-1}\mathbf{B_m})))$ and $\mathbf{b_u} = G_1(\mathbf{B_u^+V_m})-\mathbf{B_u^+A_n}-G_2\mathbf{B_u^+}$, ($\mathbf{b_u} \in \mathbb{R}^{1\times q}$). From (44), (45) and (47), we have

$$\begin{aligned} X_r = &\frac{\mathbf{C_p}(((s\mathbf{I}-\mathbf{A_p})^{-1}\mathbf{B_p})a_uF)}{1-\mathbf{b_u}((s\mathbf{I}-\mathbf{A_p})^{-1}\mathbf{B_p})}R \\ &+\frac{\mathbf{C_p}((s\mathbf{I}-\mathbf{A_p})^{-1}\mathbf{B_p}))}{1-\mathbf{b_u}((s\mathbf{I}-\mathbf{A_p})^{-1}\mathbf{B_p})}D \\ -&\frac{-\mathbf{C_p}(((s\mathbf{I}-\mathbf{A_p})^{-1}\mathbf{B_p})(\mathbf{b_um}))}{1-\mathbf{b_u}((s\mathbf{I}-\mathbf{A_p})^{-1}\mathbf{B_p})}N \end{aligned} \tag{48}$$

From (46) and (48), we have

$$\begin{aligned} Y_r = &\frac{\mathbf{C_p}(((s\mathbf{I}-\mathbf{A_p})^{-1}\mathbf{B_p})a_uF)}{1-\mathbf{b_u}((s\mathbf{I}-\mathbf{A_p})^{-1}\mathbf{B_p})}R \\ &+\frac{\mathbf{C_p}((s\mathbf{I}-\mathbf{A_p})^{-1}\mathbf{B_p}))}{1-\mathbf{b_u}((s\mathbf{I}-\mathbf{A_p})^{-1}\mathbf{B_p})}D \\ &+\frac{Z+1-\mathbf{b_u}((s\mathbf{I}-\mathbf{A_p})^{-1}\mathbf{B_p})}{1-\mathbf{b_u}((s\mathbf{I}-\mathbf{A_p})^{-1}\mathbf{B_p})}N \end{aligned} \tag{49}$$

where, $Z = \mathbf{C_p}(((s\mathbf{I}-\mathbf{A_p})^{-1}\mathbf{B_p})(\mathbf{b_um}))$.

3.7. Robustness and Performance Analysis

This section presents a robustness and performance analysis approach using GoF equations for five DOBC schemes. DOBC structures generally require a LPF design as described in the previous sections. LPF characteristics are important as they directly affect the disturbance rejection performance of DOBC approaches. If the LPF bandwidth is chosen too high, the robustness and stability of the system are adversely affected [10]. Therefore, the choice of LPF order and its bandwidth is critical. In this study, the following first order LPF is selected for all DOBC approaches to be able to compare all DOBC approaches under the same conditions. The bandwidth of the LPF is chosen wide enough for all simulation studies.

One could choose higher order LPF structures but this would increase the computational burden of the design.

$$LPF(s) = \frac{T}{s+T} \tag{50}$$

where, T is the cutoff frequency of the LPF.

3.7.1. The Gang of Four (GoF) Equations

In the previous subsections, nine TFs of the five DOBC approaches are derived. These nine TFs provide useful insights for understanding and analyzing control systems employing disturbance observer sub-dynamics. They can be reduced to six equations because some of them are the same under certain rules (e.g., $F = 1$). In this section, the only GoF equations are considered as performance and robustness equations, and they are shown in Table 3.1 as a relationship transfer functions described in the previous subsections.

Table 3.1 GoF equations(* Irrelevant inputs are taken as zero).

Strategy	CSF*	SF*	DSF*	NSF*
CFC	U/D or X_r/N	Y_r/N	X_r/D	U/N
CDOBC	U/D or X_r/N	Y_r/N	X_r/D	U/N
OEBDOBC	U/D or X_r/N	Y_r/N	X_r/D	U/N
EID	U/D or X_r/N	Y_r/N	X_r/D	U/N
TDDOBC	U/D or X_r/N	$(1-U/D)$ or $(1-X_r/N)$	X_r/D	U/N
UDE	U/D or X_r/N	$(1-U/D)$ or $(1-X_r/N)$	X_r/D	U/N

3.7.2. Simulation Parameters

It should be noted that as this study gives a comprehensive comparison of disturbance observer based robust control approaches, structural details and complexity of each approach, instead of a particular plant model with its own challenges, a second order plant model with some uncertainty in the form of time delay is considered. Although the studied plant model

is an abstract one, this makes it possible to compare the most critical aspects aside from the plant specific difficulties.

3.7.3. Minimum-Phase Uncertain Plant

Nominal plant and the uncertain plant considered in this part are as follows [11],

$$P(s) = \frac{s+5}{s^2+5s+6}, \hat{P}(s) = P(s)(1+\Delta W_T(s)) \tag{51}$$

where, $\Delta = 0.3$ and uncertainty weighting function is $W_T(s) = (5s+100)/(s+500)$.

3.7.4. Minimum-Phase Uncertain Plant with Time-Delay

Nominal plant and uncertain plant with time delay for this part are considered as follows [11],

$$\hat{P}(s) = P(s)(1+\Delta W_T(s))e^{-\tau s} \tag{52}$$

where, $\Delta = 0.3$, $W_T(s) = (5s+100)/(s+500)$ and the time delay $\tau = 0.01$ sec.

3.7.5. CFC Parameters

It is well known that cancellation of slow or unstable poles by zeros adversely affects the disturbance rejection performance of a controller. Therefore, classical feedback controller (53) is designed using pole placement method with the specifications given in Table 3.2. At the same time, for UDE approach, reference model meeting the criteria in Table 3.2 is selected as given in (54).

Table 3.2 Controller design performance criteria.

Rising Time	Settling Time	Max. Overshoot
< 0.3 sec.	< 0.8 sec.	$< \%5$

$$C(s) = \frac{6.75(s + 12.25s + 18)}{s + 12.25s} \tag{53}$$

$$\mathbf{A_m} = \begin{bmatrix} -5 & -6.25 \\ 1 & 0 \end{bmatrix}, \mathbf{B_m} = \begin{bmatrix} 6.25 \\ 0 \end{bmatrix}, \mathbf{C_m} = \begin{bmatrix} 0 & 1 \end{bmatrix} \tag{54}$$

3.7.6. CDOBC Parameters

$Q(s)$ filter is selected as follows.

$$Q(s) = \frac{100}{s + 100} \tag{55}$$

3.7.7. OEBDOBC Parameters

Together with the Q in (55), $K_{obs}(s)$ is selected as follows.

$$K_{obs}(s) = \frac{Q(s)}{G_n(s)(1 - Q(s))} \tag{56}$$

3.7.8. EID Parameters

$Q_e(s)$ filter is selected as follows.

$$Q_e(s) = \frac{100}{s + 100} \tag{57}$$

$\mathbf{L_e}$ is designed by using Ackermann formula as follows.

$$\mathbf{L_e} = \begin{bmatrix} 20 \\ 1 \end{bmatrix} \tag{58}$$

3.7.9. TDDOBC Parameters

$\mathbf{L_a}$ is designed by using Ackermann formula as follows.

$$\mathbf{L_a} = \begin{bmatrix} 112.66 \\ -17.33 \end{bmatrix} \tag{59}$$

3.7.10. UDE Parameters

$G_f(s)$ filter is selected as follows.

$$G_f(s) = \frac{100}{s + 100} \tag{60}$$

3.8. Performance and Robustness Discussion

Order of the LPF and its bandwidth directly affect the disturbance rejection capability of a DOBC scheme. For all DOBC approaches presented in this paper, a first order LPF for relevant approaches is used, and bandwidths of them are set to 100 rad/sec. While Figs. 3.7-3.10 show the response of GoF for uncertain minimum phase plant without time delay, Figs. 3.11-3.14 illustrate the results for uncertain minimum phase plant containing time delay.

In Fig. 3.7, we illustrate the step responses of the Disturbance Sensitivity Function given in (51). Because of our identical LPF selections and the choice in (56), spectral views of the GoF TFs are identical for CDOBC and OEBDOBC. Clearly CFC in this figure displays

the poorest performance. According to the figure, all schemes produce acceptable results. Their disturbance suppression capability ranking from best to worst is as follows: TDDOBC, CDOBC-OEBDOBC, UDE, EID and CFC. In this sorting, we consider the peak magnitude and the convergence speed as the major metrics.

Fig. 3.8 depicts the Noise Sensitivity Function behaviors. Looking at the results, we see some approaches produce higher sensitivity at low frequencies and some in high frequencies. Assuming the disturbances are low frequency inputs and the chosen Q filters have a bandwidth of 100 rad/sec, the poorest performance in this picture is obtained with UDE approach because of the ≈ 15 dB gain in the low frequency region. Other approaches have a small sensitivity in the low frequencies, yet the sensitivity curves increase as the frequency increases. Interestingly, EID approach displays a peak around 50 rad/sec and the curve falls as the frequency approaches 100 rad/sec and the insensitivity to noise is recovered for high frequencies. In terms of noise input, we desire smaller magnitudes in high frequencies, and this is obtained best with CFC approach. The level of insensitivity to noise from highest to lowest: CFC, EID, TDDOBC, CDOBC-OEBDOBC and UDE.

In Fig. 3.9, we show the frequency responses of the Complementary Sensitivity Functions for each approach. In this figure, we see that EID approach is poorer than the other DOBC schemes, which maintain the 0 dB level over a fairly large bandwidth without displaying any resonant peaks. EID approach is more vulnerable to waterbed effect, which shows itself as a peak provoked in between 6.77 rad/sec and 59 rad/sec., than its alternatives. We sort the approaches according to the bandwidth, and from the largest to the smallest bandwidth are TDDOBC, CDOBC-OEBDOBC, UDE, EID and CFC. CSF figure recommends the TDDOBC as it displays the highest bandwidth.

Fig. 3.10 presents the frequency responses of the Sensitivity Functions. In the figure, all DOBC schemes fairly suppress the components below 6.77 rad/sec. The suppression capability in the low frequency region is sorted from the strongest to the weakest is TDDOBC, CDOBC-OEBDOBC, UDE, EID and CFC. EID approach has a weaker disturbance attenuation performance for the components between 6.77 rad/sec and 34 rad/sec

than the other schemes. Additionally, EID approach amplifies the components between 34 rad/sec and 150 rad/sec, which is a negative observation. For high frequencies, all approaches feature high pass filters. In producing these results, the weighting performance function of SF is selected as $W_S(s) = (0.707s + 30)/(s + 2)$.

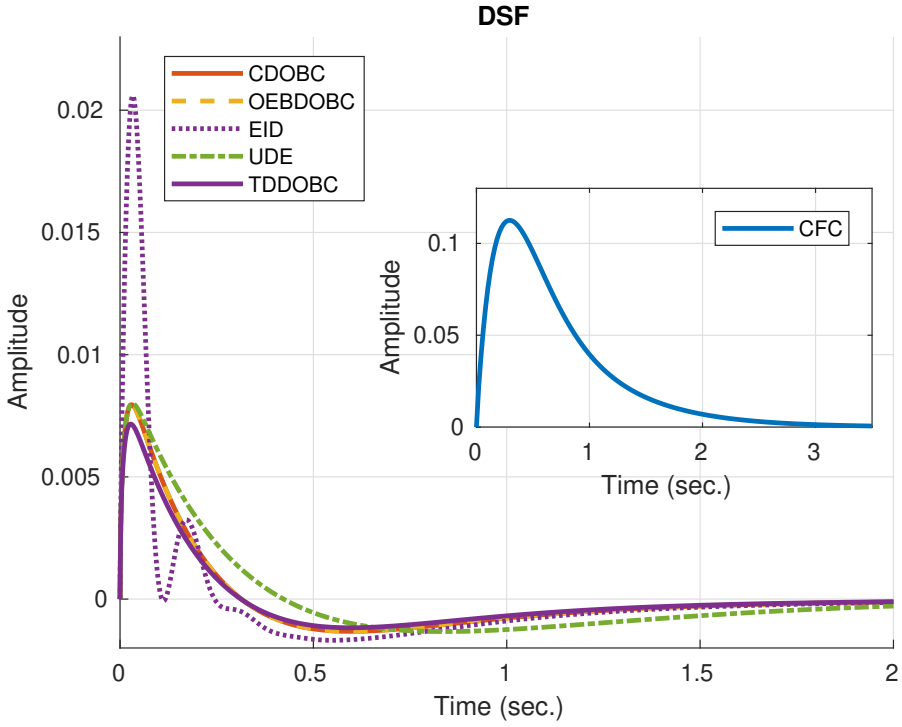

Figure 3.7 Step response of the Disturbance Sensitivity Function without time delay.

In the next GoF plots, we will consider the time delay effect in the overall performance. Fig. 3.11 illustrates the step responses of the Disturbance Sensitivity Function given in (52). The worst disturbance rejection performance among the studied approaches is CFC approach, which is shown separately in the window plot. As can be seen from Fig. 3.11, disturbance rejection performances can be sorted from the best to worst as CDOBC-OEBDOBC, UDE, TDDOBC, EID and CFC. Time delay increases the oscillations in the step responses for almost all DOBC schemes. However, the figure shows that it severely affects EID and TDDOBC approaches, the responses of which display an oscillatory initial transient.

Fig. 3.12 shows frequency responses of the Noise Sensitivity Function under time delay conditions. We see that the time delay increases the sensitivity to noise for all DOBC

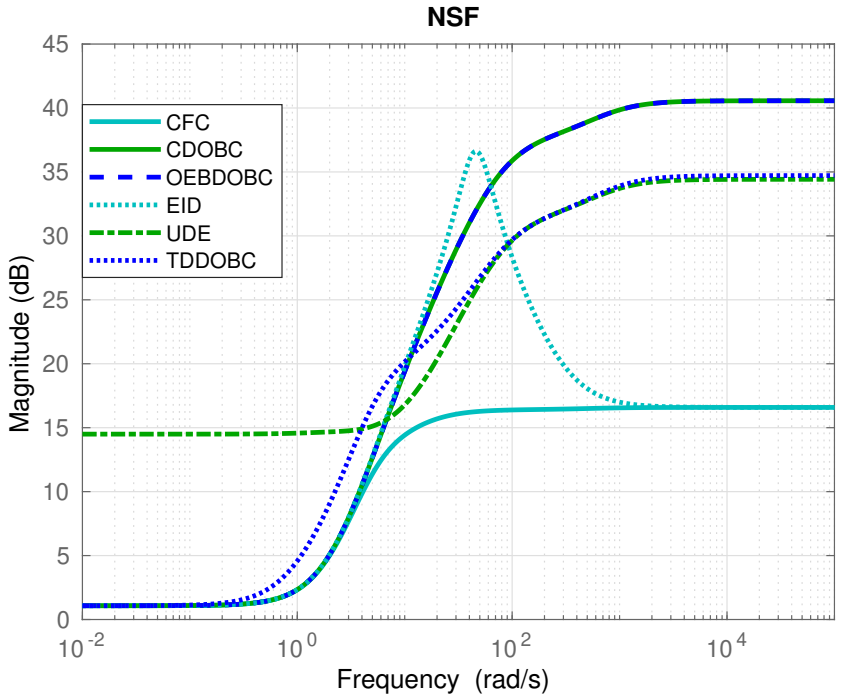

Figure 3.8 Frequency response of the Noise Sensitivity Function without time delay.

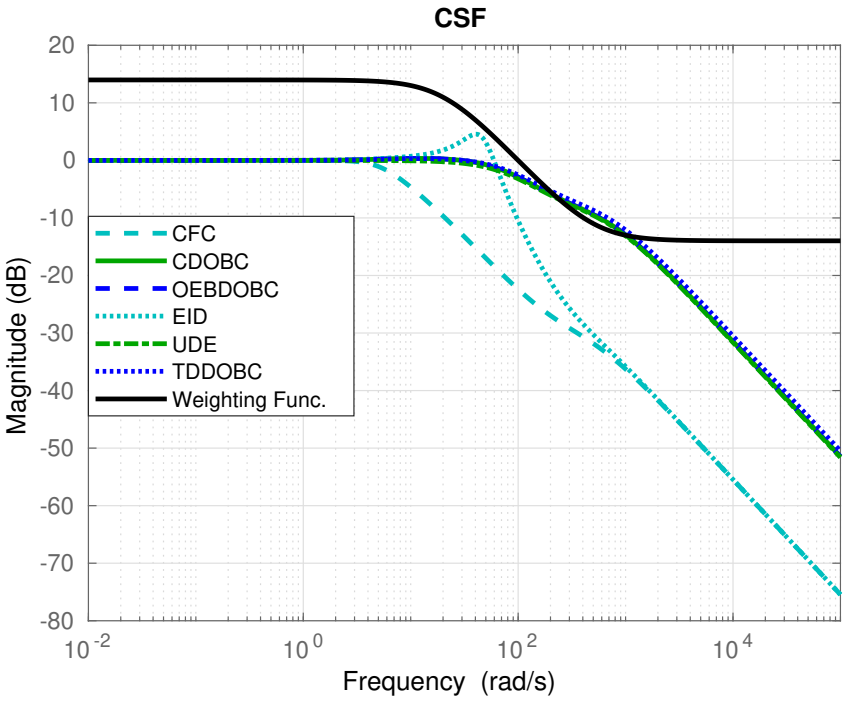

Figure 3.9 Frequency response of the Complementary Sensitivity Function without time delay.

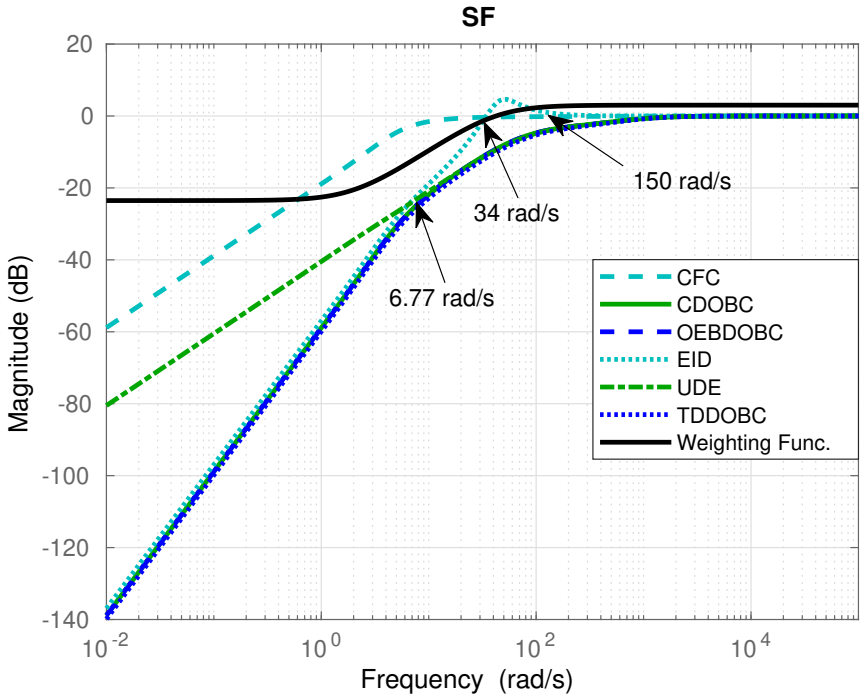

Figure 3.10 Frequency response of the Sensitivity Function frequency response without time delay.

approaches in high frequencies except CFC approach. The noise sensitivity responses from the strongest to weakest can be sorted as CFC (most insensitive to noise), EID, TDDOBC, CDOBC-OEBDOBC and UDE (most sensitive to noise).

In Fig. 3.13, we present the Complementary Sensitivity Function behaviors under time delay conditions. Time delay makes the EID approach more vulnerable to waterbed effect than other approaches. This is visible from the peak observed between 5 rad/sec and 67 rad/sec. Yet, EID recovers for high frequencies with a poor bandwidth. In this figure, CFC displays the poorest performance then comes the EID approach. This is mainly because of the bandwidth comparison with the other approaches, which display a resonant peak around 190 rad/sec and the ordering is done by considering the magnitude at this frequency. This leads to the following sorting UDE, CDOBC-OEBDOBC, TDDOBC, EID and CFC.

Fig. 3.14 depicts frequency responses of the Sensitivity Function under time delay conditions. When Fig. 3.14 are examined, it can be seen that the time delay increases the amplification magnitude of EID approach between 31 rad/sec and 150 rad/sec. The

other approaches try to preserve the high pass filter properties with some oscillations after 100 rad/sec. As discussed for Fig. 3.10, the attenuation capability order for the low frequency components from strongest to weakest is TDDOBC, CDOBC-OEBDOBC, UDE, EID and CFC. EID approach has a better suppression performance than UDE approach below 6.77 rad/sec. Considering the resonant peak magnitude around 190 rad/sec UDE approach produces the smallest peak magnitude, which is a good property.

As discussed above, OEBDOBC approach produces identical results with CDOBC approach since K_{obs} is chosen as in (56). Although they have the same performance, OEBDOBC proposed in [54] does not require the inverse of nominal plant model and it is advisable also for non-minimum phase systems when compared to CDOBC structure.

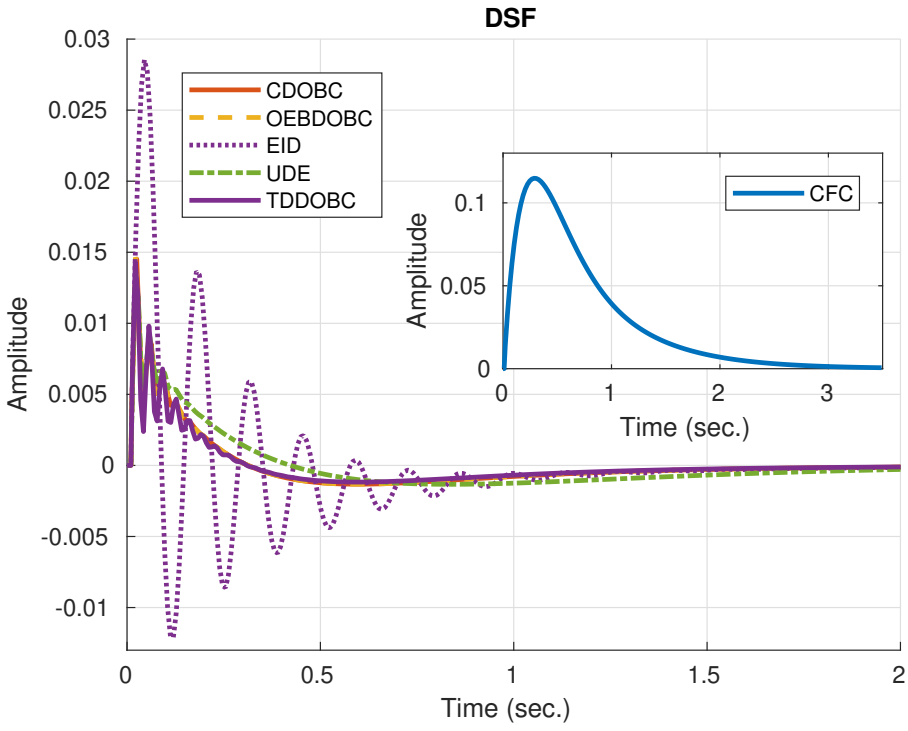

Figure 3.11 Step response of the Disturbance Sensitivity Function with time delay.

Table 3.3 gives a summary of fundamental properties of the approaches, namely, the necessity to an inverse nominal model, vulnerability to waterbed effect, insensitivity to noise and time delays and the structural representation are listed for each approach.

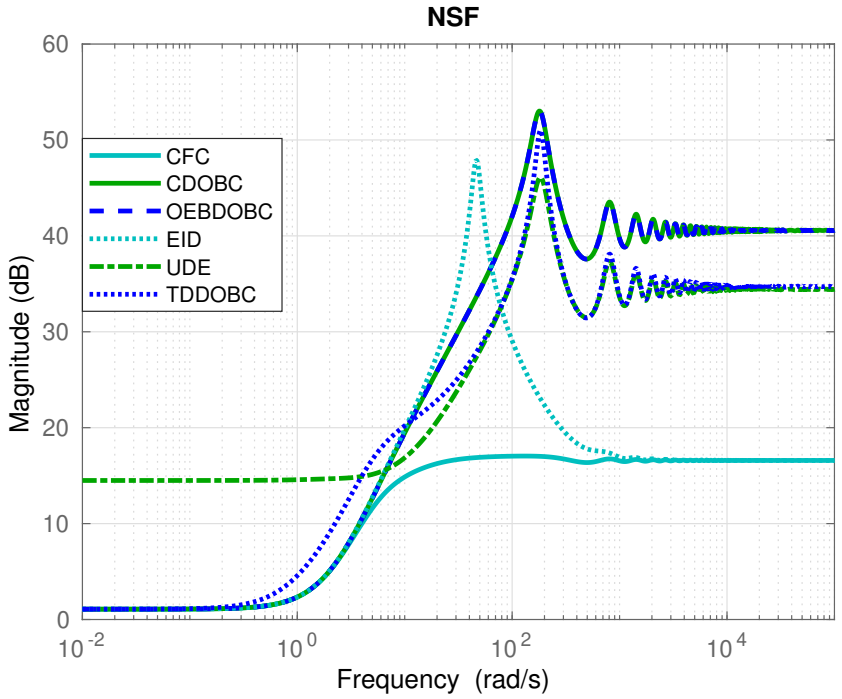

Figure 3.12 Frequency response of the Noise Sensitivity Function with time delay.

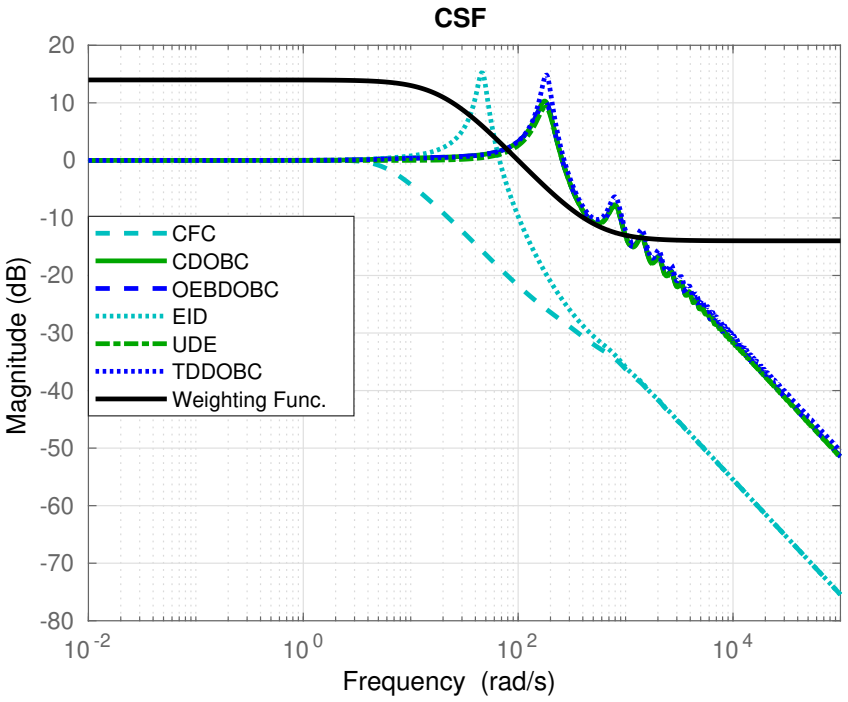

Figure 3.13 Frequency response of the Complementary Sensitivity Function with time delay.

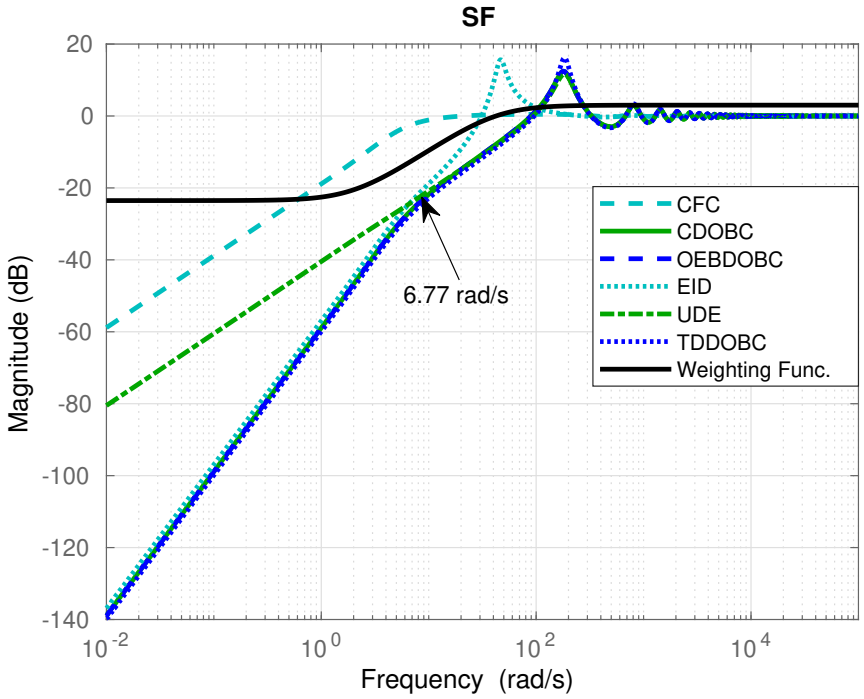

Figure 3.14 Frequency response of the Sensitivity Function with time delay.

Table 3.3 Fundamental properties of the approaches.

	CDOBC	OEBDOBC	EID	TDDOBC	UDE
Inverse Required	Yes	No	No	No	No
Waterbed Effect Vulnerability	No	No	Yes	No	No
Insensitivity to Measurement Noise	Poor	Poor	Good	Poor	Very Poor
Insensitivity to Time Delay	Good	Good	Very Poor	Poor	Very Good
Structure	TF	TF	TF-CCF	CCF	OCF

Table 3.4 lists the rankings given above for the practicing engineers, who may give more importance to one quality than the others. In the table, column 1 represents the well performing approach(es) whereas the column 5 gives the poor performing one(s). According to the table, if there is no time delay in the process model, TDDOBC is a satisfactorily successful approach with average performance in NSF measure. Under time delay conditions, TDDOBC provides average performance, yet, we see that the CDOBC-OEBDOBC approaches perform well in general. The table does not recommend a

particular approach persistently, and the contribution of this work is to unfold the approaches, which perform well and poor for which of the measures named DSF, NSF, CSF and SF.

Table 3.4 DOBC performance rankings for the measures DSF, NSF, CSF and SF (* denotes time delay).

	1	2	3	4	5
DSF	TDDOBC	CDOBC-OEBDOBC	UDE	EID	CFC
NSF	CFC	EID	TDDOBC	CDOBC-OEBDOBC	UDE
CSF	TDDOBC	CDOBC-OEBDOBC	UDE	EID	CFC
SF	TDDOBC	CDOBC-OEBDOBC	UDE	EID	CFC
DSF*	CDOBC-OEBDOBC	UDE	TDDOBC	EID	CFC
NSF*	CFC	EID	TDDOBC	CDOBC-OEBDOBC	UDE
CSF*	UDE	CDOBC-OEBDOBC	TDDOBC	EID	CFC
SF*	TDDOBC	CDOBC-OEBDOBC	UDE	EID	CFC

4. DISTURBANCE OBSERVER BASED CONTROL ARCHITECTURES FOR QUADROTORS

Uncertainty and unavoidable external disturbances such as wind, unmodeled dynamics, neglected aerodynamic effects, variable weight suspended payloads, measurement and input noise make controller design even more difficult. While wind and variable weight suspended payloads are the environmental factors, unmodeled dynamics and measurement noise are caused by the modelling errors and available sensors, respectively. Some of these unknown factors are the matched external disturbances as they effect the control input signal for the rotational motion of the quadrotor. For better understanding, while the effect of wind on rotational movement of a quadrotor is considered as matched disturbance, the effect of wind on translational movement of a quadrotor is considered as unmatched disturbance. The rejection of unmatched disturbances is the out of scope for this thesis study. Disturbance resistant control systems generally reject the disturbances up to a certain limit. Therefore, bounded matched external disturbances will be considered.

Morover, a nonlinear controller that is designed by taking into account nonlinear quadrotor dynamics namely BSC is used in all simulation studies. Whether a linear or nonlinear controller is preferred, it has been confirmed by simulation studies that when the DOBC structures presented here are integrated into the general quadrotor control system, the system becomes more robust.

4.1. Mathematical Model of a Quadrotor

This section presents the mathematical equations required for a quadrotor unmanned aerial vehicle control. We select the quadrotor model as in Fig. 4.1.

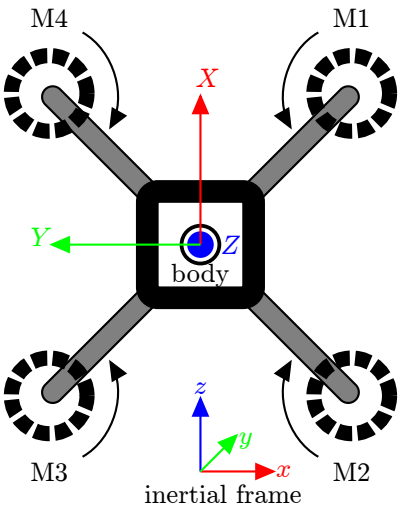

Figure 4.1 The quadrotor model in cross configuration (ENU frame)

$$\begin{bmatrix} m\ddot{x} \\ m\ddot{y} \\ m\ddot{z} \end{bmatrix} = \begin{bmatrix} (c_\psi s_\theta c_\phi + s_\psi s_\phi)U_z + d_x \\ (s_\psi s_\theta c_\phi - c_\psi s_\phi)U_z + d_y \\ (c_\theta c_\phi)U_z - mg + d_z \end{bmatrix} \tag{61}$$

$$\begin{bmatrix} I_x\dot{p} \\ I_y\dot{q} \\ I_z\dot{r} \end{bmatrix} = \begin{bmatrix} (U_\phi + (I_y - I_z)qr - Jq\Omega_S) + d_\phi \\ (U_\theta + (I_z - I_x)pr + Jp\Omega_S) + d_\theta \\ (U_\psi + (I_x - I_y)pq) + d_\psi \end{bmatrix} \tag{62}$$

Eq. (61) and (62) are the translational and rotational dynamics of a quadrotor, respectively. Where, $c : cos$ and $s : sin$, x, y, z are the relative position of a quadrotor in the inertial frame, ϕ, θ, ψ are the Euler angles, p, q, r are the body angular rates, m is the quadrotor mass, I is the quadrotor body diagonal inertia matrix, g is the gravity acceleration, U_z is the total lift control force input, U_ϕ, U_θ, U_ψ are the torque control inputs, J is the propeller moment inertia value, d_x, d_y are the bounded unknown mismatched external disturbances, $d_z, d_\phi, d_\theta, d_\psi$ are the bounded unknown matched external disturbances, and finally Ω_S is $\Omega_2 + \Omega_4 - \Omega_1 - \Omega_3$. Ω_i is the i^{th} motor speed. Eq. (63) shows the conversion from the body angular rates to the Euler angle rates.

$$\begin{bmatrix} \dot{\phi} \\ \dot{\theta} \\ \dot{\psi} \end{bmatrix} = \begin{bmatrix} 1 & s_\phi t_\theta & c_\phi t_\theta \\ 0 & c_\phi & -s_\phi \\ 0 & \frac{s_\phi}{c_\theta} & \frac{c_\phi}{c_\theta} \end{bmatrix} \begin{bmatrix} p \\ q \\ r \end{bmatrix} \tag{63}$$

Eq. (64) shows the rotation matrix from body to inertial frame.

$$\mathbf{R} = \begin{bmatrix} c_\psi c_\theta & c_\psi s_\theta s_\phi - s_\psi c_\phi & c_\psi s_\theta c_\phi + s_\psi s_\phi \\ s_\psi c_\theta & s_\psi s_\theta s_\phi + c_\psi c_\phi & s_\psi s_\theta c_\phi - c_\psi s_\phi \\ -s_\theta & c_\theta s_\phi & c_\theta c_\phi \end{bmatrix} \tag{64}$$

We can write the following control input equations by using the quadrotor model in Fig. 4.1.

$$\mathbf{U} = \begin{bmatrix} U_z \\ U_\phi \\ U_\theta \\ U_\psi \end{bmatrix} = \begin{bmatrix} 1 & 1 & 1 & 1 \\ -\frac{l}{\sqrt{2}} & -\frac{l}{\sqrt{2}} & \frac{l}{\sqrt{2}} & \frac{l}{\sqrt{2}} \\ -\frac{l}{\sqrt{2}} & \frac{l}{\sqrt{2}} & \frac{l}{\sqrt{2}} & -\frac{l}{\sqrt{2}} \\ -\kappa & \kappa & -\kappa & \kappa \end{bmatrix} \begin{bmatrix} f_1 \\ f_2 \\ f_3 \\ f_4 \end{bmatrix} \tag{65}$$

$$\begin{bmatrix} \Omega_1^2 \\ \Omega_2^2 \\ \Omega_3^2 \\ \Omega_4^2 \end{bmatrix} = \begin{bmatrix} \frac{1}{4K_F} & -\frac{\sqrt{2}}{4K_F l} & -\frac{\sqrt{2}}{4K_F l} & -\frac{1}{4\kappa K_F} \\ \frac{1}{4K_F} & -\frac{\sqrt{2}}{4K_F l} & \frac{\sqrt{2}}{4K_F l} & \frac{1}{4\kappa K_F} \\ \frac{1}{4K_F} & \frac{\sqrt{2}}{4K_F l} & \frac{\sqrt{2}}{4K_F l} & -\frac{1}{4\kappa K_F} \\ \frac{1}{4K_F} & \frac{\sqrt{2}}{4K_F l} & -\frac{\sqrt{2}}{4K_F l} & \frac{1}{4\kappa K_F} \end{bmatrix} \begin{bmatrix} U_1 \\ U_2 \\ U_3 \\ U_4 \end{bmatrix} \tag{66}$$

where, $\mathbf{U}$ is the control signal, $\mathbf{\Omega} = [\Omega_1\ \Omega_2\ \Omega_3\ \Omega_4]^T$ is the actual rotor speed in rad/sec, f_i is the thrust value generated by each rotor, l is the arm length of the quadrotor, and κ is the conversion factor between the thrust and the torque values. $\tau_i = \kappa f_i$. τ_i is the torque value generated by each rotor. $f_i = K_F \Omega_i^2$. K_F is the positive motor thrust factor. We use the below first-order transfer function as a rotor dynamics model.

$$\frac{\Omega_i(s)}{\Omega_{di}(s)} = \frac{1}{T_{rot}s + 1} \tag{67}$$

where, T_{rot} is time constant of the rotor dynamics and $\mathbf{\Omega_d} = [\Omega_{d1}\ \Omega_{d2}\ \Omega_{d3}\ \Omega_{d4}]^T$ is the desired rotor speed in rad/sec.

4.2. Robust Control Schemes for the Quadrotors

In this section, we present in detail five disturbance observer based control schemes for the quadrotors, three in frequency domain and two in time domain. Let $\mathbf{r_d} = [z_d\ \phi_d\ \theta_d\ \psi_d]^T$ denote the reference signals for altitude and attitude behaviors. Let $\mathbf{y_r} = [z\ \phi\ \theta\ \psi]^T$ denote the actual altitude and attitude states. $\mathbf{d}$, $\mathbf{n}$ and $\hat{\mathbf{d}}$ are the external disturbance input, measurement noise input and estimation of the lumped disturbances, respectively. Reference signal tracking error $\mathbf{e}$ is as follows.

$$\mathbf{e} = \mathbf{r_d} - \mathbf{y_r} \tag{68}$$

In the given DOBC block diagrams in the next subsections, 'Att&Altitude Controller' block is the baseline controller. 'Quadrotor Dynamics' block is the nonlinear equations of the quadrotor and contains Eq. (61), (62), (63) and (64). While 'Force&Torques to Speed' block is the square root of Eq. (66), 'Speed to Force&Torques' block includes Eq. (65). Finally, 'Actuator Dynamics' block includes Eq. (67) for each rotor. Altitude variables for DOE parts of the approaches presented in this paper are taken zero as we take into account the external disturbances in attitude behavior of the quadrotor.

4.2.1. Conventional Disturbance Observer Based Control (CDOBC) Scheme

Fig. 4.2 shows the overall attitude and altitude control scheme using CDOBC approach for the quadrotors. As shown in Fig. 4.2, Disturbance Observer structure consists of a combination of the inverse of nominal plant and $\mathbf{Q(s)}$ low pass filter. LPF design directly effects the disturbance rejection capability of the overall system. To achieve a good disturbance rejection performance in the attitude control of the quadrotors, we recommend designing $\mathbf{Q(s)}$ LPF by following the steps below instead of first-order LPF.

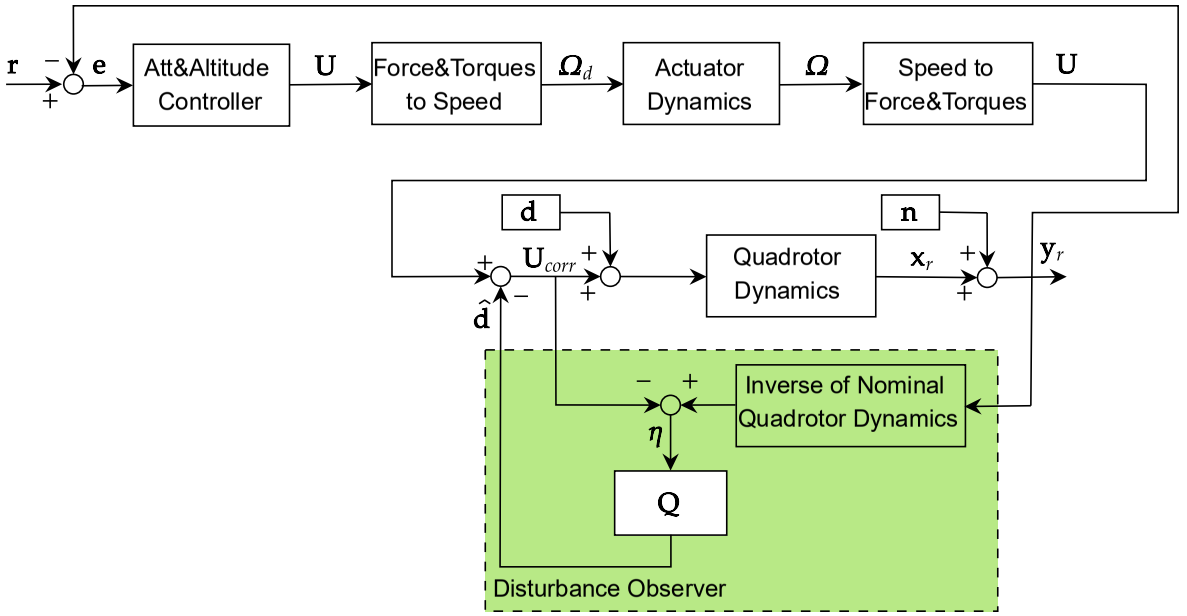

Figure 4.2 CDOBC scheme for the quadrotors

1. Develop a simple and fast Proportional-Derivative (PD) controller under the unit step reference input function for the nominal plant of the quadrotor.

2. Take overall closed loop system as $\mathbf{Q(s)}$ LPF.

To find the inverse of nominal plant and design a $\mathbf{Q(s)}$ LPF, we obtain the following nominal plant of the quadrotor after the linearization process of nonlinear quadrotor dynamics.

$$\begin{bmatrix} \ddot{z} & \ddot{\phi} & \ddot{\theta} & \ddot{\psi} \end{bmatrix}^T = \begin{bmatrix} 0 & \frac{1}{I_x s^2} & \frac{1}{I_y s^2} & \frac{1}{I_z s^2} \end{bmatrix}^T \tag{69}$$

As a consequence, 'Inverse of Nominal Quadrotor Dynamics' block generates the following output.

$$\varepsilon = diag(0, I_x s^2, I_y s^2, I_z s^2)\mathbf{y_r} \tag{70}$$

'$\mathbf{Q(s)}$' block is found as follows from the above LPF design steps.

$$\begin{aligned} \mathbf{Q(s)} = diag(0, & \frac{\frac{K_d}{I_x}s + \frac{K_p}{I_x}}{s^2 + \frac{K_d}{I_x}s + \frac{K_p}{I_x}}, \\ & \frac{\frac{K_d}{I_y}s + \frac{K_p}{I_y}}{s^2 + \frac{K_d}{I_y}s + \frac{K_p}{I_y}}, \frac{\frac{K_d}{I_z}s + \frac{K_p}{I_z}}{s^2 + \frac{K_d}{I_z}s + \frac{K_p}{I_z}}) \end{aligned} \tag{71}$$

where, K_p and K_d are the PD controller parameters for LPF design.

4.2.2. Output Error Based Disturbance Observer Based Control (OEBDOBC) Scheme

Fig. 4.3 shows the overall control structure based the output error based disturbance observer estimator presented in the study of [1]. Their D/UE structure is adapted for the quadrotors. In D/UE structure, 'Quadrotor Dynamics' block includes (69). '$\mathbf{K_{obs}}$' block has a simple

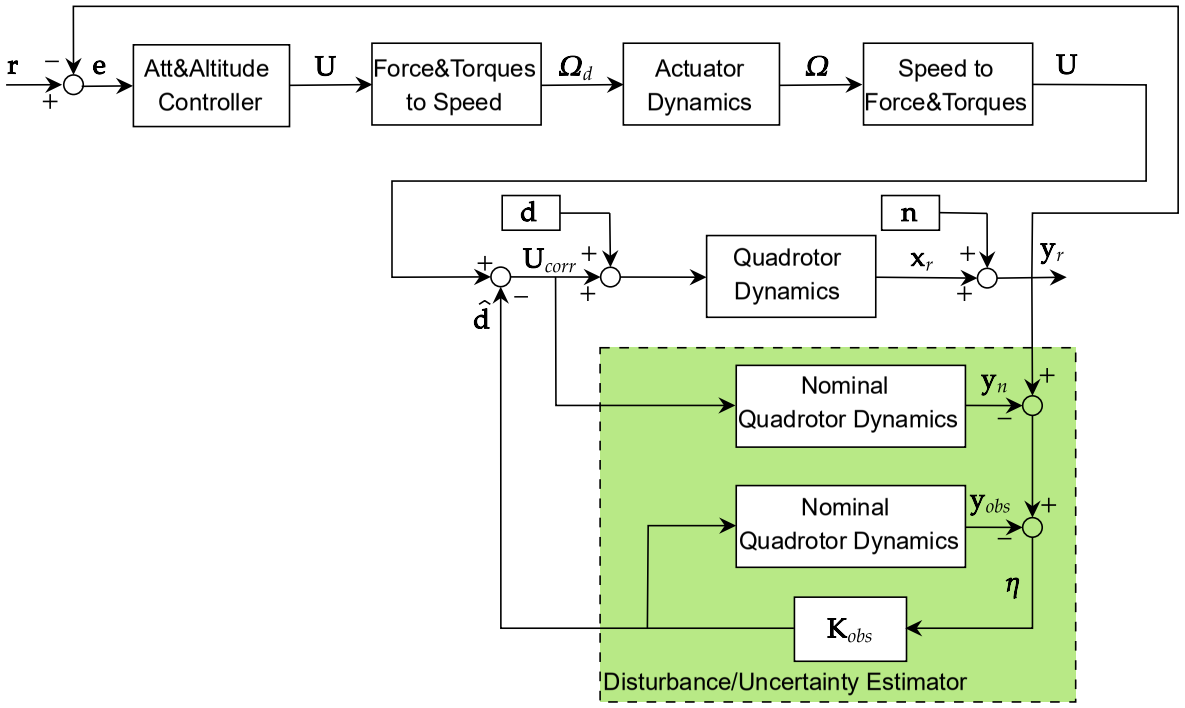

Figure 4.3 OEBDOBC scheme for the quadrotors

PD control structure obtained for the nominal plant (69) under the unit step reference input function (LPF design step 1). The following equation can be written for the observer part.

$$\varepsilon = \mathbf{y_r} - \mathbf{y_{rn}} - \mathbf{y_{robs}} \tag{72}$$

where, $\mathbf{y_{rn}} = [0\ \phi_n\ \theta_n\ \psi_n]^T$ is the nominal output of the quadrotor and $\mathbf{y_{robs}} = [0\ \phi_{obs}\ \theta_{obs}\ \psi_{obs}]^T$ is the output of observer part.

4.2.3. Equivalent Input Disturbance Based Control (EIDBC) Scheme

Fig. 4.4 illustrates the equivalent input disturbance-based control structure. We adapt it from the work of [18] for the quadrotors. EIDBC scheme requires a state observer design part and LPF design part independently.

State observer design block diagram is demonstrated in Fig. 4.5. It includes the following equation and '$\mathbf{B}_i^+$' block.

$$\dot{\hat{\mathbf{x}}}_\mathbf{i}(t) = \mathbf{A_{n}}_i\hat{\mathbf{x}}_i(t) + \mathbf{B_{n}}_i U_i(t) + \mathbf{L}_i[y_{ri}(t) - \hat{y}_i(t)] \tag{73}$$

$$\mathbf{B}_i^+ = (\mathbf{B_{n}}_i^T\mathbf{B_{n}}_i)^{-1}(\mathbf{B_{n}}_i^T\mathbf{L}_i) \tag{74}$$

where, $i \in (\phi, \theta, \psi)$, $\hat{\mathbf{x}}_i(t)$ and $\hat{y}_i(t) = \mathbf{C_{n}}_i\hat{\mathbf{x}}_i(t)$ are the observer plant state and its output, respectively. $\mathbf{L}_i$ is the observer gain. $\mathbf{A_{n}}_i$, $\mathbf{B_{n}}_i$ and $\mathbf{C_{n}}_i$ matrices are system matrix, control matrix and output matrix of nominal plant in controllable canonical form, respectively. U_i is control signal for roll, pitch and yaw movements. ($\mathbf{A_{n}}_i \in \Re^{2\times2}$, $\mathbf{B_{n}}_i \in \Re^{2\times1}$, $\mathbf{C_{n}}_i \in \Re^{1\times2}$, $\mathbf{L}_i \in \Re^{2\times1}$, $\mathbf{B_i^+} \in \Re^{1\times2}$, $\hat{\mathbf{x}}_i \in \Re^{2\times1}$, $\hat{y}_i \in \Re^{1\times1}$) LPF '$\mathbf{F(s)}$' is chosen as follows.

$$\mathbf{F(s)} = diag(0, \frac{T_e}{s+T_e}, \frac{T_e}{s+T_e}, \frac{T_e}{s+T_e}) \tag{75}$$

where, T_e is the LPF cutoff frequency.

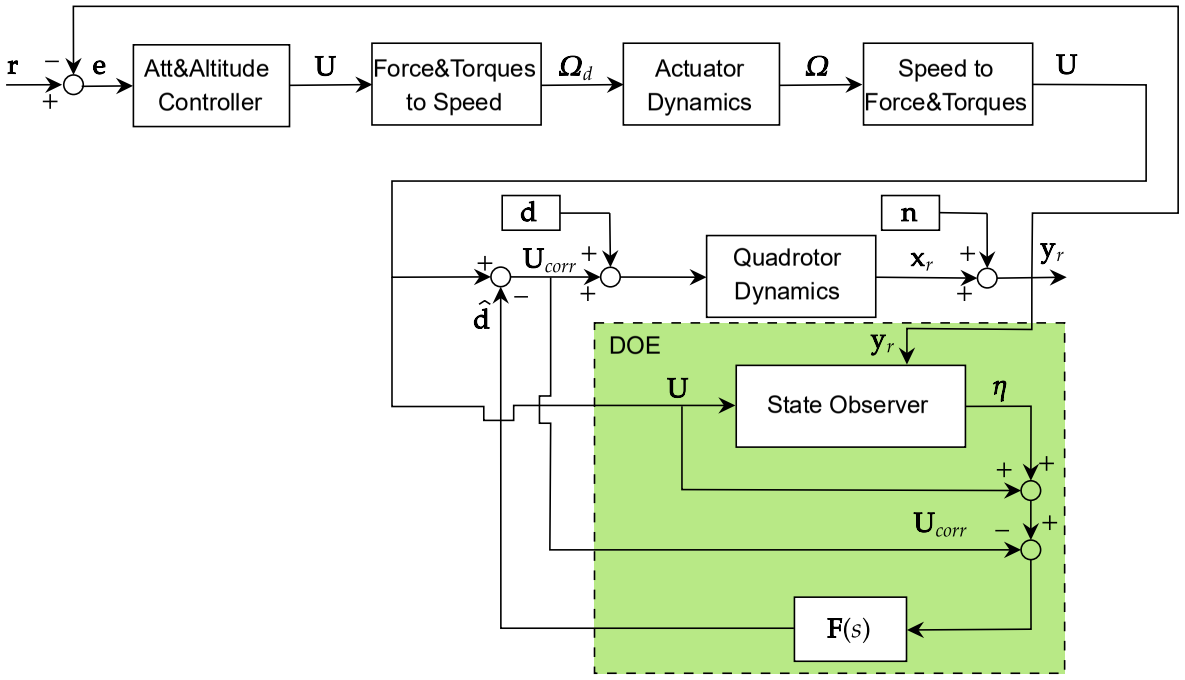

Figure 4.4 EID scheme for the quadrotors

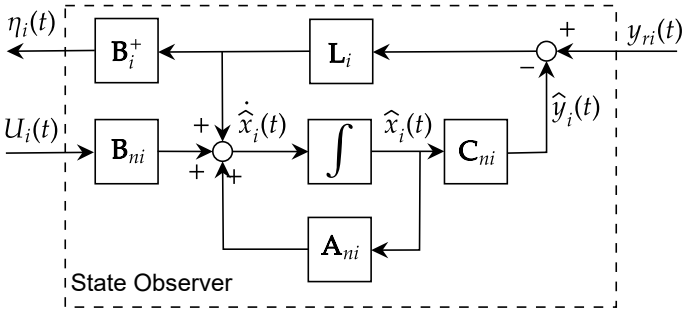

Figure 4.5 State Observer block diagram in EID scheme

4.2.4. Time Domain Disturbance Observer Based Control (TDDOBC) Scheme

Time domain disturbance observer based control scheme is presented in Fig. 4.6 ([**?**]). Fig. 4.7 shows Disturbance Observer block diagram in DOE part of it. Disturbance Observer design introduces the following dynamics.

$$\hat{d}_i = v_i(t) + \mathbf{L}_i\tilde{\mathbf{x}}_i(t) \tag{76}$$

$$\dot{v}_i(t) = -\mathbf{L}_i\mathbf{B}_{\mathbf{n}i}(v_i(t) + \mathbf{L}_i\tilde{\mathbf{x}}_i(t)) - \mathbf{L}_i(\mathbf{A}_{\mathbf{n}i}\tilde{\mathbf{x}}_i(t) + \mathbf{B}_{\mathbf{n}i}U_{corri}(t)) \tag{77}$$

$$\tilde{\mathbf{x}}_i(t) = \begin{bmatrix} y_{ri}(t) & \dot{y}_{ri}(t) \end{bmatrix}^T \tag{78}$$

where, $i \in (\phi, \theta, \psi)$, $\tilde{\mathbf{x}}_i(t)$ is the disturbance observer plant state. $\mathbf{L}_i$ is the observer gain. $\mathbf{A}_{\mathbf{n}i}$, $\mathbf{B}_{\mathbf{n}i}$ and $\mathbf{C}_{\mathbf{n}i}$ matrices are system matrix, control matrix and output matrix of nominal plant in observable canonical form, respectively. U_{corri} is corrected control signal for roll, pitch and yaw movements. ($\mathbf{A}_{\mathbf{n}i} \in \Re^{2\times2}$, $\mathbf{B}_{\mathbf{n}i} \in \Re^{2\times1}$, $\mathbf{C}_{\mathbf{n}i} \in \Re^{1\times2}$, $\mathbf{L}_i \in \Re^{1\times2}$, $\tilde{\mathbf{x}}_i \in \Re^{2\times1}$)

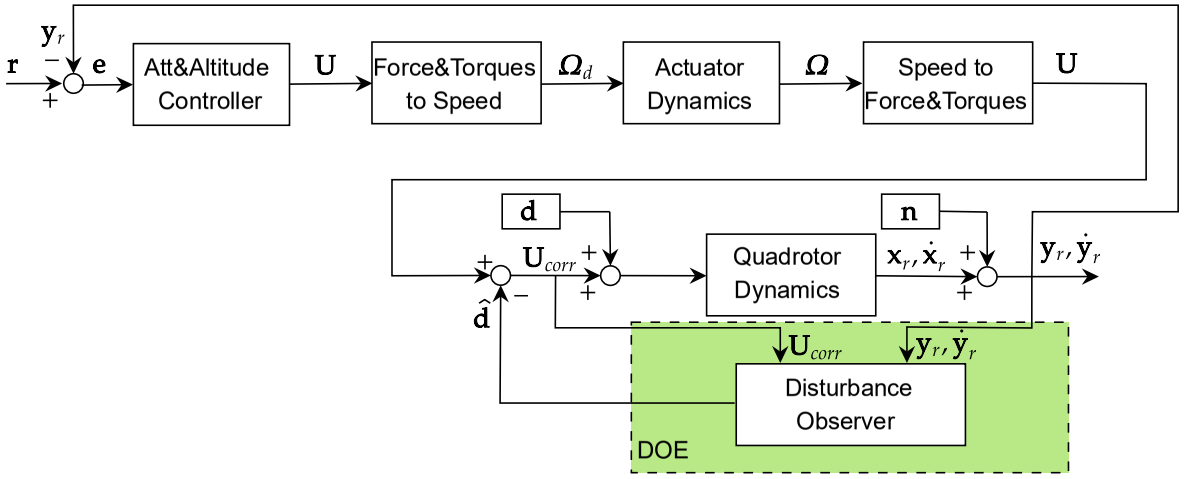

Figure 4.6 TDDOBC scheme for the quadrotors

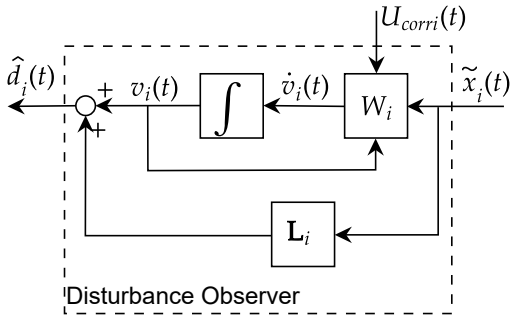

Figure 4.7 Disturbance Observer block diagram in TDDOBC scheme

4.2.5. Uncertainty Disturbance Estimator Based Control (UDEBC) Scheme

Fig. 4.8 demonstrates the uncertainty and disturbance estimator based control scheme ([20]). The main idea for designing a UDE based controller for the quadrotors is to obtain coupled dynamics from decoupled dynamics of the quadrotors, and to treat their nonlinear terms as uncertainty and disturbance. As a consequence, when we follow the procedures in the study of [49], we obtain the following UDE controller rule by simplifying the equations.

$$U_i = I_i((K_i + \tfrac{1}{T_i})e_s + \tfrac{K_i}{T_i}\int e_{si} + \lambda_i \dot{e}_{si} + \ddot{r}_{di}) \tag{79}$$

where, $i \in (\phi, \theta, \psi)$, $[I_\phi \ I_\theta \ I_\psi] = [I_x \ I_y \ I_z]$ and $e_{si} = \lambda_i e_i + \dot{e}_i$. K_i, T_i, λ_i are the UDE controller parameters. T_i determines the required low pass filter cutoff frequency for the uncertainty and disturbance estimation. UDE controller rule includes the low pass filter $G_f = 1/(Ts + 1)$.

4.2.6. Baseline Controller Design

As linear controllers such as PID and LQR are obtained for the simplified model of the quadrotors, strong disturbances are poorly rejected ([40]). However, even if there is a controller with the worst performance in disturbance rejection, DOBC approaches with 2-DoF structures remove this disadvantage and add strong robustness against disturbances

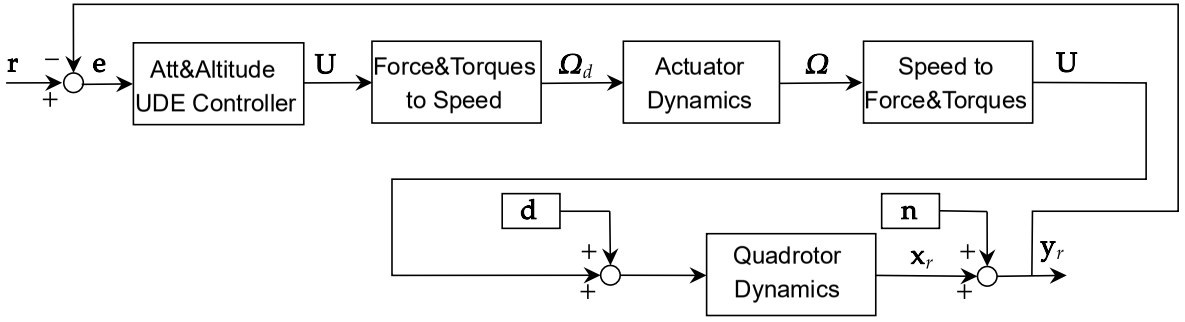

Figure 4.8 UDEBC scheme for the quadrotors

and uncertainties. We chose the BSC approach which has better disturbance rejection capability than linear controllers as baseline attitude and altitude control to take into account all the nonlinear dynamics of the quadrotor. When we execute the rules presented in the work of [38], we obtain the following BS control signals.

$$U_z = \frac{m}{cos(\phi)cos(\theta)}(\ddot{r}_{dz} + e_z + g - \alpha_{z1}(e_{bz} + \alpha_{z1} * e_z) - \alpha_{z2}e_{bz}) \tag{80}$$

where, α_{z1}, α_{z2} are the BS controller parameters for altitude control, $e_z = r_{dz} - y_{rz}$ and $e_{bz} = \dot{y}_{rz} - \dot{r}_{dz} - \alpha_{z1}e_z$.

$$U_\phi = I_x(\ddot{r}_{d\phi} + e_\phi - a_1\dot{\theta}\dot{\psi} - a_2\dot{\theta}\Omega_S - \alpha_{\phi1}(e_{b\phi} + \alpha_{\phi1}e_\phi) - \alpha_{\phi2}e_{b\phi}) \tag{81}$$

where, $\alpha_{\phi1}, \alpha_{\phi2}$ are the BS controller parameters for roll angle control, $e_\phi = r_{d\phi} - y_{r\phi}$, $e_{b\phi} = \dot{y}_{r\phi} - \dot{r}_{d\phi} - \alpha_{\phi1}e_\phi$, $a_1 = (I_y - I_z)/I_x$ and $a_2 = -J/I_x$.

$$U_\theta = I_y(\ddot{r}_{d\theta} + e_\theta - a_3\dot{\phi}\dot{\psi} - a_4\dot{\phi}\Omega_S - \alpha_{\theta1}(e_{b\theta} + \alpha_{\theta1}e_\theta) - \alpha_{\theta2}e_{b\theta}) \tag{82}$$

where, $\alpha_{\theta1}, \alpha_{\theta2}$ are the BS controller parameters for pitch angle control, $e_\theta = r_{d\theta} - y_{r\theta}$, $e_{b\theta} = \dot{y}_{r\theta} - \dot{r}_{d\theta} - \alpha_{\theta1}e_\theta$, $a_3 = (I_z - I_x)/I_y$ and $a_4 = J/I_y$.

$$U_\psi = I_z(\ddot{r}_{d\psi} + e_\psi - a_5\dot{\theta}\dot{\phi} - \alpha_{\psi1}(e_{b\psi} + \alpha_{\psi1}e_\psi) - \alpha_{\psi2}e_{b\psi}) \tag{83}$$

where, $\alpha_{\psi1}, \alpha_{\psi2}$ are the BS controller parameters for yaw angle control, $e_\psi = r_{d\psi} - y_{r\psi}$, $e_{b\psi} = \dot{y}_{r\psi} - \dot{r}_{d\psi} - \alpha_{\psi1}e_\psi$ and $a_5 = (I_x - I_y)/I_z$.

4.3. Simulation Parameters

4.3.1. Physical Parameters of the Quadrotor Model

We chose the Crazyflie 2.0 nanoquadrotor platform to show the effectiveness of the control schemes presented in this paper. The Crazyflie 2.0 nanoquadrotor platform parameters are

given in Table 4.1 ([55]).

Table 4.1 Physical parameters of the Crazyflie 2.0 nanoquadrotor

Symbol	Value(Unit)
m	0.028 (kg)
l	0.065 (m)
K_F	1.61×10^{-8} (N.s^2)
κ	0.006
I_x	16.571710×10^{-6} (kg.m^2)
I_y	16.655602×10^{-6} (kg.m^2)
I_z	29.261652×10^{-6} (kg.m^2)
g	9.8 (m/s^2)
J	0
T_{rot}	0.05
Ω_{max}	3050 (rad/sec)
Ω_{min}	0 (rad/sec)
U_{1max}	0.71 (N)
U_{1min}	0.07 (N)
τ_{max}	1×10^{-3} (Nm)
τ_{min}	-1×10^{-3} (Nm)

4.3.2. Baseline Controller Parameters

Table 4.2 shows the BS controller parameters presented in subsection "Baseline Controller Design". These parameters were found by trial and error such that the settling time is less than 1 second for attitude control, 3 seconds for altitude control and no overshoot. It should be noted here that we do not concentrate on finding the most appropriate parameters for baseline controller preferred as it will affect the tracking performance rather than the robustness of the system, regardless of the way the parameters are found.

Table 4.2 BSC approach parameters

	z	ϕ	θ	ψ
α_{*1}	2	6	6	6
α_{*2}	1	6	6	6

4.3.3. CDOBC Approach Parameters

Table 4.3 illustrates the parameters required for the LPF design proposed by us in subsection "CDOBC Scheme".

Table 4.3 CDOBC approach LPF design parameters

K_p	K_d
0.2	0.005

4.3.4. OEBDOBC Approach Parameters

The following equation is the output of '$\mathbf{K_{obs}}$' block for each rotational movement of a quadrotor.

$$\hat{d}_i = K_{pi}\varepsilon_i + K_{di}\dot{\varepsilon}_i \tag{84}$$

where, $i \in (\phi, \theta, \psi)$.

Observer parameters required for the design of '$\mathbf{K_{obs}}$' block are given in Table 4.4.

Table 4.4 OEBDOBC approach observer parameters

	z	ϕ	θ	ψ
K_{p*}	0	0.2	0.2	0.2
K_{d*}	0	0.005	0.005	0.005

4.3.5. EIDBC Approach Parameters

The following equations show the system matrix, control matrix and output matrix of quadrotor nominal plant for each rotational motion.

$$\mathbf{A}_{\mathbf{n}\phi} = \begin{bmatrix} 0 & 0 \\ 1 & 0 \end{bmatrix} \mathbf{B}_{\mathbf{n}\phi} = \begin{bmatrix} 1 \\ 0 \end{bmatrix} \mathbf{C}_{\mathbf{n}\phi} = \begin{bmatrix} 0 & 60344 \end{bmatrix} \tag{85}$$

$$\mathbf{A}_{\mathbf{n}\theta} = \begin{bmatrix} 0 & 0 \\ 1 & 0 \end{bmatrix} \mathbf{B}_{\mathbf{n}\theta} = \begin{bmatrix} 1 \\ 0 \end{bmatrix} \mathbf{C}_{\mathbf{n}\theta} = \begin{bmatrix} 0 & 60040 \end{bmatrix} \tag{86}$$

$$\mathbf{A}_{\mathbf{n}\psi} = \begin{bmatrix} 0 & 0 \\ 1 & 0 \end{bmatrix} \mathbf{B}_{\mathbf{n}\psi} = \begin{bmatrix} 1 \\ 0 \end{bmatrix} \mathbf{C}_{\mathbf{n}\psi} = \begin{bmatrix} 0 & 34174 \end{bmatrix} \tag{87}$$

We give the EIDBC approach observer gain parameters in Table 4.5. These parameters were found by the Ackermann method. Moreover, for LPF '$\mathbf{F}(\mathbf{s})$' block, we set T_e cutoff frequency in Eq. 75 as 100 rad/sec.

Table 4.5 EIDBC approach observer gain parameters

	ϕ	θ	ψ
$\mathbf{L}_i$	$[0.4972\ 0.0058]^T$	$[0.4997\ 0.0058]^T$	$[0.8778\ 0.0102]^T$

4.3.6. TDDOBC Approach Parameters

The following equations show the system matrix, control matrix and output matrix of quadrotor nominal plant for each rotational motion.

$$\mathbf{A}_{\mathbf{n}\phi} = \begin{bmatrix} 0\ 0 \\ 1\ 0 \end{bmatrix} \mathbf{B}_{\mathbf{n}\phi} = \begin{bmatrix} 60344 \\ 0 \end{bmatrix} \mathbf{C}_{\mathbf{n}\phi} = \begin{bmatrix} 0\ 1 \end{bmatrix} \tag{88}$$

$$\mathbf{A}_{\mathbf{n}\theta} = \begin{bmatrix} 0\ 0 \\ 1\ 0 \end{bmatrix} \mathbf{B}_{\mathbf{n}\theta} = \begin{bmatrix} 60040 \\ 0 \end{bmatrix} \mathbf{C}_{\mathbf{n}\theta} = \begin{bmatrix} 0\ 1 \end{bmatrix} \tag{89}$$

$$\mathbf{A}_{\mathbf{n}\psi} = \begin{bmatrix} 0\ 0 \\ 1\ 0 \end{bmatrix}, \mathbf{B}_{\mathbf{n}\psi} = \begin{bmatrix} 34174 \\ 0 \end{bmatrix}, \mathbf{C}_{\mathbf{n}\psi} = \begin{bmatrix} 0\ 1 \end{bmatrix} \tag{90}$$

Table 4.6 presents the observer gain parameters found by the Ackermann method.

Table 4.6 TDDOBC approach observer gain parameters

	ϕ	θ	ψ
$\mathbf{L}_i$	$[0.008\ 0.003]$	$[0.008\ 0.003]$	$[0.008\ 0.003]$

4.3.7. UDEBC Approach Parameters

UDEBC approach controller parameters in Eq. 79 are given in Table 4.7. The UDE controller parameters were selected by following the parameter finding steps in the reference study of [56].

Table 4.7 UDEBC approach parameters

	ϕ	θ	ψ
K_i	4	4	4
T_i	0.001	0.001	0.001
λ_i	2	2	2

4.4. Simulation Experiments

In this section, two flight simulation scenarios are considered to verify the presented disturbance observer schemes. The goal of the first scenario is to show that external disturbances (d_ϕ, d_θ, d_ψ) in the rotational dynamics of the quadrotor are rejected under the attitude trajectory commands while the altitude are maintained at a constant value. In the second scenario, we aim to demonstrate the practical applicability of the disturbance observer based control approaches under the certain reference way-point and trajectory commands. All simulation parameters are given in the appendix section.

For the first scenario, we selected the magnitudes of the external disturbances in the rotational dynamics as shown in Fig. 4.9 and applied them to the quadrotor for 80 seconds under the given roll, pitch and yaw reference signals. Fig. 4.10 presents the attitude and altitude behaviours of the quadrotor. Under a constant altitude reference value, while all DOBC approaches rejected the applied external disturbances, BSC approach could not perform the same disturbance rejection performance. When we zoom in the roll behavior of the quadrotor in Fig. 4.11, it can be seen that EIDBC and UDEBC approaches have worse disturbance rejection performance than other DOBC approaches. It should be kept in mind that disturbance suppression performances of EIDBC and UDEBC approaches can be improved after adjusting the parameters like bandwidth parameters in the DOE structures. For our simulation studies, their rejection performances are within acceptable limits without any adjusting. Fig. 4.12 illustrates the actuator behaviors of the quadrotor under the disturbance. From Fig. 4.12, we can see that BSC and UDEBC transmit the external disturbance effects to

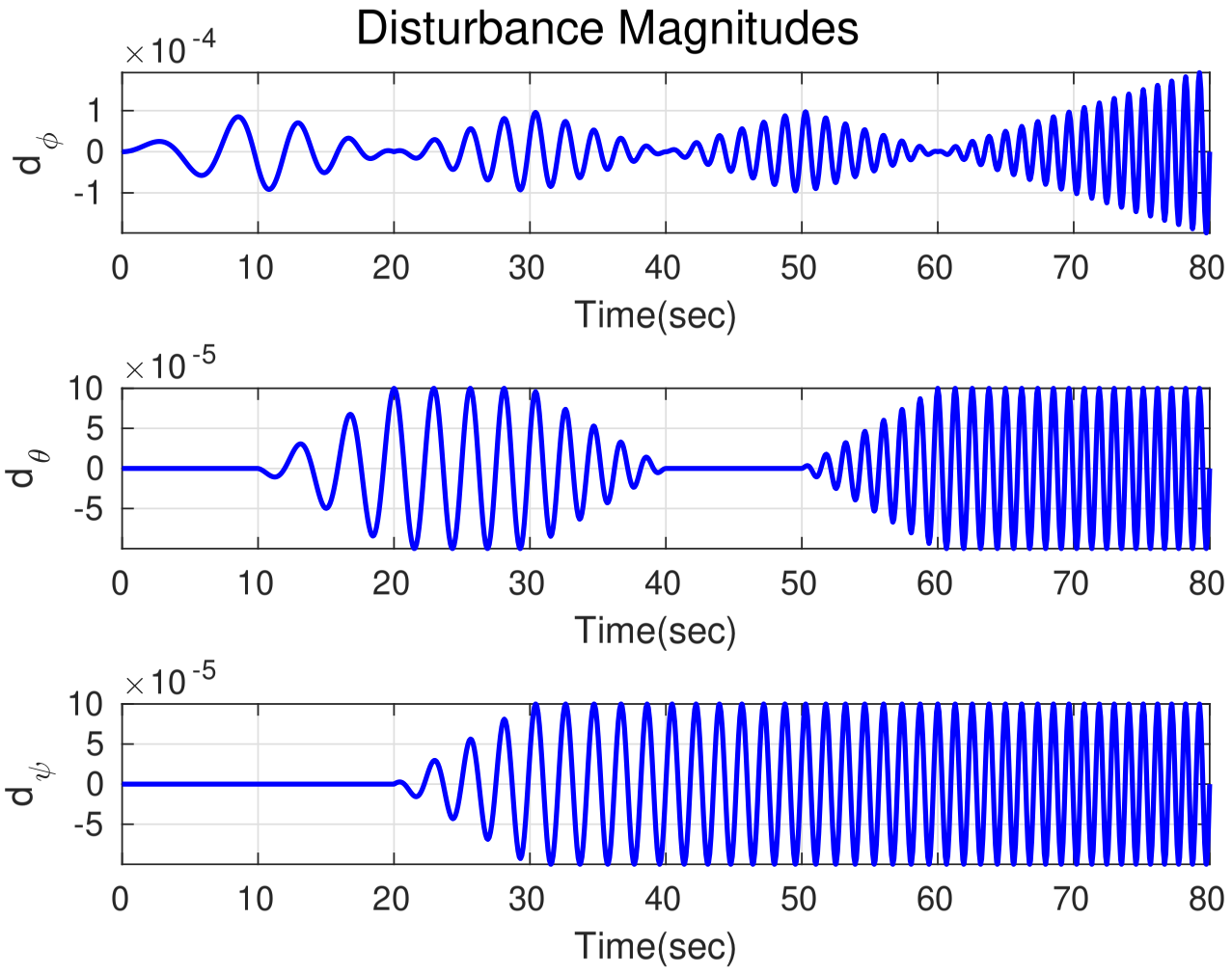

Figure 4.9 Magnitudes of external disturbances for rotational motion of Crazyflie 2.0.

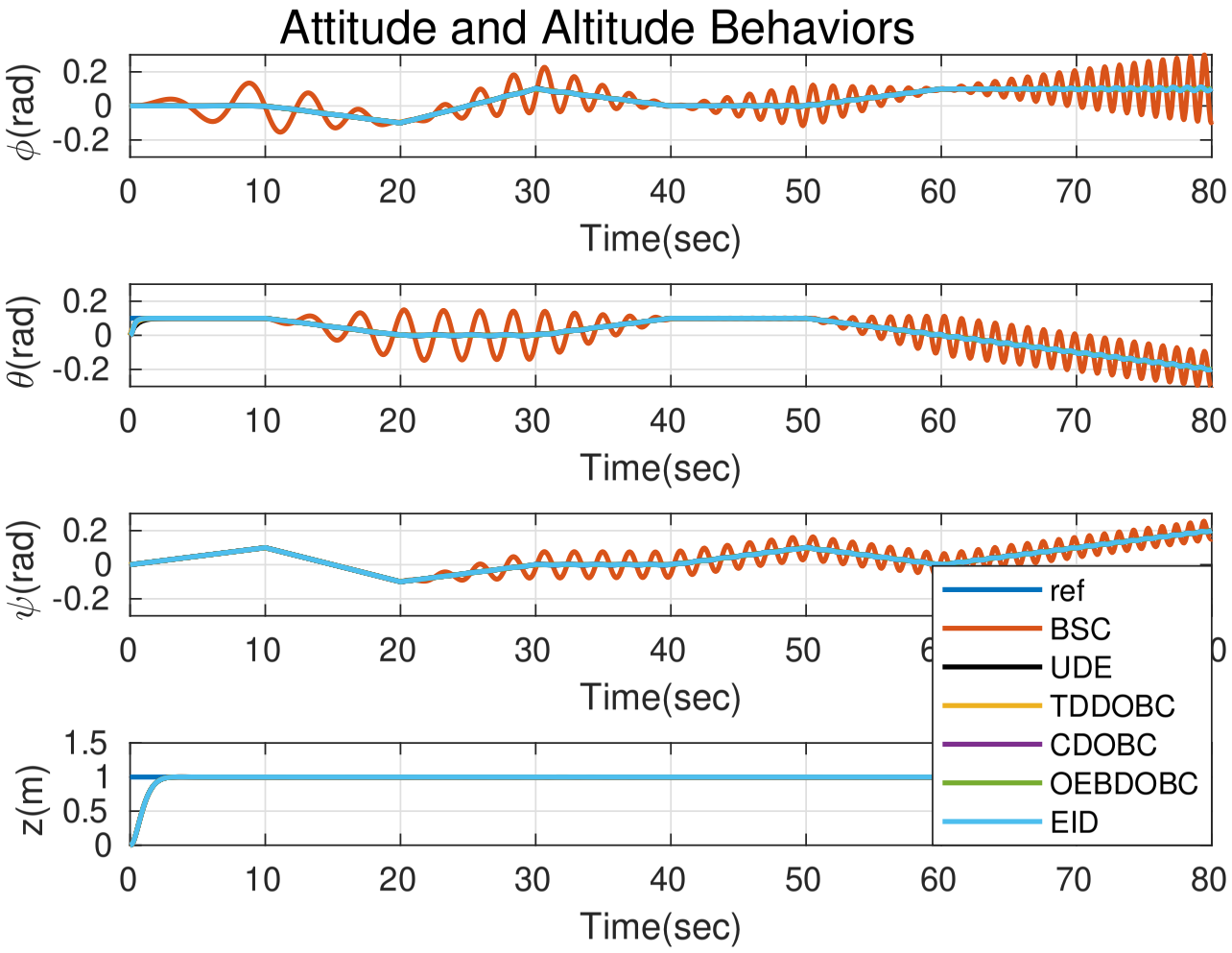

Figure 4.10 Attitude and altitude behaviors of the quadrotor.

the actuators. These actuator oscillations in the BSC and UDEBC approaches cause actuator ESCs to overheat in case of continuous exposure to external disturbances. It should not be forgotten that flight accidents may occur as a result.

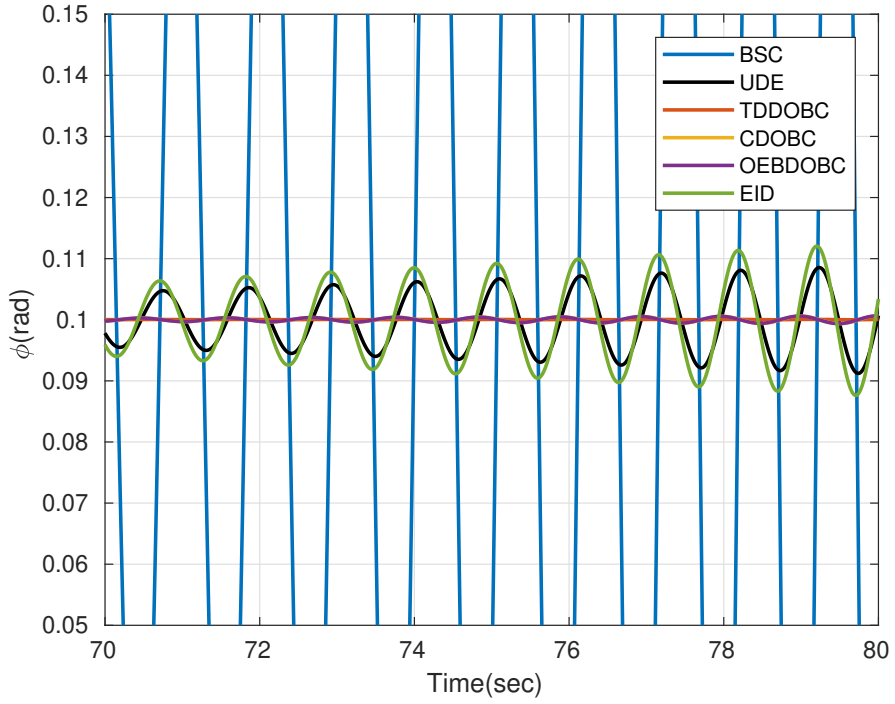

Figure 4.11 Roll behavior of the quadrotor (zoomed in).

For the second scenario, we added an outer loop controlling translational motions to attitude control mechanism in Fig. 4.13, and issued both the reference way-point and trajectory commands after setting the magnitudes of the external disturbances in the rotational dynamics as shown in Fig. 4.14. Position block control rule in Fig. 4.13 includes Eq. (91)-(92) and (93).

$$\begin{bmatrix} \phi_d \\ \theta_d \end{bmatrix} = \begin{bmatrix} \frac{c(\theta)c(\phi)}{g}(s(\psi)\dot{x}_p - c(\psi)\dot{y}_p) \\ \frac{c(\theta)c(\phi)}{g}(c(\psi)\dot{x}_p + s(\psi)\dot{y}_p) \end{bmatrix} \tag{91}$$

$$\begin{bmatrix} \dot{x}_p \\ \dot{y}_p \end{bmatrix} = \begin{bmatrix} K_{vx}\dot{e}_{vx} \\ K_{vy}\dot{e}_{vy} \end{bmatrix} \tag{92}$$

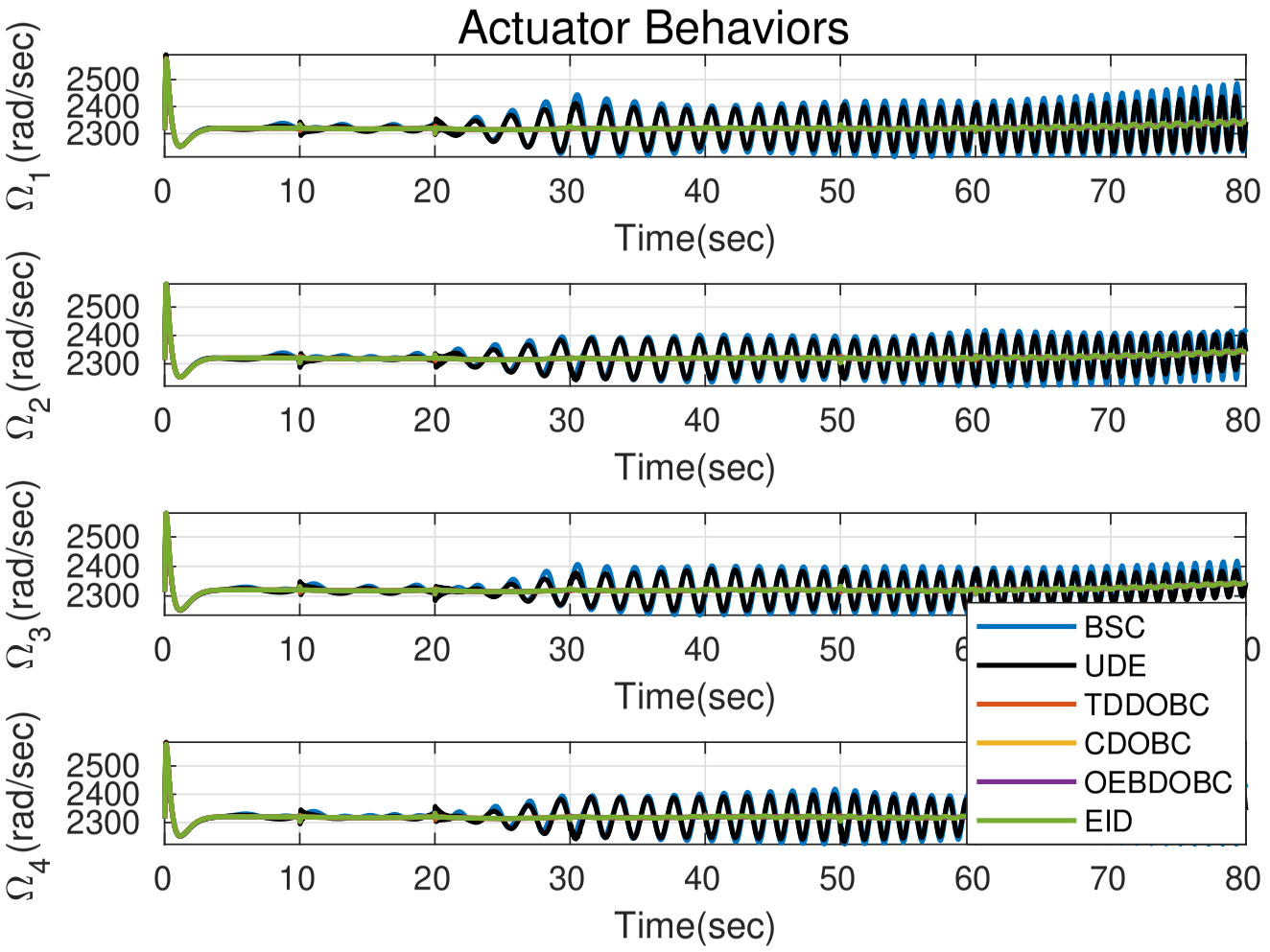

Figure 4.12 Actuator behaviors of the quadrotor.

Figure 4.13 Position controller block for the quadrotors.

where, $\dot{e}_{vp} = v_{dp} - \dot{p}$ is the velocity errors and $K_{vp} = 3$ is velocity control coefficient ($p = x, y$). v_{dp} is found as Eq.(93).

$$\begin{bmatrix} v_{dx} \\ v_{dy} \end{bmatrix} = \begin{bmatrix} K_x e_x \\ K_y e_y \end{bmatrix} \tag{93}$$

where, $e_p = p_d - p$ is the position errors and $K_p = 1$ is position control coefficient.

Table 4.8 presents the simulation parameters. We took into account measurement noise as well as external disturbances to demonstrate the practical applicability of DOBC approaches. While we gave commands that change in one direction in Cartesian space for the way-point command case, we gave the following simultaneously changing commands for the trajectory command case.

$$x_d = \begin{cases} 0 & t < 20sec. \\ \frac{t-20}{2}\sin(\frac{2\pi t}{20}) & 20 \leq t < 80sec. \\ \frac{140-t}{2}\sin(\frac{2\pi t}{20}) & t \geq 80sec. \end{cases} \tag{94}$$

$$y_d = \begin{cases} 0 & t < 20sec. \\ \frac{t-20}{2}\cos(\frac{2\pi t}{20}) & 20 \leq t < 80sec. \\ \frac{140-t}{2}\cos(\frac{2\pi t}{20}) & t \geq 80sec. \end{cases} \tag{95}$$

$$z_d = \begin{cases} 10\tanh(\frac{t}{5}) & t < 20sec. \\ 10 & 20 \leq t < 80sec. \\ \frac{140-t}{6} & t \geq 80sec. \end{cases} \tag{96}$$

Table 4.8 Simulation settings for the second scenario

Δt	Simulation step size	0.001 sec.
T	Flight time	140 sec.
σ_p	Variance of positional noise	0.001
σ_v	Variance of velocity noise	0.001
Δt_n	Noise step size	0.1 sec.

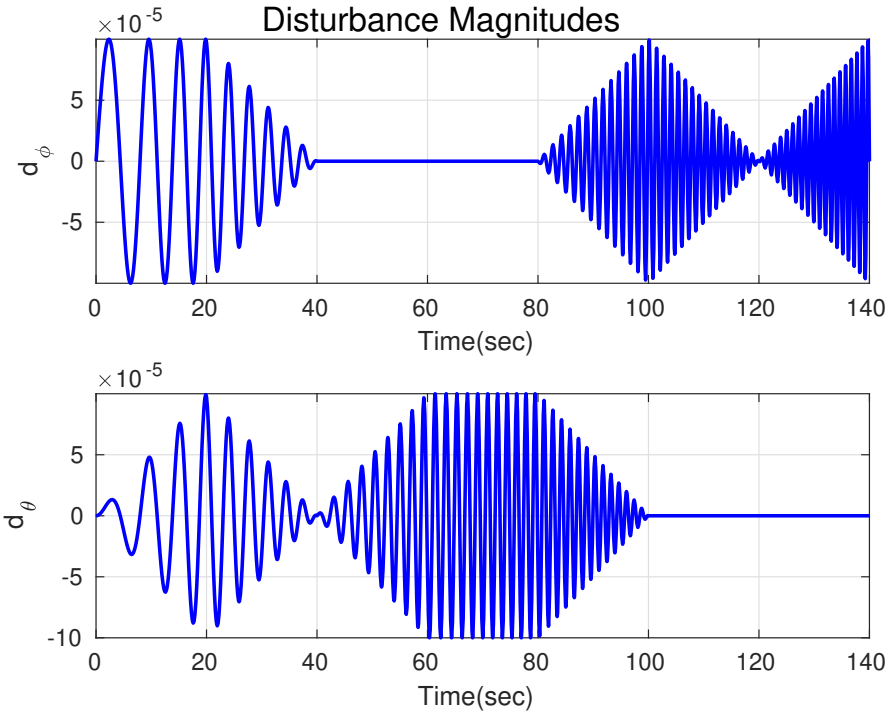

Figure 4.14 Magnitudes of external disturbances for way-point and trajectory tracking of Crazyflie 2.0.

Fig. 4.15 shows the roll, pitch and altitude behaviours of the quadrotor under the way-point reference commands. Fig. 4.16 depicts the angular speeds of the quadrotor for the same command set. In Fig. 4.17 and 4.18, translational behaviours of the quadrotor are presented. For the trajectory commands case, Fig. 4.19-4.22 illustrate the orientational, actuator and trajectory tracking behaviorsof the quadrotor. Scenario 2 simulation studies (Fig. 4.16 and 4.20) have shown that the UDE method is also more sensitive to measurement noise.

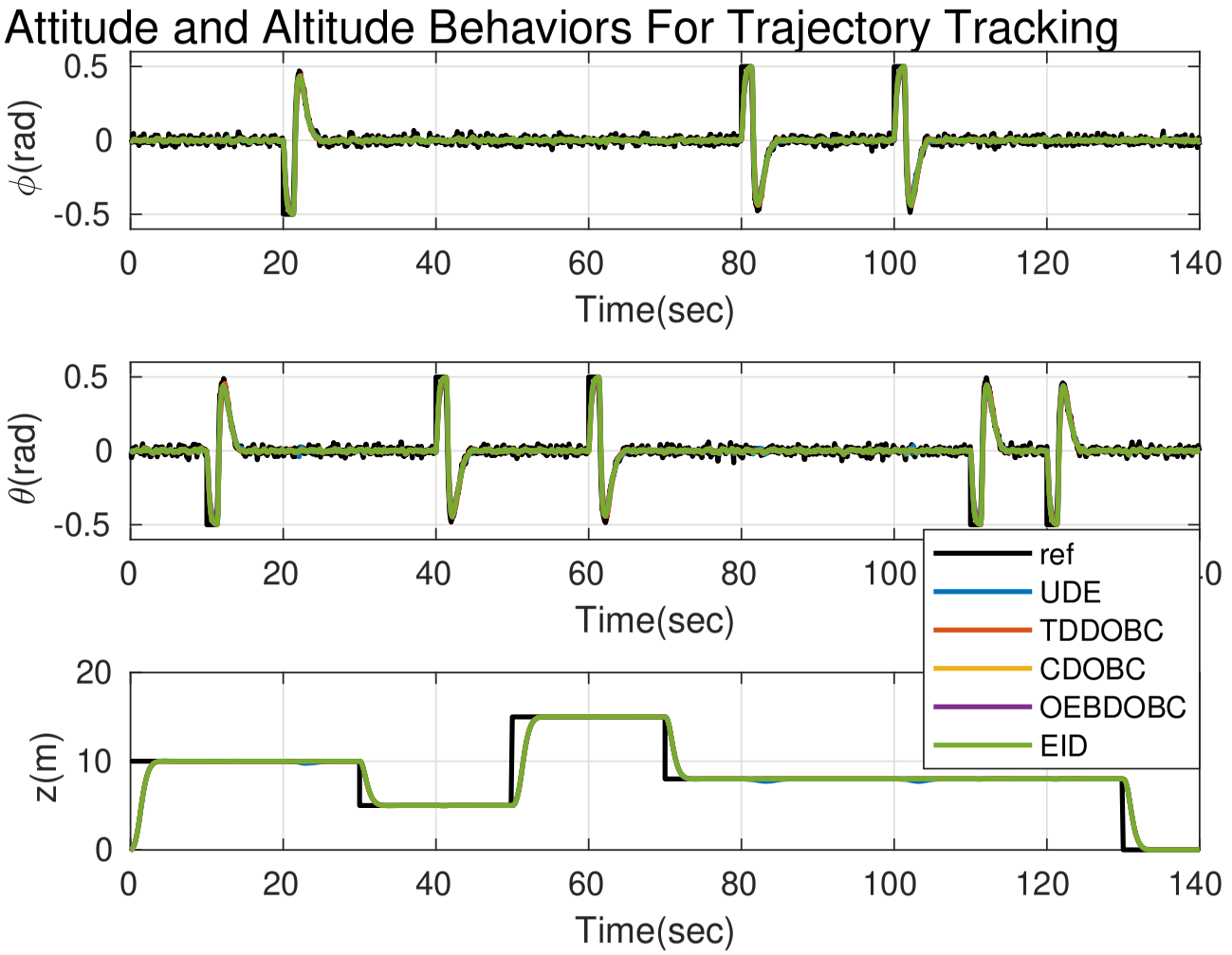

Figure 4.15 Attitude and altitude behaviors of the quadrotor for way-point tracking.

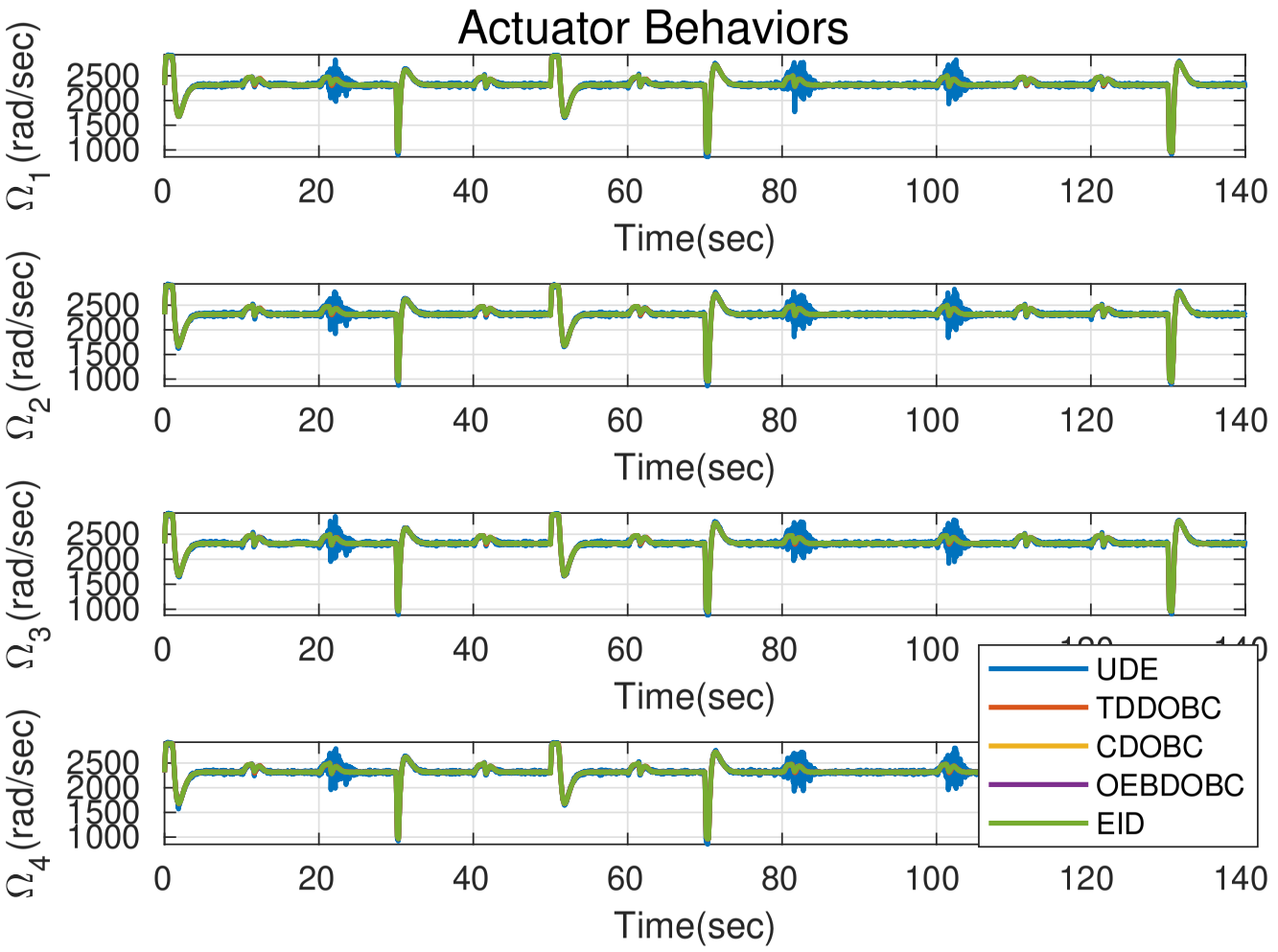

Figure 4.16 Actuator behaviors of the quadrotor for way-point tracking.

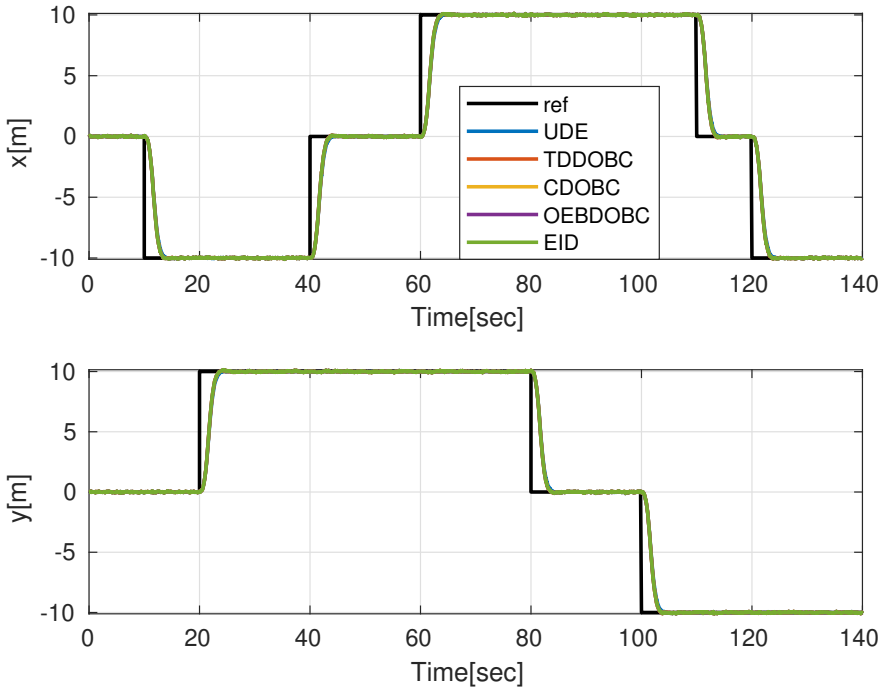

Figure 4.17 Way-point tracking position behaviors of the quadrotor.

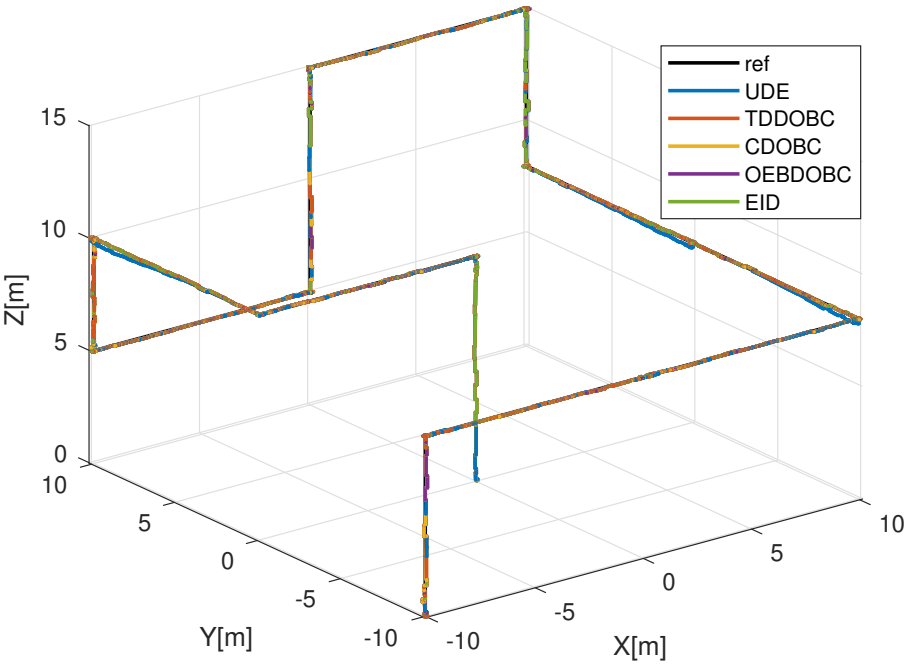

Figure 4.18 Way-point tracking 3D behaviors of the quadrotor.

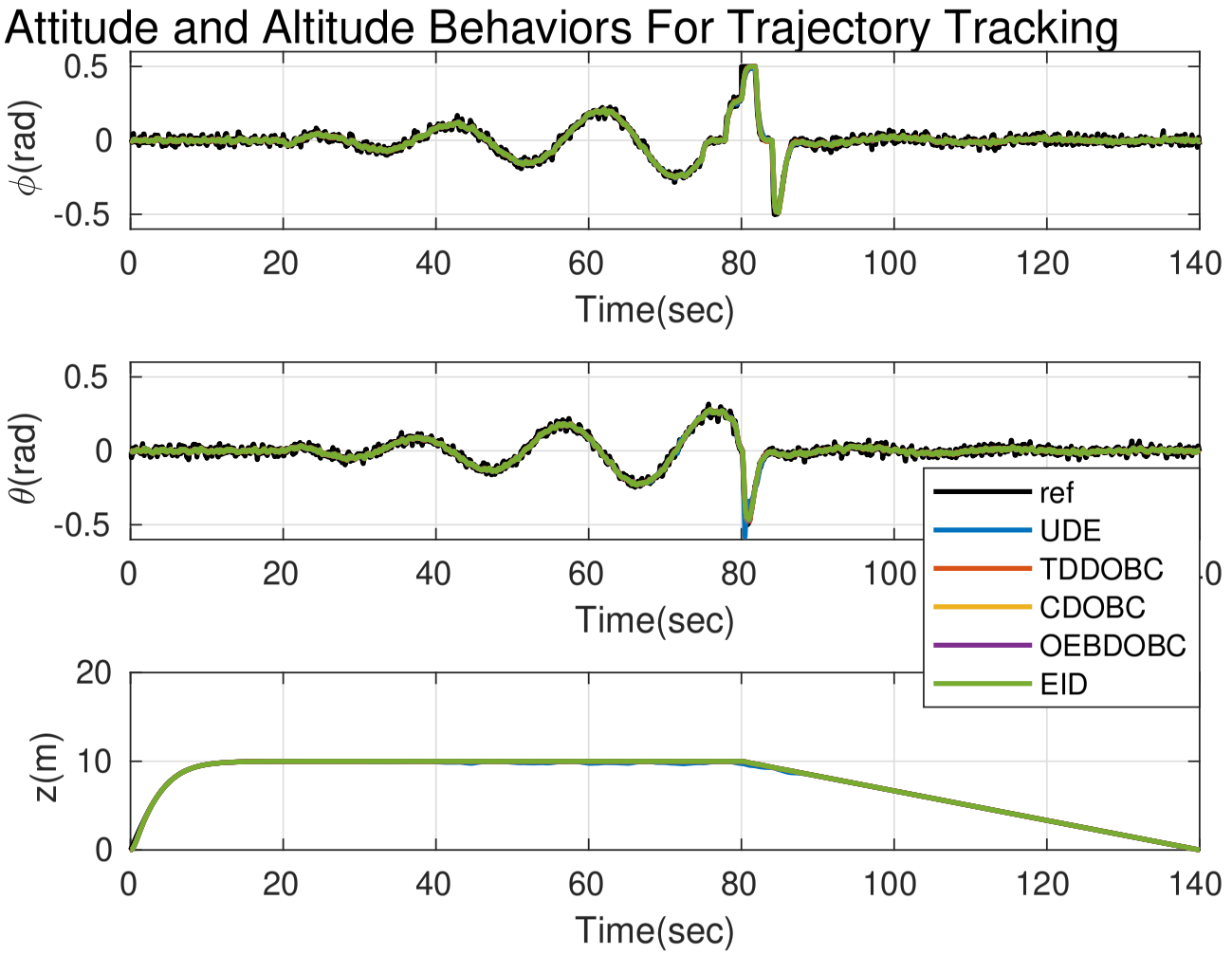

Figure 4.19 Attitude and altitude behaviors of the quadrotor for trajectory tracking.

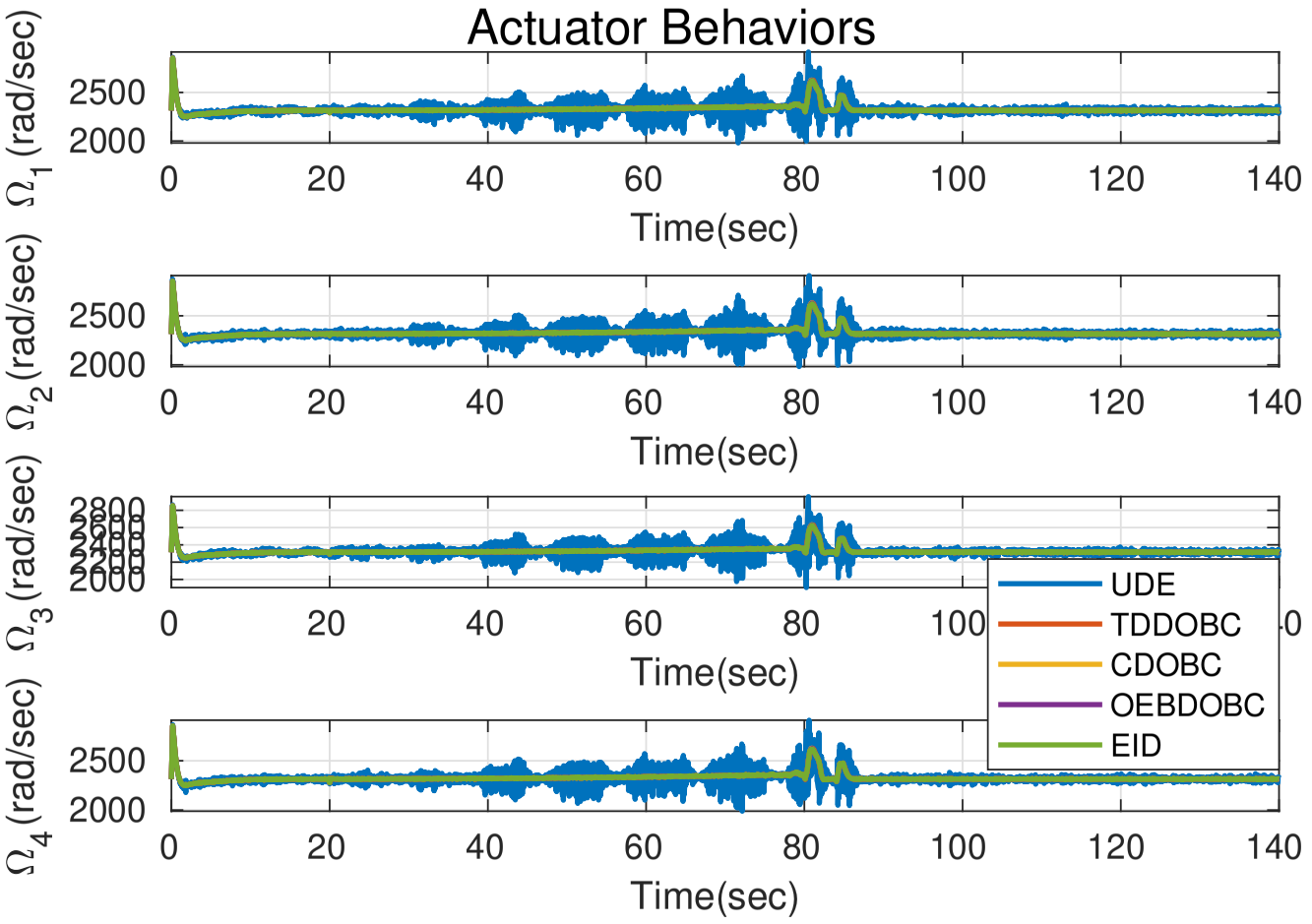

Figure 4.20 Actuator behaviors of the quadrotor for trajectory tracking.

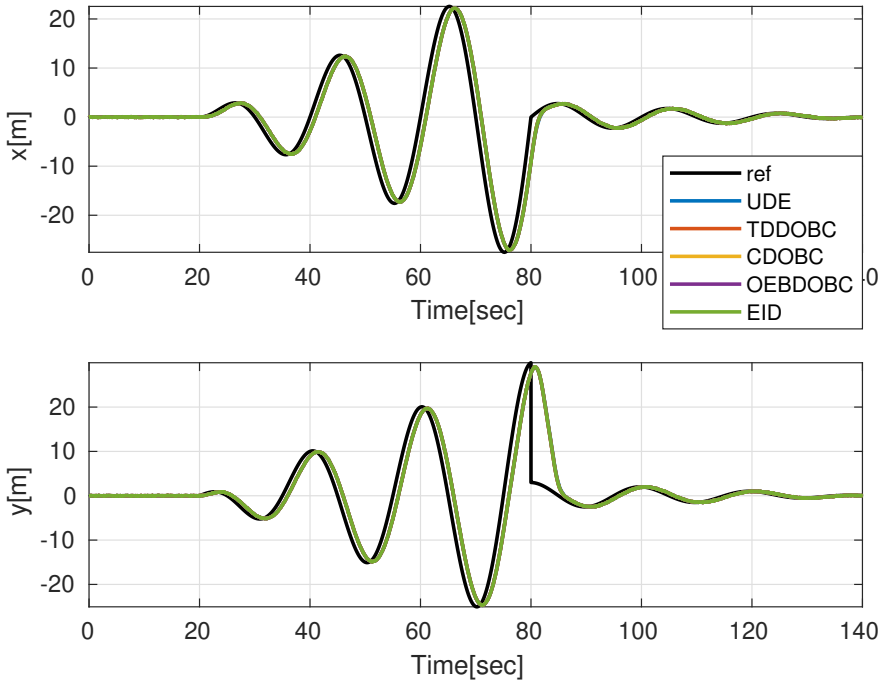

Figure 4.21 Trajectory tracking position behaviors of the quadrotor.

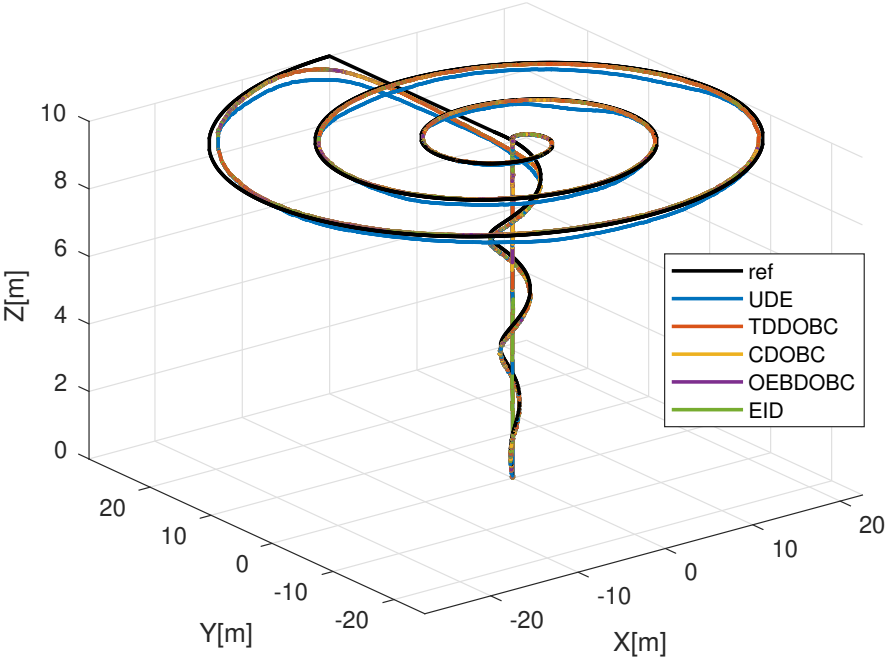

Figure 4.22 Trajectory tracking 3D behaviors of the quadrotor.

BSC scheme failed to follow the both way-point and trajectory reference commands. However, all DOBC approaches have successfully completed the given way-point and trajectory commands. The experiments made proved the practical applicability of these methods, which are successful even under measurement noise.

5. PROPOSED METHOD

5.1. Disturbance/Uncertainty Estimator based Control Scheme

For an LTI system, the general equivalent input disturbance representation of it can be given as

$$\dot{x}(t) = \mathbf{A}x(t) + \mathbf{B}(u(t) + d(t)), \quad y(t) = \mathbf{C}x(t), \tag{97}$$

where $\mathbf{A} \in \mathbb{R}^{n\times n}$, $\mathbf{B} \in \mathbb{R}^{n\times 1}$, $\mathbf{C} \in \mathbb{R}^{1\times n}$, $x(t) \in \mathbb{R}^{n\times 1}$, $y(t) \in \mathbb{R}$, $u(t) \in \mathbb{R}$ and $d(t) \in \mathbb{R}$.

Fig. 5.1 illustrates the disturbance/uncertainty based control scheme proposed in [1], where, K is the main controller, $u(t) \in \mathbb{R}$ is the output of the main controller, $\eta(t) \in \mathbb{R}$ is the observer error, K_{obs} is the observer controller, $d(t) \in \mathbb{R}$ is the equivalent input disturbance and $\hat{d}(t) \in \mathbb{R}$ is the mixed estimations of disturbance/uncertainty. The perturbed plant $\hat{P}$ is as follows:

$$\hat{P} \in P(1 + \Delta W_T) \ \mid \ \forall \|\Delta\|_\infty \leq 1, \tag{98}$$

where P, W_T and Δ are the nominal plant, robustness weight function and unstructured uncertainty function, respectively. The transfer function of the nominal plant (P) is given as below.

$$P = \mathbf{C}(s\mathbf{I} - \mathbf{A})^{-1}\mathbf{B}. \tag{99}$$

5.2. Proposed Scheme

Controller design procedures of K and K_{obs} in Fig. 5.1 are given in [1, 54] for equivalent LTI systems (97). Robustness figures of the closed loop system can be generated for designed K and K_{obs} using the following co-sensitivity and sensitivity expressions.

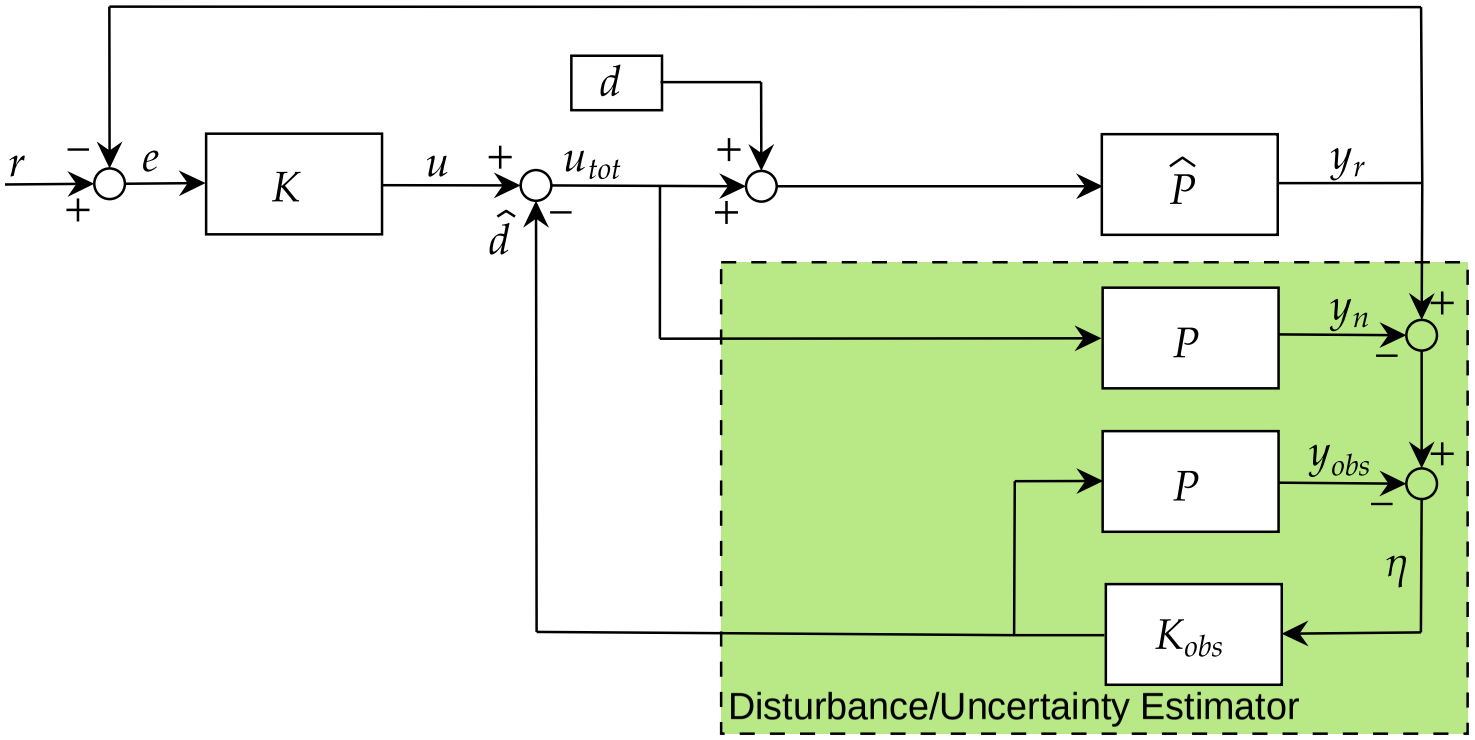

Figure 5.1 Disturbance/Uncertainty estimator based control scheme proposed by Kürkçü et al., [1]

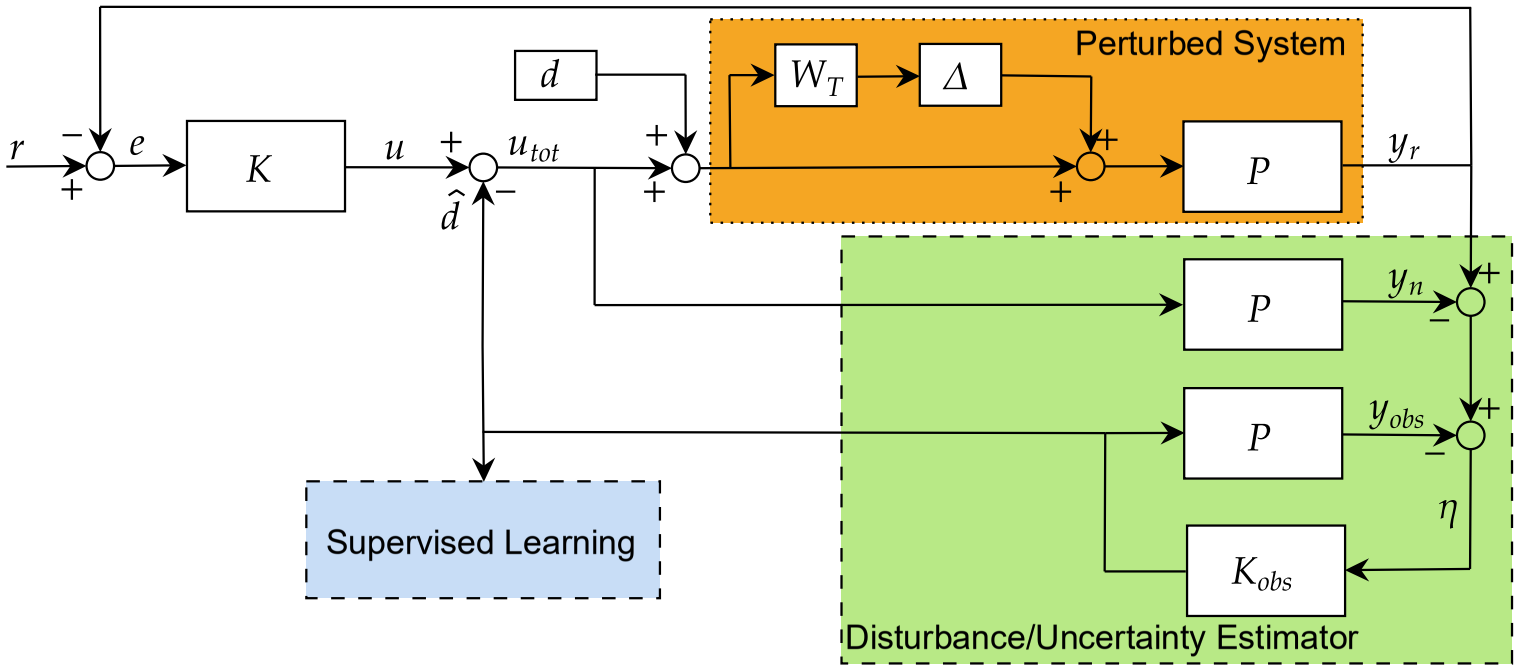

Figure 5.2 Proposed ML assisted disturbance/uncertainty estimator based control scheme-learning phase.

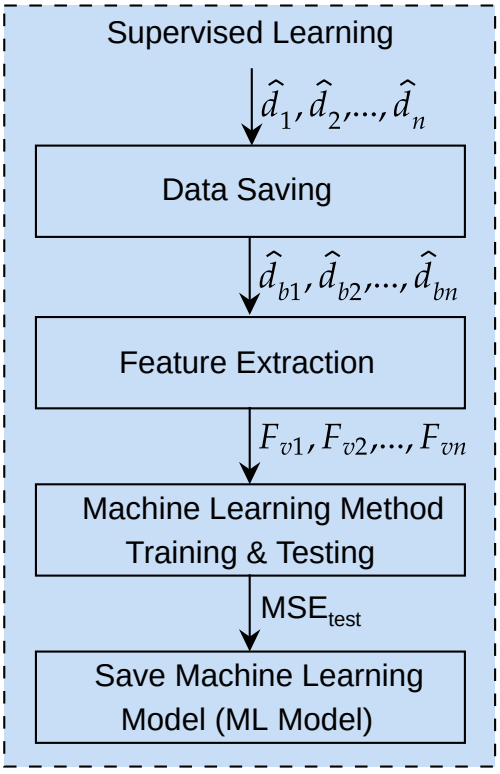

Figure 5.3 Learning phase steps.

$$T = \frac{\hat{P}K(1 + PK_{obs})}{1 + \hat{P}K + \hat{P}K_{obs} + P\hat{P}KK_{obs}}. \tag{100}$$

$$S = 1 - T. \tag{101}$$

After designing the main controller and observer controller structures, we implemented an adaptive method using support vector machine approach, which is a powerful machine learning technique for regression and classification problems, presented in Figs. 5.2-5.4. While Figs. 5.2-5.3 illustrate the learning phase of proposed scheme, Fig. 5.4 shows the overall online adaptation scheme after learning phase. According to the figure, one understands that the adaptive scheme matches the plant uncertainty iteratively using ML techniques and the new nominal system is used in the lowest disturbance prediction loop to cancel out the disturbance d.

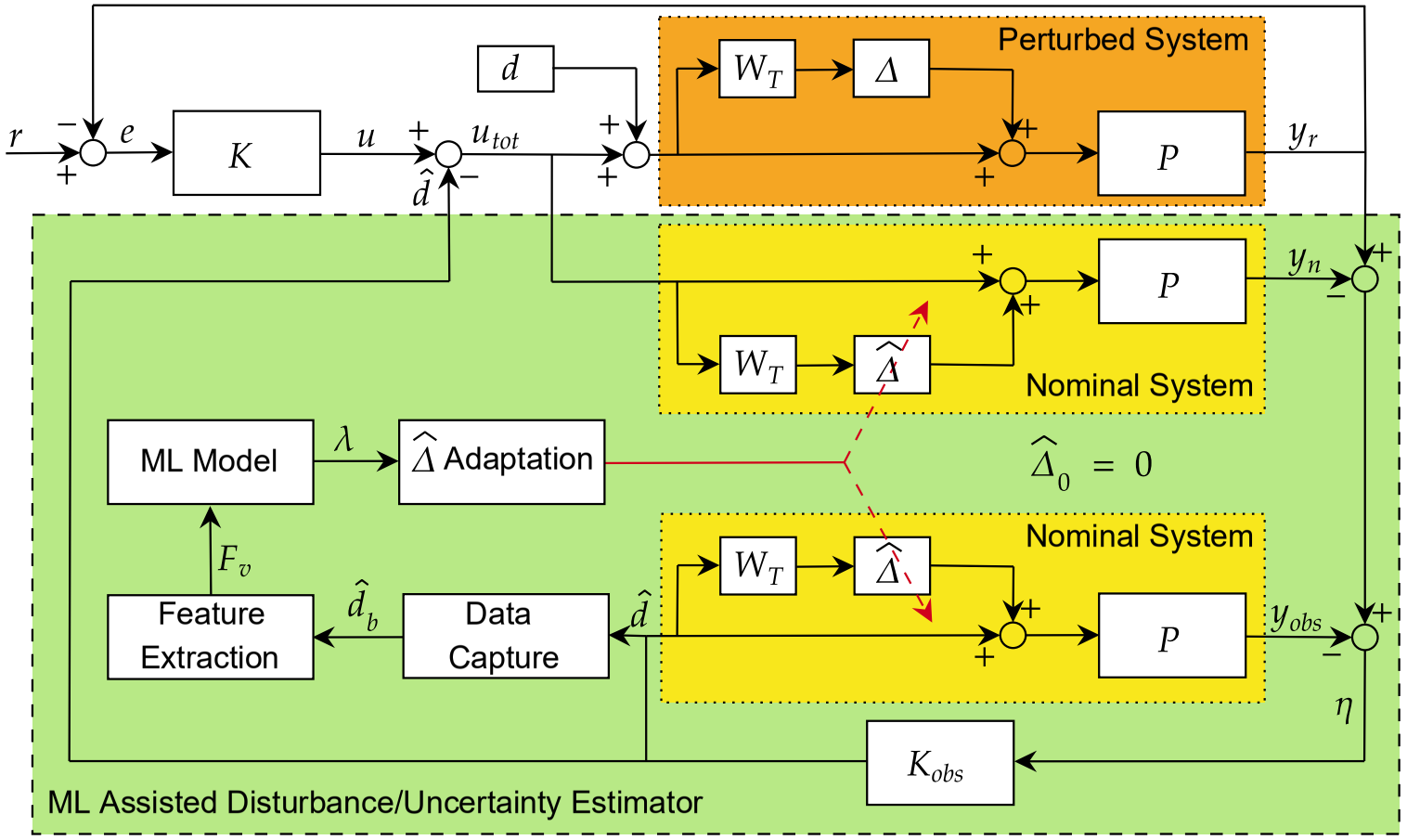

Figure 5.4 Proposed ML assisted disturbance/uncertainty estimator based control overall scheme.

Supervised learning process in the block diagram presented in Fig. 5.2 consists of four steps and is depicted in Fig. 5.3. Receiving and saving data periodically constitute the first step of this process. An important issue in this step is to save data-sets that contain as much variation as possible in the time-domain using different disturbance and uncertainty models. This is critically important to distinguish the components of a mixed signal. In this thesis study, we consider harmonic disturbance model and constant unstructured uncertainty model, i.e. $|\Delta| \leq 1$, $\Delta \in \mathbb{R}$. Time-domain sinusoidal disturbance model is defined as

$$d(t) = A\sin(2\pi f t). \tag{102}$$

For constant unstructured uncertainty model, while weight function W_T in (98) is *i* th-order transfer function with poles and zeros in a Butterworth pattern to meet the specified gain constraints, $\Delta \in (\Delta_{min}, \Delta_{max})$.

The data-sets constitute the crux of the approach. We perform several experiments to collect the numerical data. In the first set, input disturbances ($d(t)$) are available yet there is no plant uncertainty ($\Delta \equiv 0$). In the second set, we have plant uncertainty (Δ) yet no disturbance ($d(t) \equiv 0$) in the control channel. Such a data-set describes the decoupled effect of each factor on the output signal and constitutes a labeled input to a learning agent. Each data-set contains a certain duration time-domain D/U estimation signal sampled at a certain period the system is in the steady regime. In a real scenario, the experiments without plant uncertainty might not be conducted and the best known nominal model could be used to generate the training data to execute the proposed algorithm.

In the feature extraction step, N-point Fast Fourier Transform (FFT) is computed and the FFT magnitudes are used in the sequel. For each data-set, a feature vector is created. Feature vector is an m-dimensional vector consisting of the single sided magnitude of calculated FFT (SSMoFFT), the mean absolute value (MAV) of it and the zero crossing (ZC) value of time-domain signal. ZC value represents the number of signal crossings of the given input signal. The feature vector structure is defined as

$$F_v = [\text{SSMoFFT} \quad \text{MAV} \quad \text{ZC}] \in \mathbb{R}^m \tag{103}$$

After feature extraction step, machine learning approaches can be applied to the obtained data-sets. For the proposed ML assisted disturbance/uncertainty estimator based control scheme, we have used ϵ-Support Vector Regression (ϵ-SVR) as the regression machine learning model. ϵ-SVR solves the following primal problem:

$$\begin{aligned} \min_{\mathbf{w},b,\zeta,\zeta^*} \quad & \frac{1}{2}\mathbf{w}^T\mathbf{w} + C\sum_{i=1}^{n}(\zeta_i - \zeta_i^*) \\ \text{subject to} \quad & y_i - \mathbf{w}^T\phi(x_i) - b \leq \epsilon + \zeta_i, \\ & \mathbf{w}^T\phi(\mathbf{x}_i) + b - y_i \leq \epsilon + \zeta_i^*, \\ & \zeta_i, \zeta_i^* \geq 0, i = 1, ..., n \end{aligned} \tag{104}$$

where $\mathbf{x}_i \in \mathbb{R}^p$ is training input vectors ($i = 1, ..., n$), $\mathbf{y} \in \mathbb{R}^n$ is a vector containing regression (output) values and C is a penalty term. The value of ϵ defines a margin of tolerance where no penalty is enforced over errors. In the above optimization problem, ϕ stands for the kernel trick, [57]. The main goal is to find $\mathbf{w} \in \mathbb{R}^p$ and $b \in \mathbb{R}$.

The dual problem is as given below and it is a convex optimization problem that can be solved.

$$\begin{aligned} \min_{\alpha,\alpha^*} \quad & \frac{1}{2}(\alpha - \alpha^*)^T\mathbf{Q}(\alpha - \alpha^*) + \\ & \epsilon\mathbf{e}^T(\alpha + \alpha^*) - \mathbf{y}^T(\alpha - \alpha^*) \\ \text{subject to} \quad & \mathbf{e}^T(\alpha - \alpha^*) = 0, \\ & 0 \leq \alpha, \alpha^* \leq C, i = 1, ..., n \end{aligned} \tag{105}$$

where $\mathbf{e}$ is a vector composed of all ones, $\mathbf{Q}$ is $n \times n$ positive semi-definite matrix, $\mathbf{Q}_{ij} = \mathbf{K}(\mathbf{x}_i, \mathbf{x}_j) := \phi(\mathbf{x}_i)^T\phi(\mathbf{x}_j)$ with $\mathbf{K}$ being the kernel. $(\alpha - \alpha^*)$ is the vector of coefficients of the dual problem. An in-depth treatment of support vector machines and the optimization algorithms can be found in [57, 58].

The data-sets used for the optimization of ϵ-SVR contain samples, in which the output is *zero* if only uncertainty is active, *one* if only input disturbance is active. Input vector of the ϵ-SVR is m-dimensional feature vector given in the feature extraction step. Such a data-set structure enables us to define the boundary of disturbance-active region and uncertainty-active region in the input space and it further lets us interpolate between these regions if both disturbance and uncertainty are active and mixed at different levels. The machine learning model obtained with the minimum mean squared error (MSE) value after the training and testing processes is obtained first and it is used in the online plant adaptation process as shown in Fig. 5.4.

Fig. 5.4 presents the proposed overall control scheme including online adaptation process. The main purpose is to update the nominal model iteratively to match its response to that of the perturbed/uncertain system. The adjustable nominal plant is defined as

$$\widehat{P}(s) = P(s)(1 + \widehat{\Delta} W_T(s)), \tag{106}$$

where $\widehat{\Delta}$ is the estimate of Δ. $\widehat{\Delta} \in [\Delta_{min}, \Delta_{max}) \subset \mathbb{R}$ and initial $\widehat{\Delta}$ value $\widehat{\Delta_0} = 0$. As a result, initially $\widehat{P}(s) = P(s)$.

The following items describe the modules in the proposed scheme seen in Fig. 5.4.

- **Data Capture:** The module receives the D/U estimation values ($\hat{d}$) at a certain duration intervals and transmits the relevant part of the received data ($\hat{d}_b$) to the "Feature Extraction" module. This operation is maintained continuously for every new finite duration data frame.

- **Feature Extraction:** The module creates an m-dimensional feature vector (F_v) of the $\hat{d}_b$ signal each time a new $\hat{d}_b$ signal is received.

- **ML Model:** This module generates a regression value (λ) related to how much of the lumped D/U estimations are associated to the disturbance and how much is associated

to uncertainty for the given feature vector (F_v) by using the machine learning model that has already been obtained in the learning phase. $\lambda \in [0, 1]$.

- **$\widehat{\Delta}$ Adaptation:** "$\widehat{\Delta}$ Adaptation" module updates $\widehat{\Delta}$ value with δ_{Δ} step resolution according to the ML Model output (λ) by considering a threshold value in the range of $(threshold, 1)$. Algorithm 1 describes the algorithmic flow of the proposed method including online adaptation processes.

Algorithm 1 Online adaptation overall process.

$\widehat{\Delta}_0 \leftarrow 0$
$\widehat{\Delta}_p \leftarrow \widehat{\Delta}_0$ //auxiliary variable
$\widehat{\Delta} \leftarrow \widehat{\Delta}_0$
$\lambda_{set} \leftarrow \emptyset$ //to append $[\widehat{\Delta}\ \lambda]$ pair
Set δ_Δ
Set threshold
Run the system
while true **do**
  //***input:*** *time domain mixed D/U estimations-*$\hat{d}$
  //***output:*** Δ *estimation value-*$\widehat{\Delta}$
  //*Data Capture Module*
  //***input:*** $\hat{d}$
  //***output:*** $\hat{d}_b$
  Capture time-domain data
  if $\widehat{\Delta}$ not found & $\hat{d}_b$ is ready **then**
    //*Feature Extraction Module*
    //***input:*** $\hat{d}_b$
    //***output:*** F_v
    Extract feature vector
    //*ML Model Module*
    //***input:*** F_v
    //***output:*** λ
    Run the machine learning model
    //$\widehat{\Delta}$ *Adaptation Module*
    //***input:*** λ
    //***output:*** $\widehat{\Delta}$
    Append $[\widehat{\Delta}_p\ \lambda]$ to λ_{set}
    if $\lambda <$ threshold **then**
      $\widehat{\Delta}_0 \leftarrow \widehat{\Delta}_p$
      $\widehat{\Delta}_p \leftarrow \widehat{\Delta}_p + \delta_\Delta$
      if $\widehat{\Delta}_p > \Delta_{max} - \delta_\Delta$ **then**
        $\widehat{\Delta}_p \leftarrow$ find maximum of λ_{set}
        $\widehat{\Delta}$ found
      else
        $\widehat{\Delta}$ not found
      end if
    else
      $\widehat{\Delta}$ found
    end if
  end if
  $\widehat{\Delta} \leftarrow \Delta_p \times rampFunction(slope = 0.5)$
    $+\ \Delta_0 \times (1 - rampFunction(slope = 0.5))$
end while

6. EXPERIMENTAL RESULTS

In order to exemplify the proposed scheme, we consider a second order LTI system, which allows the user to reproduce the results. The dynamic system in (107) represents the nominal plant transfer function of the system under consideration.

$$P(s) = \frac{1}{s^2 + 10s + 20}. \tag{107}$$

Remark 1: The plant model is chosen deliberately simple to demonstrate the goals of this study. We aim to devise an algorithm that senses the effect of the proportions of disturbance and uncertainty in an observed output variable. Choosing a more complicated (possibly nonlinear and multidimensional) model would make understanding the contributions of the current work difficult. We avoided the plant specific difficulties to discuss and unfold the algorithm-specific issues.

The main controller K is designed for the nominal plant and it is a proportional-integral-derivative (PID) controller meeting the performance criteria, i) 32 rad/s bandwidth and ii) 90 degrees phase margin. These specifications indicate that a reasonably fast response is requested. The controller K satisfying these specifications is defined as

$$K(s) = K_p + K_i\frac{1}{s} + K_d s, \tag{108}$$

where, $K_p = 320$, $K_i = 796$ and $K_d = 32.2$ are proportional, integral and derivative gains, respectively. Fig. 6.1 illustrates the step response of the nominal closed loop system.

The perturbed plant is chosen as

$$\hat{P}(s) = P(s)(1 + \Delta W_T(s)), \tag{109}$$

where $\Delta = 0.67$ and $W_T(s) = \frac{3s+5.774}{s+28.87}$.

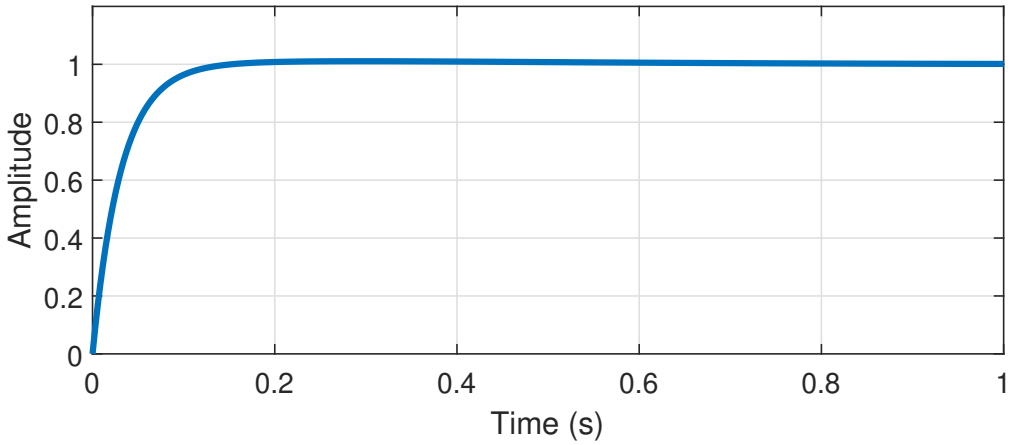

Figure 6.1 Step response of the nominal closed loop system.

K and K_{obs} can be designed together as defined in [1, 54] by considering weighting function (W_T) defining performance requirements. For simplicity, we set $K_{obs} \equiv K$. We have depicted sensitivity (S) and co-sensitivity (T) functions in Fig. 6.2 by using (100) and (101). When we inspect the data in Fig 6.2, we see that K_{obs} is enough to estimate and reject disturbance/uncertainty, yet one can pursue better K_{obs} designs than the choice $K_{obs} \equiv K$.

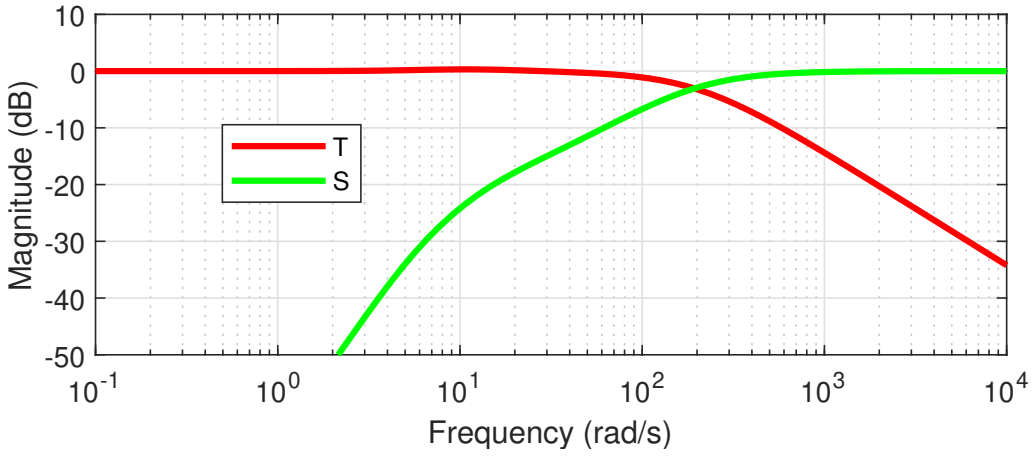

Figure 6.2 Sensitivity and complementary sensitivity functions.

Fig. 6.3 illustrates predicted mixed disturbance/uncertainty results for the perturbed plant given in (109) and below harmonic disturbance model is adopted.

$$d(t) = \sin(4\pi t). \tag{110}$$

According to Fig. 6.3 and its window plots, we observe that uncertainty (Δ) causes steady state errors in estimating the disturbance that enter through the control channel. The response seen in the figure displays a fast transient and the steady regime is reached after almost 1 second. The window plot (a) shows the initial transient, (b) shows the predicted disturbance and (c) demonstrates the ground truth. It is evident that the presence of constant Δ causes a constant shift in the disturbance estimations. Our goal is to improve the disturbance estimation performance by eliminating these steady state errors to approximate to the true value of $d(t)$.

Remark 2: In a general scenario, for a ML model to distinguish the effects of input disturbances and structural uncertainties, the design engineer is expected to perform a number of tests that guide the ML model and develop a reasonable decision boundary to unmix the mutual effects. This tightly depends on the numerical data and the feature set that embodies the ML model's input vector.

Table 6.1 Data-set features characterizing input disturbance and plant uncertainty

Features of the Input Disturbance	
Type	$A\sin(2\pi ft)$ $(f_{min} \leq f < f_{max})$
Feature Vector F_v Size	40
Data-Set Size $(n/2)$	500
A	1
f_{min}	1 Hz
f_{max}	5 Hz
Features of the Model Uncertainty	
Type	$\Delta \in (\Delta_{min}, \Delta_{max}) \subset \mathbb{R}$
Feature Vector F_v Size	40
Data-Set Size $(n/2)$	500
Δ_{min}	0
Δ_{max}	1

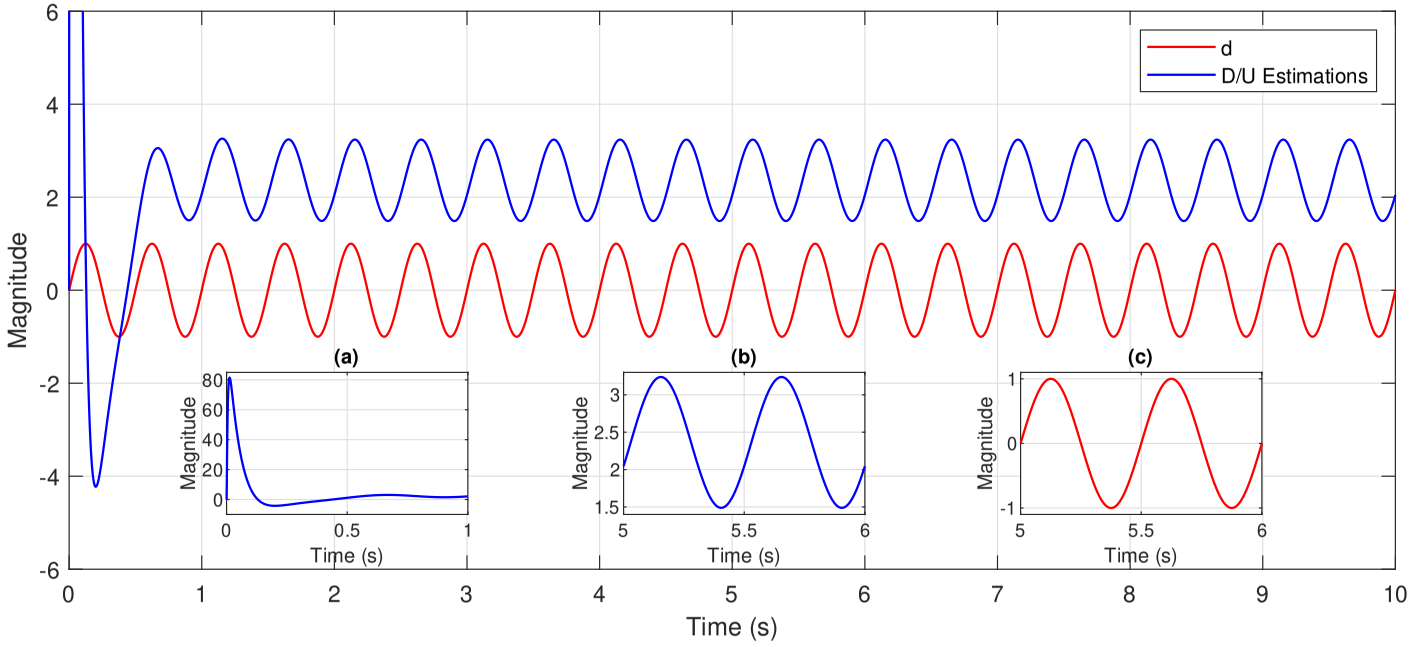

Figure 6.3 D/U ($\hat{d}$) estimations ($\Delta = 0.67$, $d(t) = \sin(4\pi t)$). Window plots show the transient response in (a), estimation of disturbance in (b) and its ground truth in (c).

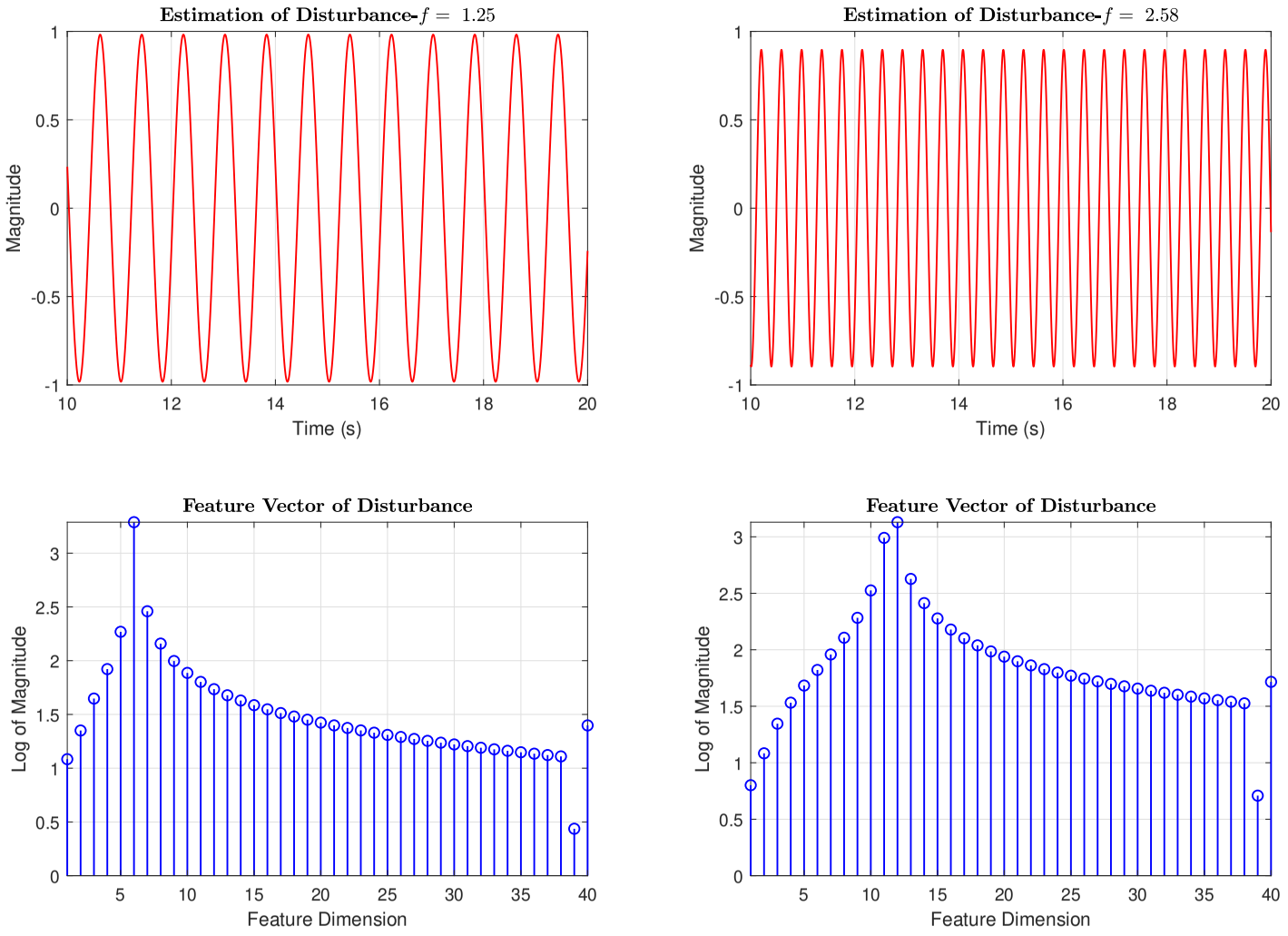

Figure 6.4 Sample disturbance data-set.

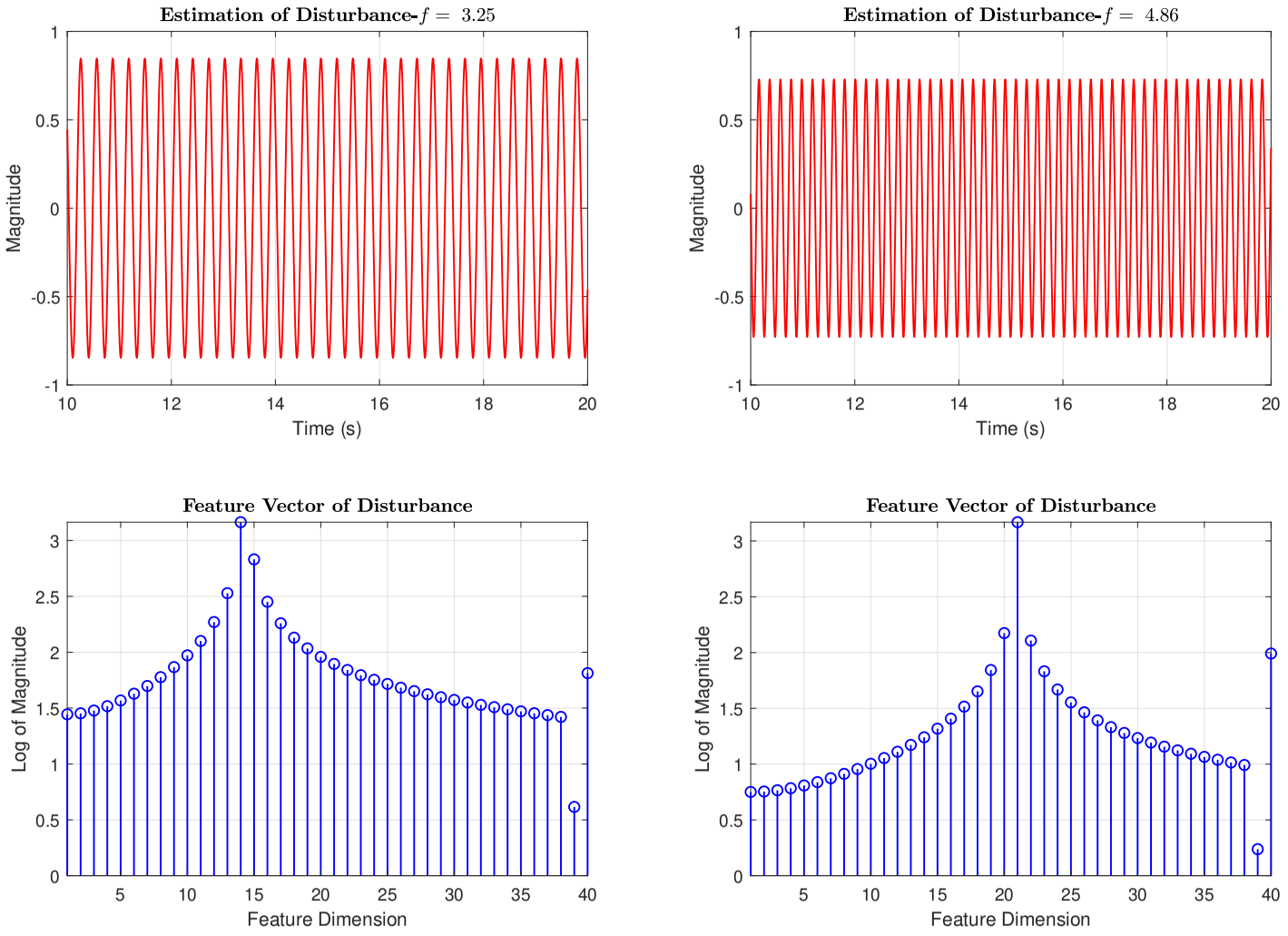

Figure 6.5 Sample disturbance data-set.

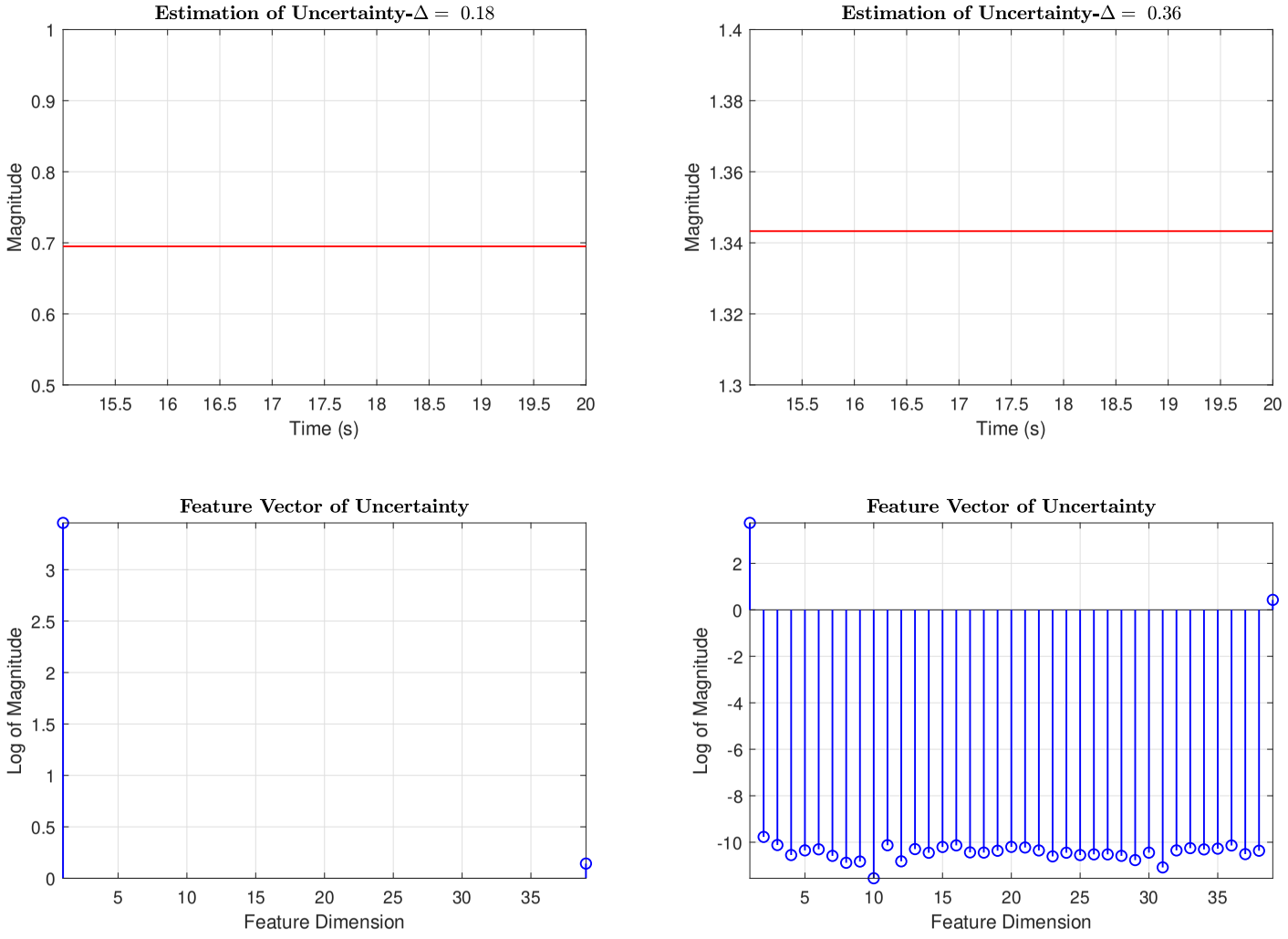

Figure 6.6 Sample uncertainty data-set. Except for the first and 39th dimensions of the feature vector, remaining components are zero or at the order of 10^{-10}. This is visible in the bottom left subplot.

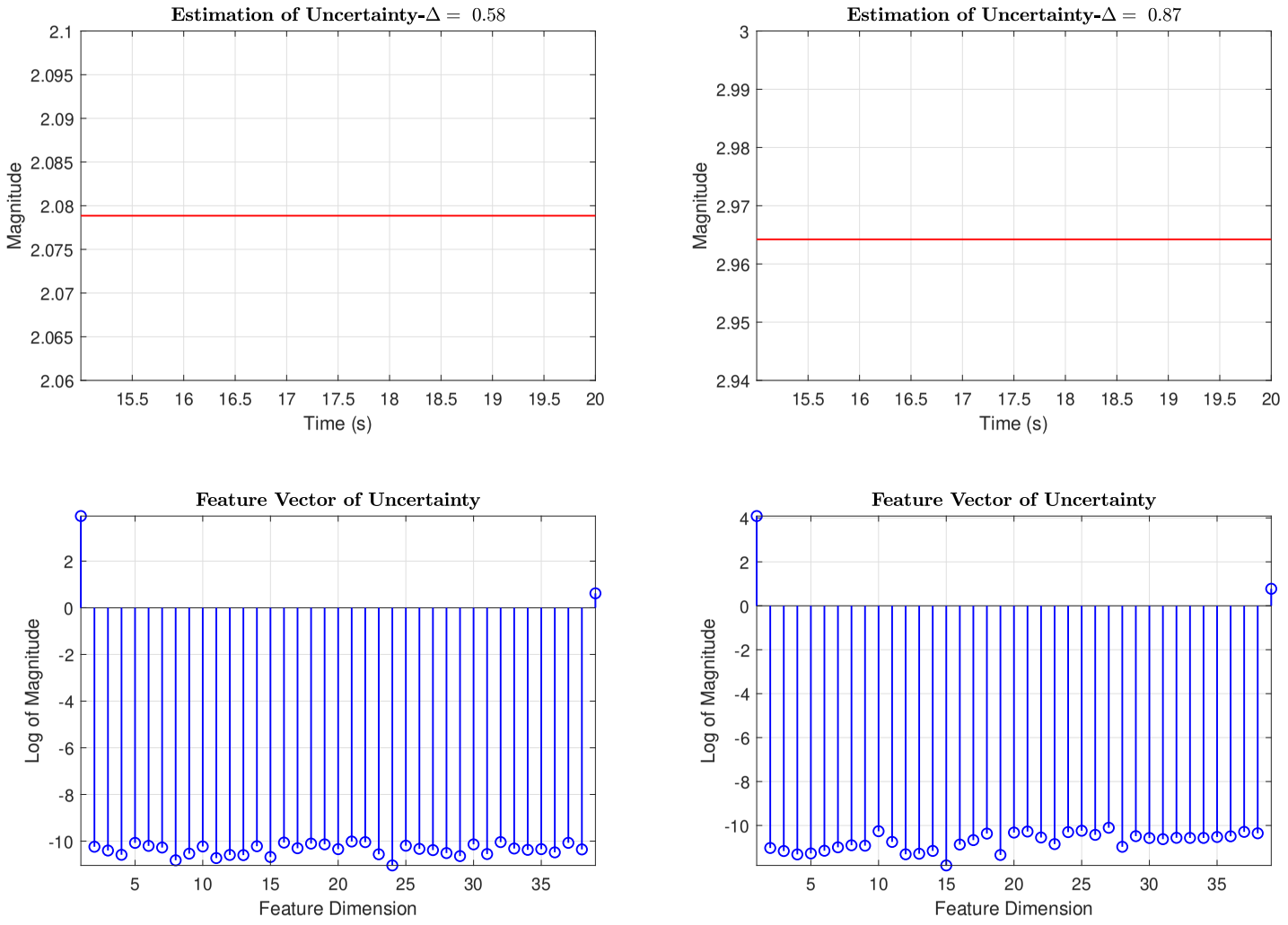

Figure 6.7 Sample uncertainty data-set.

In order to apply the proposed method to the D/U estimator based control scheme in Fig 5.1, we first need to create a data-set as described in the learning phase steps. In Table 6.1, the data-set features are given. A total of 1000 data-sets are created. Each data set has a size of 5-seconds time-domain D/U estimation signal sampled at 1 ms during the steady state regime of the system and is generated. Random numbers adopted here distribute uniformly over the ranges determined by the maximum and minimum values given in Table 6.1. Then, the feature vectors of them are created by adding the associated MAV and ZC values. Each feature vector is $m = 40$ dimensional vector and its first N values ($N = 38$) come from the single sided magnitude of calculated 4096-point FFT. The 39^{th} entry is the mean absolute value (MAV) and the 40^{th} entry is the zero crossing (ZC) value of time-domain signal.

Fig. 6.4-6.7 show sample disturbance and uncertainty data-sets, where the rightmost components augment the selected N-element FFT magnitude array with MAV and ZC values. While Fig. 6.4 demonstrates disturbance estimations and feature vectors of them for 1.25 Hz and 2.58 Hz harmonic input disturbance frequencies, Fig. 6.5 displays the same graphics for 3.25 Hz and 4.86 Hz harmonic input disturbance frequencies. In Fig. 6.6 and 6.7, uncertainty estimations and feature vectors of them are given for 0.18, 0.36, 0.58 and 0.86 constant uncertainty values. In the figures, feature vectors are shown as log of magnitude. Fig. 6.8 illustrates the 3D principal component analysis (PCA) plot of the whole data-set. PCA analysis clearly demonstrates that the disturbance and uncertainty are separable and the usability of data-sets with the learners of machine learning approaches.

As the next learning phase step, we have imported ϵ-SVR regression model from the support vector machine (SVM) class of *scikit-learn* Python library, [59]. We have chosen the model parameters as SVR(kernel = 'rbf') (with default parameters) and reserved 75% of the data-sets for the training. After training process terminates, we observed that the obtained model reaches a mean squared error value of 0.00708 (MSE_{test}) for the testing data-set.

Remark 3: In machine learning applications, the eventual performance depends the critically on the available numerical data. As the number of observations decreases, the performance deteriorates. However, the abundance of recorded observations enables the designer to obtain

an accurate model. In the current paper, the number of experiments determines the eventual performance of the SVM based machine learning model. Therefore, one may not assure absolute success or absolute failure in such applications. In our experiments, the number of training data is sufficient to show the enhancement in the overall performance. If the number of training data is increased, naturally, one should expect better performance.

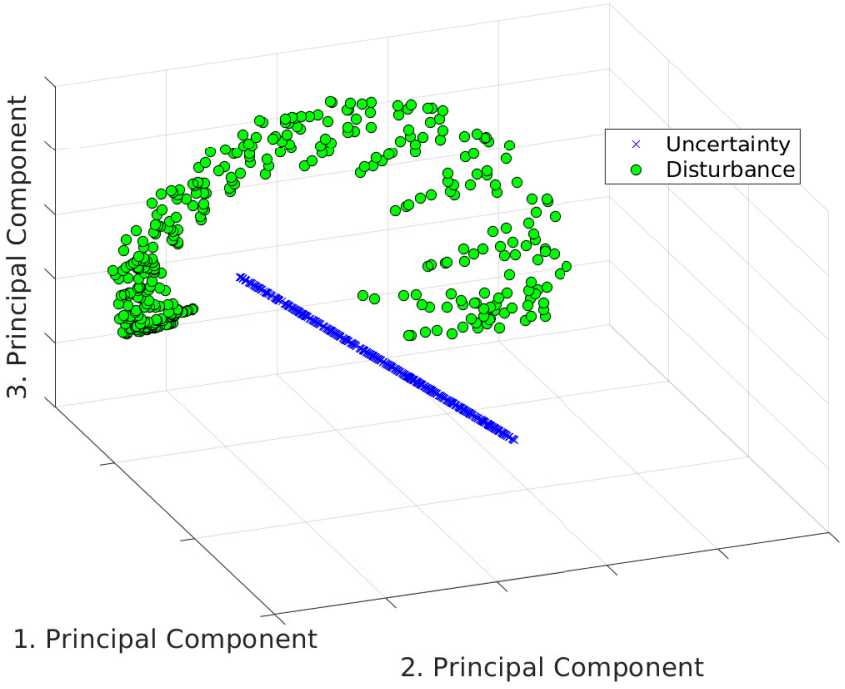

Figure 6.8 3D PCA plot of the whole data-set.

For simulation test cases, the "Data Capture" unit receives the D/U estimation values ($\hat{d}$) at 1 ms intervals for 15 seconds time frame and transmits the last 5 seconds of received data ($\hat{d}_b$) to the "Feature Extraction" module to ensure that the steady state regime is reached.

Figs. 6.9-6.17 illustrate the simulation results. Fig. 6.9 and Fig. 6.10 show the $\widehat{\Delta}$ update rule behaviors stated in Algorithm 1 code lines 38-39 for two simulation test cases ($\Delta = 0.27$, $d(t) = sin(2.12\pi t)$)-($\Delta = 0.84$, $d(t) = sin(4.37\pi t)$). In Fig. 6.11 and Fig. 6.12, ML Model outputs (λ) corresponding to $\widehat{\Delta}$ are depicted for these test cases. For the first test case, we can see from Fig. 6.11 that the value of $\widehat{\Delta}$ is correctly found above the specified threshold line. The same can be said for the second simulation test case. However, in Fig.

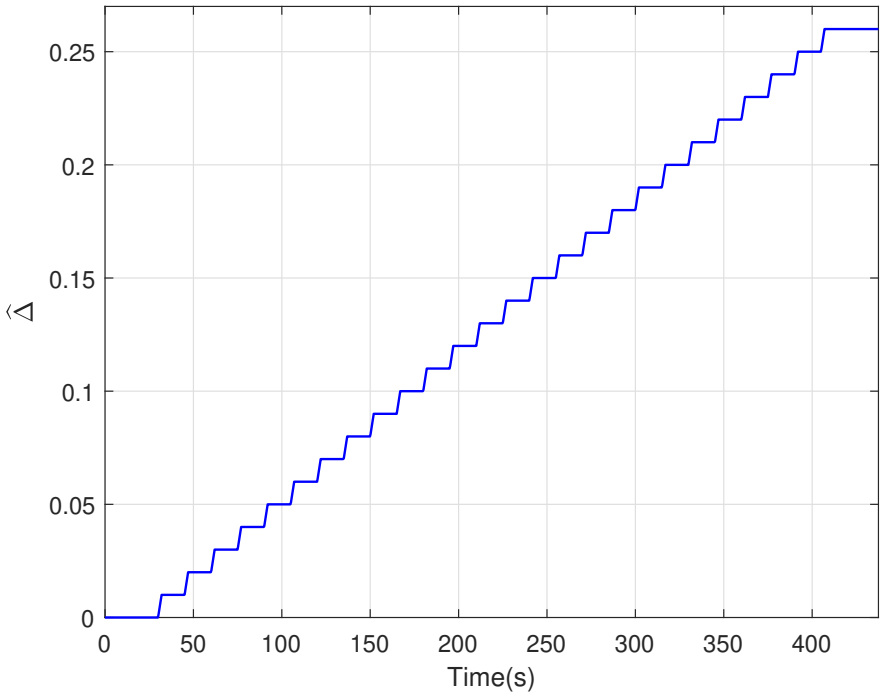

Figure 6.9 $\widehat{\Delta}$ update rule behavior ($\Delta = 0.27$, $d(t) = \sin(2.12\pi t)$, threshold=0.95 and $\delta_{\Delta} = 0.01$).

6.12, we see that the ML Model generates a result close to the threshold line when $\widehat{\Delta}$ is approximately equal to 0.13 value. From this, it can be deduced that the obtained ML Model may find wrong $\widehat{\Delta}$ values when there is a mixed D/U including features close to Δ_{min} and f_{max} values in the system. This problem can be called the early convergence problem. The sharp drop in ML Model output after early convergence can be used to solve this problem. In addition, increasing the data-set size and adding the new feature extraction methods will eliminate these problems. Fig. 6.13 shows the ML Model outputs of a different simulation test case that produces ML Model outputs below the specified threshold line. In such a case, $\widehat{\Delta}$ corresponding to the maximum value of λ is the correct $\widehat{\Delta}$ value.

Figs. 6.14-6.17 illustrate the D/U estimation results for two simulation test cases. In Fig. 6.14 and Fig. 6.16, the mixed D/U estimations that are predicted by conventional D/U estimator are given. Fig. 6.15 and Fig. 6.17 show the proposed ML assisted D/UE based control simulation results. Our proposed ML assisted D/U estimator found $\widehat{\Delta} = 0.26$ for the first test case and $\widehat{\Delta} = 0.84$ for the second test case ($\Delta = 0.84$). With the proposed method, the

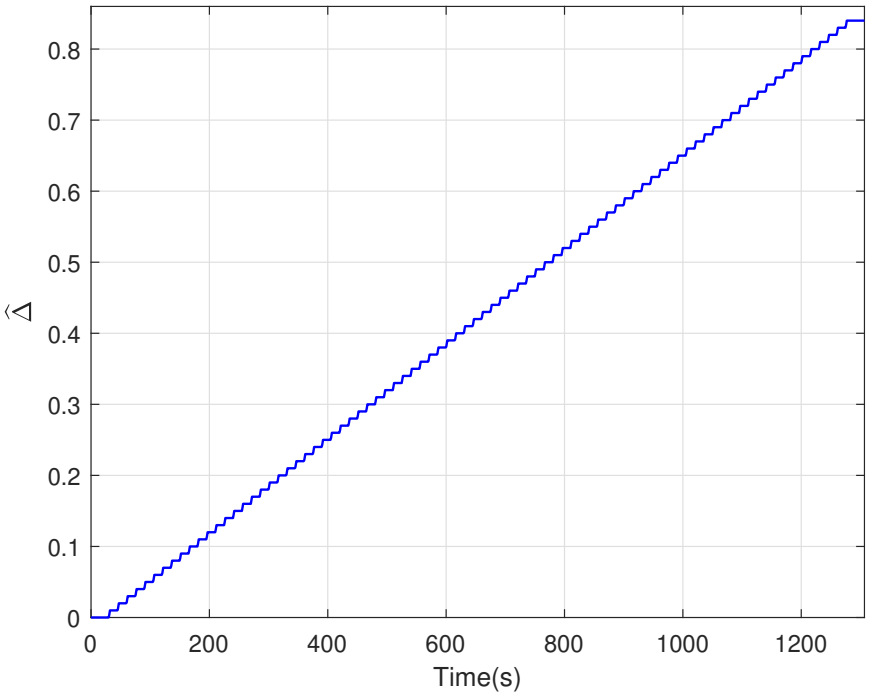

Figure 6.10 $\widehat{\Delta}$ update rule behavior ($\Delta = 0.84$, $d(t) = \sin(4.37\pi t)$, threshold=0.95 and $\delta_\Delta = 0.01$).

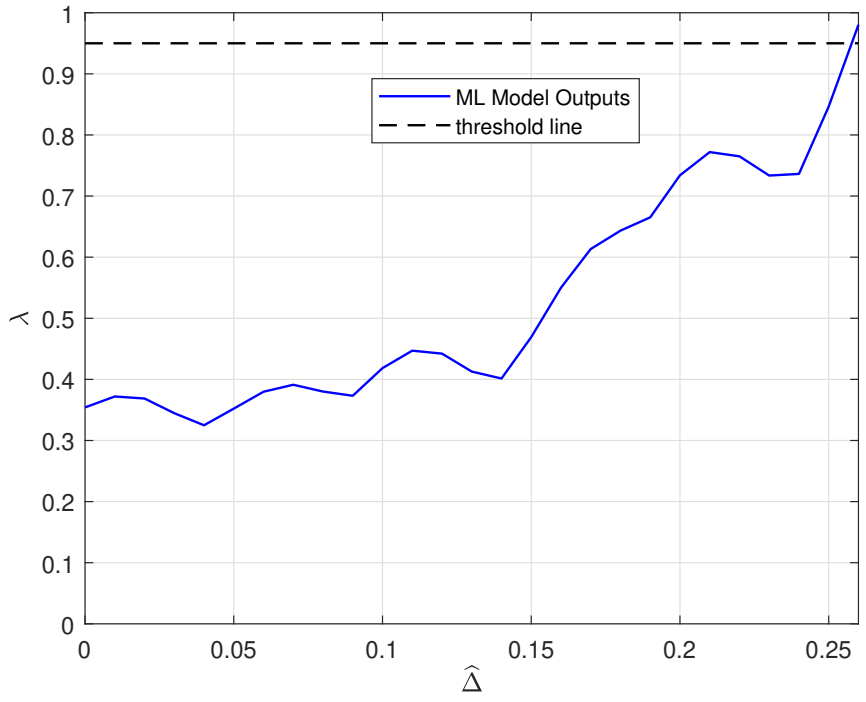

Figure 6.11 ML Model outputs ($\Delta = 0.27$, $d(t) = \sin(2.12\pi t)$, threshold=0.95 and $\delta_\Delta = 0.01$).

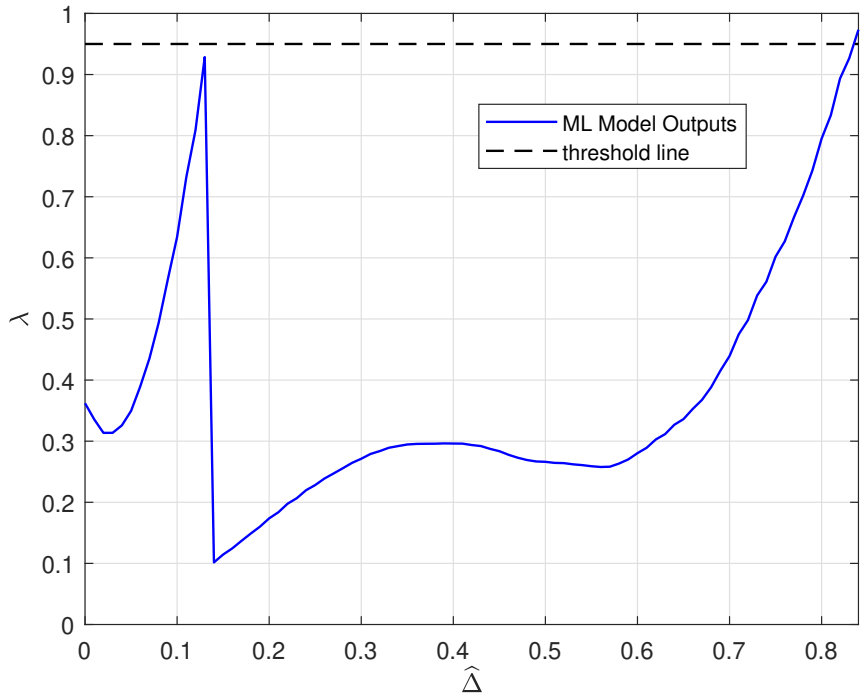

Figure 6.12 ML Model outputs ($\Delta = 0.84$, $d(t) = \sin(4.37\pi t)$, threshold=0.95 and $\delta_\Delta = 0.01$).

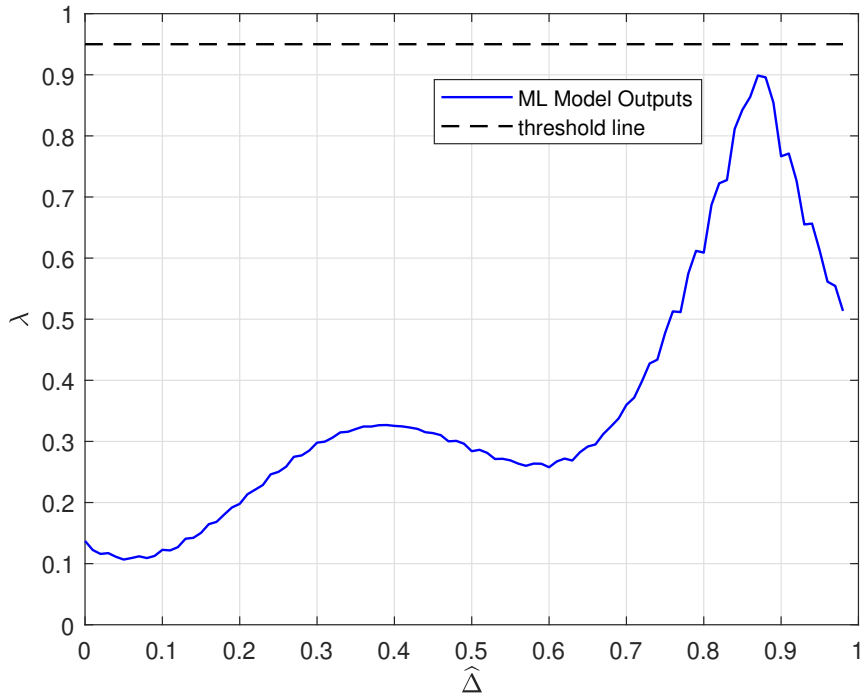

Figure 6.13 ML Model outputs ($\Delta = 0.87$, $d(t) = \sin(1.49\pi t)$, threshold=0.95 and $\delta_\Delta = 0.01$).

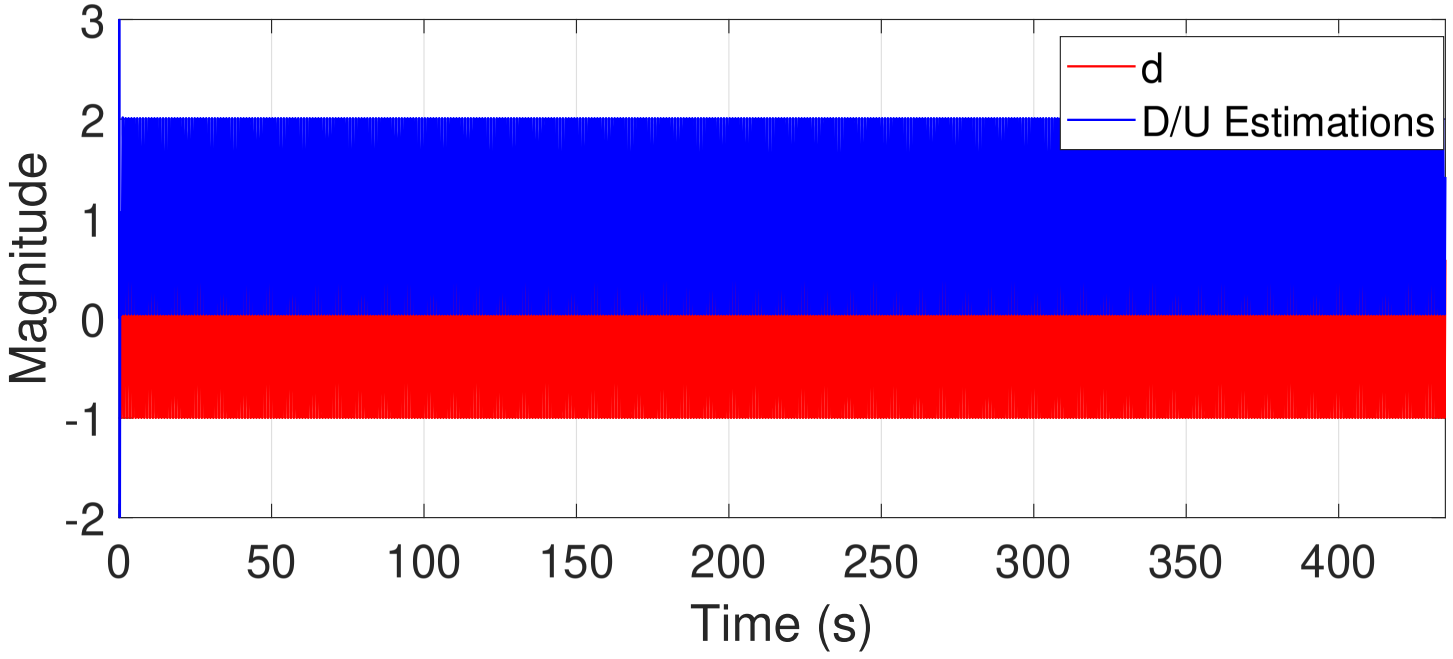

Figure 6.14 D/U estimator based control conventional scheme ($\Delta = 0.27$, $d(t) = \sin(2.12\pi t)$, threshold=0.95 and $\delta_{\Delta} = 0.01$).

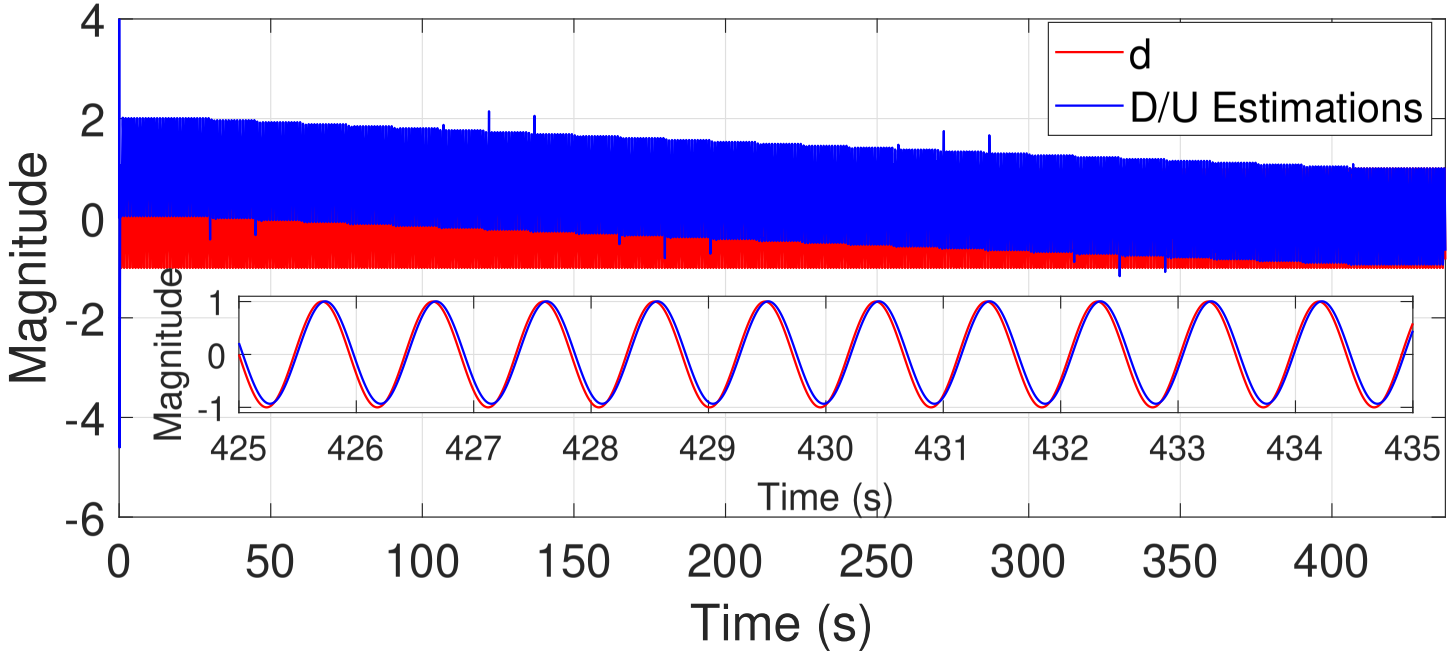

Figure 6.15 Proposed ML assisted D/U estimator based control scheme ($\Delta = 0.27$, $\widehat{\Delta} = 0.26$, $d(t) = \sin(2.12\pi t)$, threshold=0.95 and $\delta_{\Delta} = 0.01$).

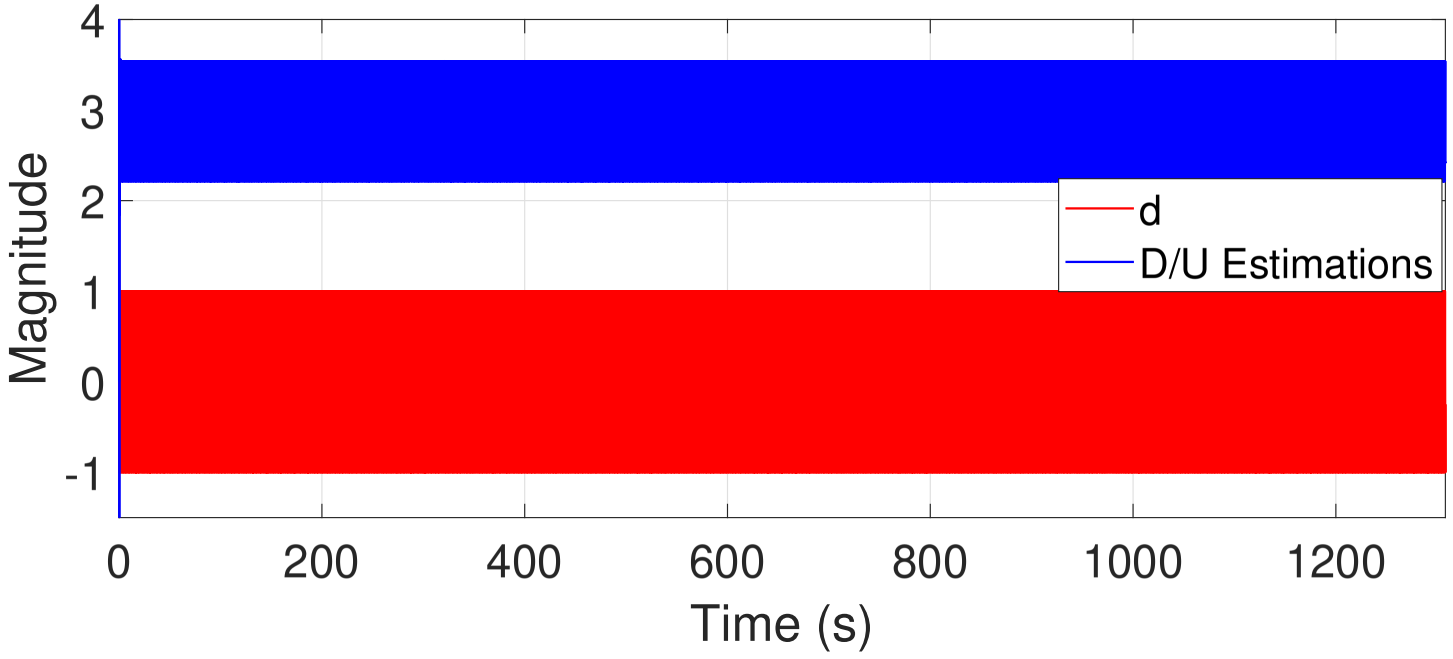

Figure 6.16 D/U estimator based control conventional scheme ($\Delta = 0.84$, $d(t) = \sin(8.74\pi t)$, threshold=0.95 and $\delta_\Delta = 0.01$).

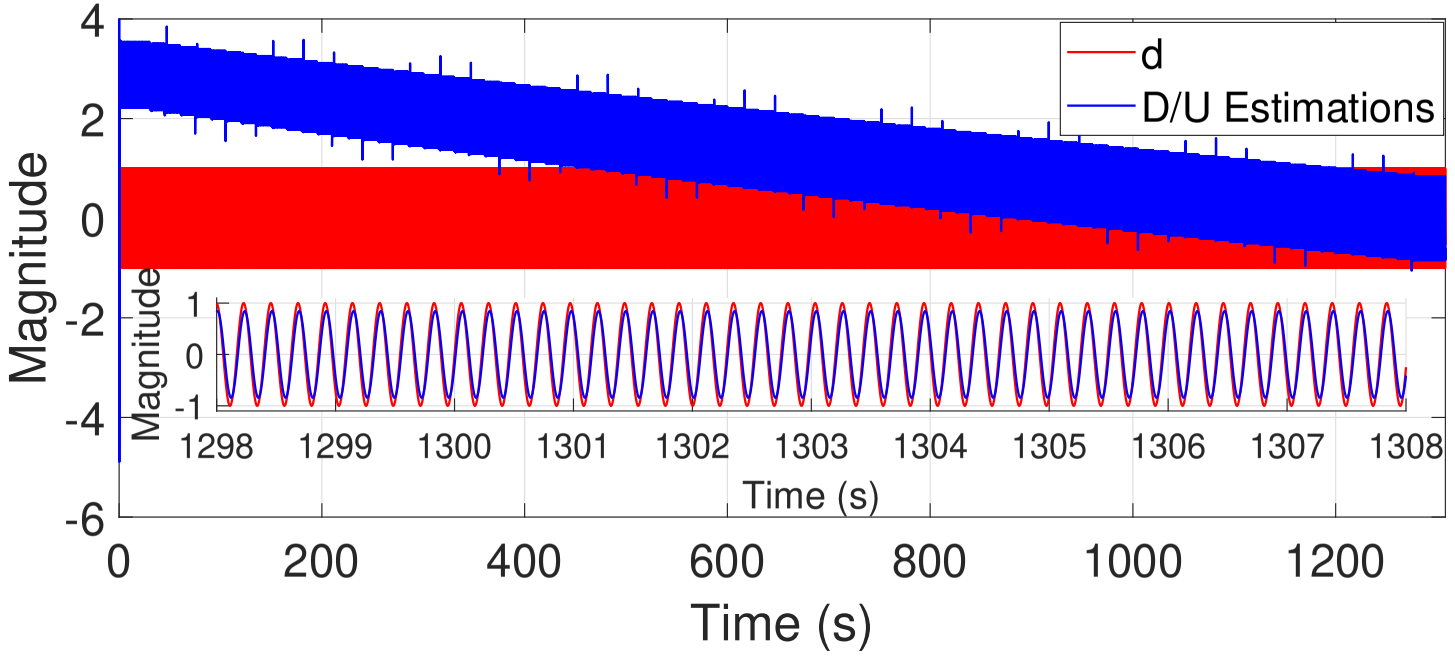

Figure 6.17 Proposed ML assisted D/U estimator based control scheme ($\Delta = 0.84$, $\widehat{\Delta} = 0.84$, $d(t) = \sin(8.74\pi t)$, threshold=0.95 and $\delta_{\Delta} = 0.01$).

actual disturbance is estimated over time. However, conventional D/U estimator predicts the disturbance with the steady state error due to uncertainty.

When the simulation results are examined, it is obvious that the proposed approach enhances the disturbance estimation capability of the system when compared to the classical D/UE based control scheme. Furthermore, Table 6.2 presents $\widehat{\Delta}$ results of 40 simulation test cases for different Δ and disturbance values. The studied set of simulation results prove that the proposed approach outperforms the classical methods by increasing disturbance estimation performance of the system. To obtain more precise $\widehat{\Delta}$ predictions, the size of the data-set can be increased and different splitting percentages for training and testing data-sets can be adopted. As in all ML applications, feeding the learning system by diverse data leads to accurate spot of the decision boundary. Enhanced input vectors may play the same role as long as the newly added features' roles are examined well.

Table 6.2 Proposed scheme test cases for threshold=0.95 and $\delta_{\Delta} = 0.01$

Test Case	$d(t)$	Δ	$\widehat{\Delta}$
1	$\sin(9.16\pi t)$	0.07	0.08
2	$\sin(9.22\pi t)$	0.18	0.18
3	$\sin(8.90\pi t)$	0.29	0.28
4	$\sin(9.90\pi t)$	0.38	0.38
5	$\sin(8.00\pi t)$	0.45	0.43
6	$\sin(9.46\pi t)$	0.56	0.53
7	$\sin(8.44\pi t)$	0.63	0.65
8	$\sin(8.18\pi t)$	0.71	0.73
9	$\sin(8.74\pi t)$	0.84	0.84
10	$\sin(9.78\pi t)$	0.97	0.97
11	$\sin(7.94\pi t)$	0.02	0.01
12	$\sin(7.50\pi t)$	0.13	0.11
13	$\sin(7.74\pi t)$	0.21	0.21
14	$\sin(7.24\pi t)$	0.30	0.30
15	$\sin(7.02\pi t)$	0.47	0.45
16	$\sin(6.96\pi t)$	0.52	0.51
17	$\sin(6.20\pi t)$	0.69	0.66
18	$\sin(6.50\pi t)$	0.76	0.78
19	$\sin(6.08\pi t)$	0.88	0.85
20	$\sin(7.18\pi t)$	0.94	0.92
21	$\sin(4.08\pi t)$	0.08	0.06
22	$\sin(4.80\pi t)$	0.16	0.16
23	$\sin(5.76\pi t)$	0.24	0.23
24	$\sin(4.62\pi t)$	0.37	0.38
25	$\sin(5.06\pi t)$	0.42	0.41
26	$\sin(4.58\pi t)$	0.55	0.53
27	$\sin(4.30\pi t)$	0.63	0.62
28	$\sin(5.28\pi t)$	0.73	0.73
29	$\sin(5.58\pi t)$	0.80	0.78
30	$\sin(4.96\pi t)$	0.92	0.92
31	$\sin(2.06\pi t)$	0.05	0.04
32	$\sin(2.62\pi t)$	0.11	0.09
33	$\sin(3.76\pi t)$	0.27	0.26
34	$\sin(2.22\pi t)$	0.31	0.31
35	$\sin(3.30\pi t)$	0.49	0.48
36	$\sin(2.54\pi t)$	0.52	0.52
37	$\sin(3.82\pi t)$	0.66	0.66
38	$\sin(3.52\pi t)$	0.75	0.74
39	$\sin(2.98\pi t)$	0.87	0.87
40	$\sin(3.16\pi t)$	0.98	0.98

7. CONCLUSION

This thesis study firstly comparatively discusses five DOBC approaches, namely, CDOBC, OEBDOBC, EID, TDDOBC, UDE. Their common and equivalent block diagram properties have been discussed, and nine performance and robustness TFs that provide an in-depth understanding of these schemes are derived. Four of these TFs are selected as a GoF equations, and for both uncertain minimum phase and time delay system, robustness and disturbance rejection performance discussion have been given for five DOBC schemes and CFC scheme. Our tests have shown that derived GoF equations can be used for qualifying the DOBC performances. A summary table considering performance and robustness analysis of DOBC methods and their design requirements are presented. In terms of robustness and disturbance rejection performance under similar operating conditions, simulation results recommend the TDDOBC scheme, which outperforms the other DOBC approaches if there is no process time time delay. Under the time delay conditions, UDE approach is more advisable than the others.

Secondly, a short tutorial introduction to DOBC approaches for the quadrotors is presented to obtain robust autopilot architectures. The modelling and controlling of a quadrotor are explained and five different DOBC approaches are adapted its overall architecture. DOBC design steps are given in detail by design challenges. To show their disturbance rejection capabilities and practical applicability, two flight simulation scenarios are carried out. For all simulation cases, we only took into account the external disturbances in rotational motions. While we gave the attitude trajectory commands to quadrotor attitude control architecture in the first scenario, we issued both way-point and trajectory commands to an outer loop controlling the translational motions in the second one. Presented DOBC approaches have successfully completed the given reference commands in the presence of the external disturbances even under the measurement noise. Moreover, simulation experiments have shown that UDEBC approach transmit the external disturbance and measurement noise effects to the actuators directly. As a result, for UDEBC approach, it should be kept in mind that flight accidents may occur due to excessive ESC heating. Baseline attitude

controller without DOBC approach have failed to follow the given reference commands. The simulation studies have also proved the practical applicability of these methods, which are successful even under measurement noise.

Finally, a novel approach to unmix the disturbance and uncertainty is presented. The classical approaches reconstruct the disturbances entering through the control channels and the process is subject to the presence of plant uncertainty, which leads to the prediction of a lumped effect that do not cancel out the input disturbance totally. The approach presented here uses an adjustable nominal model and an ϵ-SVR approach to decompose the percentages of the mixture. Such an approach distinguishes the effect of disturbance and the effect of uncertainty thereby leading to precise cancellation of the input disturbances. The performance of the presented technique is subject to that of all machine learning systems, i.e. the amount of training data, chosen learner type, representational diversity of the input vector, training termination criteria and so on. The claims have been exemplified on a second order LTI system to avoid the interference of plant specific difficulties. Results demonstrate that numerical data-oriented methods can offer alternative solutions to decompose a mixed signal and treat its components separately.

The proposed method is open to improvement and potential field of studies are given below:

- Adaptation algorithm can be changed.
- Different disturbance and uncertainty models can be added.
- Different feature extraction approaches can be suggested.
- Different supervised and reinforcement learning machine learning approaches can be applied.
- It can be applied on different linear and non-linear disturbance observer based control structures that directly use the nominal model information.
- New approaches can be suggested using proposed method in Composite Controller Design and Data-Driven Control schemes.

- It can be adapted to real physical systems.

REFERENCES

[1] Burak Kürkçü, Coşku Kasnakoğlu, and Mehmet Önder Efe. Disturbance/uncertainty estimator based integral sliding-mode control. *IEEE Transactions on Automatic Control*, 63(11):3940–3947, **2018**.

[2] Wen-Hua Chen, Jun Yang, Lei Guo, and Shihua Li. Disturbance-observer-based control and related methods—an overview. *IEEE Transactions on Industrial Electronics*, 63(2):1083–1095, **2016**. doi:10.1109/TIE.2015.2478397.

[3] Emre Sariyildiz, Roberto Oboe, and Kouhei Ohnishi. Disturbance observer-based robust control and its applications: 35th anniversary overview. *IEEE Transactions on Industrial Electronics*, 67(3):2042–2053, **2019**.

[4] Burak Kürkçü, Coşku Kasnakoğlu, Mehmet Önder Efe, and Rong Su. On the existence of equivalent-input-disturbance and multiple integral augmentation via h-infinity synthesis for unmatched systems. *ISA transactions*, **2022**.

[5] Xinjiang Wei and Lei Guo. Composite disturbance-observer-based control and h control for complex continuous models. *International Journal of Robust and Nonlinear Control: IFAC-Affiliated Journal*, 20(1):106–118, **2010**.

[6] Qi Dong, Qun Zong, Bailing Tian, Chaofan Zhang, and Wenjing Liu. Adaptive disturbance observer-based finite-time continuous fault-tolerant control for reentry rlv. *International Journal of Robust and Nonlinear Control*, 27(18):4275–4295, **2017**.

[7] Jun Yik Lau, Wenyu Liang, and Kok Kiong Tan. Adaptive sliding mode enhanced disturbance observer-based control of surgical device. *ISA transactions*, 90:178–188, **2019**.

[8] Harvey Rojas-Cubides, John Cortés-Romero, and Jaime Arcos-Legarda. Data-driven disturbance observer-based control: an active disturbance rejection approach. *Control Theory and Technology*, 19(1):80–93, **2021**.

[9] Shihua Li, Jun Yang, Wen-Hua Chen, and Xisong Chen. *Disturbance observer-based control: methods and applications*. CRC press, **2014**.

[10] Emre Sariyildiz and Kouhei Ohnishi. Analysis the robustness of control systems based on disturbance observer. *International Journal of Control*, 86(10):1733–1743, **2013**. doi:10.1080/00207179.2013.795663.

[11] Emre Sariyildiz and Kouhei Ohnishi. A guide to design disturbance observer. *Journal of Dynamic Systems, Measurement, and Control*, 136(2):021011, **2014**.

[12] Kiyoshi Ohishi. Torque-speed regulation of dc motor based on load torque estimation. In *IEEJ International Power Electronics Conference, IPEC-TOKYO, 1983-3*, volume 2, pages 1209–1216. **1983**.

[13] Kiyoshi Ohishi, Masato Nakao, Kouhei Ohnishi, and Kunio Miyachi. Microprocessor-controlled dc motor for load-insensitive position servo system. *IEEE transactions on industrial electronics*, (1):44–49, **1987**.

[14] Masato Nakao, Kouhei Ohnishi, and Kunio Miyachi. A robust decentralized joint control based on interference estimation. In *Proceedings. 1987 IEEE International Conference on Robotics and Automation*, volume 4, pages 326–331. IEEE, **1987**.

[15] Jingqing Han. A class of extended state observers for uncertain systems. *Control and decision*, 10(1):85–88, **1995**.

[16] Jingqing Han. From pid to active disturbance rejection control. *IEEE transactions on Industrial Electronics*, 56(3):900–906, **2009**.

[17] Jun Yang, Wen-Hua Chen, and Shihua Li. Autopilot design of bank-to-turn missiles using state-space disturbance observers. **2010**.

[18] Jin-Hua She, Mingxing Fang, Yasuhiro Ohyama, Hiroshi Hashimoto, and Min Wu. Improving disturbance-rejection performance based on an equivalent-input-disturbance approach. *IEEE Transactions on Industrial Electronics*, 55(1):380–389, **2008**.

[19] Jin-Hua She, Xin Xin, and Yaodong Pan. Equivalent-input-disturbance approach—analysis and application to disturbance rejection in dual-stage feed drive control system. *IEEE/ASME Transactions on Mechatronics*, 16(2):330–340, **2010**.

[20] Qing-Chang Zhong and David Rees. Control of uncertain lti systems based on an uncertainty and disturbance estimator. *J. Dyn. Sys., Meas., Control*, 126(4):905–910, **2004**.

[21] Qing-Chang Zhong, Alon Kuperman, and RK Stobart. Design of ude-based controllers from their two-degree-of-freedom nature. *International Journal of Robust and Nonlinear Control*, 21(17):1994–2008, **2011**.

[22] Hamin Chang, Hyuntae Kim, Gyunghoon Park, and Hyungbo Shim. Do-dat: A matlab toolbox for design & analysis of disturbance observer. *IFAC-PapersOnLine*, 51(25):340–345, **2018**.

[23] Tarik Uzunovic, Emre Sariyildiz, and Asif Sabanovic. A discussion on discrete implementation of disturbance-observer-based control. In *2018 IEEE 15th International Workshop on Advanced Motion Control (AMC)*, pages 613–618. IEEE, **2018**.

[24] Mehmet Önder Efe and Coşku Kasnakoğlu. An enhanced bandwidth disturbance observer based control-s-filter approach. *Turkish Journal of Electrical Engineering and Computer Sciences*, 29(4):2170–2185, **2021**.

[25] Izzuddin M Lazim, Abdul Rashid Husain, Zaharuddin Mohamed, Mohd Ariffanan Mohd Basri, Nurul Adilla Mohd Subha, and Liyana Ramli. Disturbance observer-based formation tracking control of multiple quadrotors in

the presence of disturbances. *Transactions of the Institute of Measurement and Control*, 41(14):4129–4141, **2019**.

[26] Youwu Du, Weihua Cao, Jinhua She, Min Wu, Mingxing Fang, and Seiichi Kawata. Disturbance rejection and control system design using improved equivalent input disturbance approach. *IEEE Transactions on Industrial Electronics*, 67(4):3013–3023, **2019**.

[27] Ilan Aharon, Doron Shmilovitz, and Alon Kuperman. Phase margin oriented design and analysis of ude-based controllers under actuator constraints. *IEEE Transactions on Industrial Electronics*, 65(10):8133–8141, **2018**.

[28] Tiago P Nascimento and Martin Saska. Position and attitude control of multi-rotor aerial vehicles: A survey. *Annual Reviews in Control*, 48:129–146, **2019**.

[29] Samir Bouabdallah, Andre Noth, and Roland Siegwart. Pid vs lq control techniques applied to an indoor micro quadrotor. In *2004 IEEE/RSJ International Conference on Intelligent Robots and Systems (IROS)(IEEE Cat. No. 04CH37566)*, volume 3, pages 2451–2456. IEEE, **2004**.

[30] Samir Bouabdallah. Design and control of quadrotors with application to autonomous flying. Technical report, Epfl, **2007**.

[31] L Salih Atheer, AF Mohamed Haider, and Sallom Gaeid Khalaf. Flight pid controller design for a uav quadrotor. *Scientific research and essays*, 5(23):3660–3667, **2010**.

[32] Shahida Khatoon, Mohammad Shahid, Himanshu Chaudhary, et al. Dynamic modeling and stabilization of quadrotor using pid controller. In *2014 International Conference on Advances in Computing, Communications and Informatics (ICACCI)*, pages 746–750. IEEE, **2014**.

[33] Filippo Rinaldi, Sergio Chiesa, and Fulvia Quagliotti. Linear quadratic control for quadrotors uavs dynamics and formation flight. *Journal of Intelligent & Robotic Systems*, 70(1):203–220, **2013**.

[34] Elias Reyes-Valeria, Rogerio Enriquez-Caldera, Sergio Camacho-Lara, and Jose Guichard. Lqr control for a quadrotor using unit quaternions: Modeling and simulation. In *CONIELECOMP 2013, 23rd International Conference on Electronics, Communications and Computing*, pages 172–178. IEEE, **2013**.

[35] Moses Bangura and Robert Mahony. Real-time model predictive control for quadrotors. *IFAC Proceedings Volumes*, 47(3):11773–11780, **2014**.

[36] Kostas Alexis, George Nikolakopoulos, and Anthony Tzes. Model predictive quadrotor control: attitude, altitude and position experimental studies. *IET Control Theory & Applications*, 6(12):1812–1827, **2012**.

[37] Fuyang Chen, Rongqiang Jiang, Kangkang Zhang, Bin Jiang, and Gang Tao. Robust backstepping sliding-mode control and observer-based fault estimation for a quadrotor uav. *IEEE Transactions on Industrial Electronics*, 63(8):5044–5056, **2016**.

[38] Tarek Madani and Abdelaziz Benallegue. Backstepping control for a quadrotor helicopter. In *2006 IEEE/RSJ International Conference on Intelligent Robots and Systems*, pages 3255–3260. IEEE, **2006**.

[39] Samir Bouabdallah and Roland Siegwart. Backstepping and sliding-mode techniques applied to an indoor micro quadrotor. In *Proceedings of the 2005 IEEE international conference on robotics and automation*, pages 2247–2252. IEEE, **2005**.

[40] Samir Bouabdallah and Roland Siegwart. Full control of a quadrotor. In *2007 IEEE/RSJ international conference on intelligent robots and systems*, pages 153–158. Ieee, **2007**.

[41] Andrew Zulu and Samuel John. A review of control algorithms for autonomous quadrotors. *arXiv preprint arXiv:1602.02622*, **2016**.

[42] Mukarram K Shaik and James F Whidborne. Robust sliding mode control of a quadrotor. In *2016 UKACC 11th International Conference on Control (CONTROL)*, pages 1–6. IEEE, **2016**.

[43] Juan Paul Ortiz, Luis Ismael Minchala, and Manuel Jeova Reinoso. Nonlinear robust h-infinity pid controller for the multivariable system quadrotor. *IEEE Latin America Transactions*, 14(3):1176–1183, **2016**.

[44] Xiao-Ning Shi, Yong-An Zhang, and Di Zhou. A geometric approach for quadrotor trajectory tracking control. *International Journal of Control*, 88(11):2217–2227, **2015**.

[45] Yong Zhang, Zengqiang Chen, Xinghui Zhang, Qinglin Sun, and Mingwei Sun. A novel control scheme for quadrotor uav based upon active disturbance rejection control. *Aerospace Science and Technology*, 79:601–609, **2018**.

[46] Abdurrahman Bayrak and MÖ Efe. Disturbance uncertainty estimator based robust attitude control of a quadrotor. In *10th Ankara International Aerospace Conference*. **2019**.

[47] Honglin Wang and Mou Chen. Trajectory tracking control for an indoor quadrotor uav based on the disturbance observer. *Transactions of the Institute of Measurement and Control*, 38(6):675–692, **2016**.

[48] Wenjing Cai, Jinhua She, Min Wu, and Yasuhiro Ohyama. Disturbance suppression for quadrotor uav using sliding-mode-observer-based equivalent-input-disturbance approach. *ISA transactions*, 92:286–297, **2019**.

[49] Ricardo Sanz, Pedro Garcia, Qing-Chang Zhong, and Pedro Albertos. Robust control of quadrotors based on an uncertainty and disturbance estimator. *Journal of Dynamic Systems, Measurement, and Control*, 138(7), **2016**.

[50] Ricardo Sanz, Pedro Garcia, Qing-Chang Zhong, and Pedro Albertos. Predictor-based control of a class of time-delay systems and its application to quadrotors. *IEEE Transactions on Industrial Electronics*, 64(1):459–469, **2016**.

[51] Izzuddin M Lazim, Abdul Rashid Husain, Zaharuddin Mohamed, Mohd Ariffanan Mohd Basri, Nurul Adilla Mohd Subha, and Liyana Ramli. Disturbance observer-based formation tracking control of multiple quadrotors in the presence of disturbances. *Transactions of the Institute of Measurement and Control*, 41(14):4129–4141, **2019**.

[52] Davide Invernizzi, Pietro Panizza, Fabio Riccardi, Simone Formentin, and Marco Lovera. Data-driven attitude control law of a variable-pitch quadrotor: a comparison study. *IFAC-PapersOnLine*, 49(17):236–241, **2016**.

[53] Chidentree Treesatayapun and Aldo Jonathan Muñoz-Vázquez. Discrete-time data-driven disturbance-observer control based on fuzzy rules emulating networks. *Journal of Computational Science*, 54:101426, **2021**.

[54] Burak Kürkçü, Coşku Kasnakoğlu, and Mehmet Önder Efe. Disturbance/uncertainty estimator based robust control of nonminimum phase systems. *IEEE/ASME Transactions on Mechatronics*, 23(4):1941–1951, **2018**.

[55] Julian Förster. *System identification of the crazyflie 2.0 nano quadrocopter*. B.S. thesis, ETH Zurich, **2015**.

[56] Qi Lu, Beibei Ren, Siva Parameswaran, and Qing-Chang Zhong. Uncertainty and disturbance estimator-based robust trajectory tracking control for a quadrotor in a global positioning system-denied environment. *Journal of Dynamic Systems, Measurement, and Control*, 140(3), **2018**.

[57] Rong-En Fan, Kai-Wei Chang, Cho-Jui Hsieh, Xiang-Rui Wang, and Chih-Jen Lin. Liblinear: A library for large linear classification. *the Journal of machine Learning research*, 9:1871–1874, **2008**.

[58] Chih-Chung Chang and Chih-Jen Lin. Libsvm: a library for support vector machines. *ACM transactions on intelligent systems and technology (TIST)*, 2(3):1–27, **2011**.

[59] Fabian Pedregosa, Gaël Varoquaux, Alexandre Gramfort, Vincent Michel, Bertrand Thirion, Olivier Grisel, Mathieu Blondel, Peter Prettenhofer, Ron Weiss, Vincent Dubourg, et al. Scikit-learn: Machine learning in python. *the Journal of machine Learning research*, 12:2825–2830, **2011**.